

ROLE OF microRNA-709 IN MURINE LIVER

Sneha Surendran

Submitted to the faculty of the University Graduate School  
in partial fulfillment of the requirements  
for the degree  
Doctor of Philosophy  
in the Department of Medical and Molecular Genetics,  
Indiana University

August 2014

Accepted by the Graduate Faculty, Indiana University, in partial fulfillment of the requirements for the degree of Doctor of Philosophy.

---

Núria Morral, Ph.D., Chair

---

Brittney-Shea Herbert, Ph.D.

Doctoral Committee

---

Mircea Ivan, MD, Ph.D.

May 8, 2014

---

Robert Considine, Ph.D.

---

Nadia Carlesso, M.D., Ph.D.

To my parents, Gracia and my grandparents

## ACKNOWLEDGEMENTS

My Ph.D. journey would not have been possible without the support from both my teachers and family. I would first like to thank my mentor, Dr. Núria Morral, for giving me the opportunity to pursue my Ph.D. under her guidance. I have benefited immensely from her vast knowledge of gene therapy and diabetes. Her scientific ideas, guidance and support have been instrumental in the successful completion of my research. She ensured that I stayed on course and focused on my objective. I would also like to thank the members of my research committee, Dr. Brittney-Shea Herbert, Dr. Mircea Ivan, Dr. Robert Considine and Dr. Nadia Carlesso for their critical evaluations, insights and guidance.

I would like to thank members of the Morral lab including Dr. Miwon Ahn, Dr. Jae-Seung Park, Dr. Yongyong Hou, Aisha Gamble and Victoria Jideonwo. I was fortunate to work with them on a number of projects, which enabled me to learn some of the methods used in this study. I am fortunate to have had friends in my colleagues. I am also grateful to summer research students John Murray and Chris Merchun for their help with this work. I would like to thank Dr. Janaiah Kota and Dr. Guoli Dai for sharing liver tissues for this research. I would like to thank Dr. Yunlong Liu and Chirayu Goswami for their help and guidance on statistical analyses. I am indebted to Dr. Kenn Dunn and Dr. Jennifer Ryan for their help with microscopy for hepatocyte polarization experiments. I am also grateful to Dr. William A. Truitt and Pamela Minick for all the help with TaqMan Low Density Arrays. I would also like to thank Seth Winfree and Indiana Center

for Biological Microscopy for their help with imaging labeled miRNA. I am also thankful to Dr. Edenberg and Dr. Jeanette McClintick and the Center for Medical Genomics for their help with the Affymetrix microarray. I am also immensely grateful to the DeVault Diabetes & Obesity Program and the American Heart Association Midwest for supporting me with pre-doctoral fellowships.

I would like to thank the faculty and staff at the Center for Diabetes Research. I am also thankful to the members of the Department of Medical and Molecular Genetics, especially Peggy Knople and Jean Good as well as the staff of the IUPUI Graduate Office and the Graduate Division of the Indiana University School of Medicine for their help during the course of my study.

Lastly, I would like to offer my heartfelt thanks to my family for their constant support and encouragement in the pursuit of my personal and professional objectives. I am very thankful to my parents, sister and Gracia for their unconditional love and support even from such a long distance. I wouldn't be me without my family. Their motivation and support has helped me progress along smoothly and I would like to express my sincere gratitude to them. I am also thankful to my friends and in-laws for their constant words of encouragement. Finally, this work would not have been possible without the constant love, support and encouragement from my husband.

Sneha Surendran

## ROLE OF microRNA-709 IN MURINE LIVER

MicroRNA are small RNA molecules that regulate expression of genes involved in development, cell differentiation, proliferation and death. It has been estimated that in eukaryotes, approximately 0.5 to 1% of predicted genes encode a microRNA, which in humans, regulate at least 30% of genes at an average of 200 genes per miRNA. Some microRNAs are tissue-specific, while others are ubiquitously expressed. In liver, a few microRNAs have been identified that regulate specialized functions. The best known is miR-122, the most abundant liver-specific miRNA, which regulates cholesterol biosynthesis and other genes of fatty acid metabolism; it also regulates the cell cycle through inhibition of cyclin G1. To discover other miRNAs with relevant function in liver, we characterized miRNA profiles in normal tissue and identified miR-709. Our data indicates this is a highly abundant hepatic miRNA and is dysregulated in an animal model of type 2 diabetes. To understand its biological role, miR-709 gene targets were identified by analyzing the transcriptome of primary hepatocytes transfected with a miR-709 mimic. The genes identified fell within four main categories: cytoskeleton binding, extracellular matrix attachment, endosomal recycling and fatty acid metabolism. Thus, similar to miR-122, miR-709 downregulates genes from multiple pathways. This would be predicted, given the abundance of the miRNA and the fact that the estimated number of genes targeted by a miRNA is in the hundreds. In the case of miR-709, these suggested a coordinated response during cell proliferation, when cytoskeleton remodeling requires substantial changes in gene expression. Consistently, miR-709 was found significantly

upregulated in an animal model of hepatocellular carcinoma. Likewise, in a mouse model of liver regeneration, mature miR-709 was increased. To study the consequences of depleting miR-709 in quiescent and proliferating cells, primary hepatocytes and hepatoma cells were cultured with antagomiRs (anti-miRs). The presence of anti-miR-709 caused cell death in proliferating cells. Quiescent primary hepatocytes responded by upregulating miR-709 and its host gene, Rfx1. These studies show that miR-709 targets genes relevant to cytoskeleton structural genes. Thus, miR-709 and Rfx1 may be needed to facilitate cytoskeleton reorganization, a process that occurs after liver injury and repopulation, or during tumorigenesis.

Núria Morral, Ph.D., Chair

## TABLE OF CONTENTS

<b>LIST OF TABLES</b> .....	xii
<b>LIST OF FIGURES</b> .....	xiii
<b>LIST OF ABBREVIATIONS</b> .....	xvi
<b>INTRODUCTION</b>	
A. Role of liver in metabolism.....	1
B. Liver organization .....	4
C. Hepatocyte polarity and cytoskeletal organization .....	7
D. MicroRNAs.....	11
E. Role of miRNAs in liver function .....	17
F. Thesis hypothesis and Research Aims.....	24
<b>MATERIALS AND METHODS</b>	
A. Materials.....	26
1. Plasmids.....	26
2. Primers.....	26
3. Mice.....	27
a. Liver miRNA analysis.....	27
b. Primary hepatocyte isolation.....	27
c. miRNA profiles under fed, fasted, refed conditions .....	27
d. Relative expression of pre-miR-709 vs mature miR-709 .....	27
4. Antibodies .....	28
5. Other reagents.....	28
a. Plasmid isolation .....	28



b. RNA isolation .....	29
c. Protein isolation .....	29
d. DNA gel extraction.....	29
e. Ligation .....	29
f. PCR.....	29
g. qRT-PCR.....	29
h. TaqMan miRNA Assay.....	30
i. Protein quantification.....	30
j. Western blot detection .....	30
k. LDH assay.....	30
l. Transfection .....	30
m. LB broth.....	30
n. Bacteria for subcloning.....	30
o. Cell lines .....	30
B. Methods.....	30
1. Plasmid cloning .....	31
2. Primary hepatocyte isolation .....	35
2.a. Primary hepatocyte sandwich experiments .....	35
2.b. Sodium fluorescein assay.....	36
2.c. Imaging of labeled miR-709 in primary hepatocytes.....	37
3. Cell culture .....	37
3.a. Imaging of labeled miR-709 in Hepa1c1c cells.....	38
3.b. LDH assay in Hepa1c1c cells .....	38

4. Cell transfection .....	39
a. Using plasmids and miRNA.....	39
b. Using plasmids.....	39
c. Using miRNA/siRNA/antagomiRs/anti-miRs .....	40
5. miRNA target predictions .....	40
6. Array analyses .....	40
a. miRNA microarray.....	40
b. mRNA Affymetrix analysis .....	42
c. Taqman low Density Array.....	43
7. Western blotting .....	44
8. Northern blotting .....	45
9. LDH assay .....	46
10. qPCR analysis.....	46
a. qRT-PCR.....	46
b. TaqMan assay to quantify mature miRNAs.....	47
11. Statistical analysis .....	47

**RESULTS**

A. Hepatic murine miRNA expression .....	48
A.1 Identification of miRNAs expressed in livers of normal and <i>db/db</i> mice.....	48
A.2 Differential expression of hepatic microRNAs in the fasted and refed state .....	53
B. Targets of miRNA-709 in murine liver .....	59

B.1. miR-709-3p is the mature strand of miRNA-709.....	59
B.2. miR-709-induced transcriptome.....	63
B.3. Ces1g, Rab11b and Pctp are direct targets of miR-709 .....	73
B.4. Database gene predictions.....	76
C. Biological Role of miRNA-709 In Liver .....	79
C.1. miR-709 gene targets do not regulate hepatocyte polarity.....	79
C.2. Intracellular miR-709 localization .....	87
C.3. Pre-miR-709 accumulates in liver.....	92
C.4. miR-709 inhibition elicits cell death .....	99
C.5. Mature levels of miR-709 do not increase in <i>db/db</i> livers .....	103
<b>DISCUSSION</b> .....	104
<b>FUTURE DIRECTIONS</b> .....	113
<b>REFERENCES</b> .....	114
<b>CURRICULUM VITAE</b>	

## LIST OF TABLES

Table 1. Oligonucleotides used to generate luciferase constructs and primers used for PCR.....	26
Table 2. Antibodies used for Western blotting .....	28
Table 3. miRNAs expressed in liver of normal C57BLKS/J mice. ....	51
Table 4. Blood glucose and body weight.....	54
Table 5. miRNAs differentially expressed between fasted and refed groups.....	55
Table 6. Predicted pathway regulation by miRNAs .....	58
Table 7. Genes significantly downregulated >2-fold in miR-709-treated primary hepatocytes .....	66
Table 8. Predicted versus observed miR-709 target genes .....	77
Table 9. Overlap between miR-709 target genes and hsa-miR-1827 predicted targets .....	78

## LIST OF FIGURES

Figure 1. Metabolic pathways in liver .....	3
Figure 2. Liver cross section.....	6
Figure 3. Liver lobule and portal triad.....	6
Figure 4. Hepatocyte polarity .....	9
Figure 5. Endosomal recycling in hepatocytes .....	9
Figure 6. Processing of miRNA.....	15
Figure 7. Structural components of a pre-miRNA.....	16
Figure 8. Role of miR-122 in liver.....	19
Figure 9. Schematic representation of the psi-CHECK2 plasmid used for generating constructs for luciferase reporter assays .....	31
Figure 10. Schematic representation of plasmids expressing pri-miR-709 and pri-Cel-239b .....	34
Figure 11. Hierarchical clustering analysis of miRNAs with p-value < 0.01.....	50
Figure 12. miR-709 strand selection in primary hepatocytes. ....	60
Figure 13. miR-709 strand selection in the Hepa1c1c7 cell line. ....	61
Figure 14. Strand selection of endogenous miR-709 in primary hepatocytes.....	62
Figure 15. miR-709 quantification in primary hepatocyte transfected with mimic .....	62
Figure 16. Hierarchical cluster of top 100 genes .....	64
Figure 17. Real time RT-PCR analysis of miR-709 targets.....	69
Figure 18. Prolonged downregulation of miR-709 targets over time .....	70

Figure 19. miR-709 on Rab11b, Timp3 and Dync1li1 protein levels .....	71
Figure 20. miR-709 decreases Rab11b in Hepa1c1c cells.....	72
Figure 21. miR-709 putative binding sites in the 3' UTR of Rab11b, Ces1g and Pctp.....	74
Figure 22. Rab11b, Pctp and Ces1g are direct targets of miR-709.....	75
Figure 23. Formation of bile canaliculi between primary hepatocytes cultured in a sandwich configuration .....	82
Figure 24. Uptake and secretion of sodium fluorescein .....	83
Figure 25. Sodium fluorescein transport in primary hepatocytes transfected with miR-709 and Cel-239b.....	84
Figure 26. Rab11b silencing in mouse primary hepatocytes .....	85
Figure 27. Sodium fluorescein transport in primary hepatocytes treated with siRab11b .....	86
Figure 28. Intracellular localization of miR-709 in primary hepatocytes.....	89
Figure 29. Intracellular localization of miR-709 in Hepa1c1c .....	90
Figure 30. Cytoplasmic miRNA localization in Hepa1c1c cells transfected with miRNA-709 .....	91
Figure 31. Relative abundance of pre- and mature miR-709 in an animal model of hepatocellular carcinoma.....	94
Figure 32. Relative abundance of pre- and mature miR-122 in an animal model of hepatocellular carcinoma.....	95
Figure 33. Levels of mature miR-709 in HEK293 and Hepa1c1c cells upon transfection with plasmids expressing pri-miR-709 or pri-Cel-239b.....	96

Figure 34. Relative abundance of miR-709 in an animal model of liver regeneration.....	97
Figure 35. qPCR analysis of miR-709 and Rfx1 in animal models of liver regeneration and hepatocellular carcinoma .....	98
Figure 36. miR-709, Rab11b, Ces1g and Rfx-1 expression in primary hepatocytes transfected with anti-miR-709. ....	100
Figure 37. Cell viability assay in Hepa1c1c cells transfected with miR-709 inhibitor ...	102
Figure 38. Levels of mature miR-709 in livers of <i>db/db</i> mice.....	103

## LIST OF ABBREVIATIONS

°C	Degree Celsius
μM	Micromolar
3'-UTR	3'-Untranslated region
Abca1	Adenosine triphosphate-binding cassette (ABC) transporter, member 1
Acc1	Acyl-CoA carboxylase 1
Acl	ATP-dependent citrate lysase
Acox2	Acyl-CoA oxidase 2
Adam10	A disintegrin and metalloprotease family 10
Adam17	A disintegrin and metalloprotease family 17
AGO	Argonaute
Agpat1	Acylglycerol-3-Phosphate O-Acyltransferase 1
Anova	Analysis of variance
ATCC	American Type Culture Collection
bp	Base pair
BCL-2	B-cell lymphoma 2
Bcrp	Breast Cancer Resistance Protein
Bsep	Bile Salt Export Pump
CAT-1	Cationic amino acid transporter-1
cDNA	Complementary DNA
Cel-239b	<i>Caenorhabditis elegans</i> miRNA 239b



Ces1g	Carboxylesterase 1G
CD36	Cluster of Differentiation 36
CD44	CD44 Molecule
CIDEc	Cell Death-Inducing DFFA-Like Effector C
C <sub>t</sub>	Threshold cycle
CPT1 $\alpha$	Carnitine palmitoyl transferase 1 $\alpha$
CUTL1	Cut-like homeobox 1
Cyc-A	Cyclophilin A
Db/db	Mice homozygous for a point mutation in the leptin receptor gene, rendering them deficient in leptin receptor activity
DcP2	mRNA-decapping enzyme 2
DNA	Deoxyribonucleic acid
DGAT2	Diacylglycerol acyltransferase-2
DGCR8	Digeorge syndrome critical region gene 8
Dync1li1	Dynein cytoplasmic light chain 1
ECL	Enhanced chemiluminescence
ECM	Extracellular matrix
<i>E. coli</i>	<i>Escherichia coli</i>
EGTA	Ethylene glycol tetraacetic acid
ELOVL6	ELOVL fatty acid elongase 6
ENaC	Epithelial sodium channel
ERC	Endosomal recycling compartment
FAM	6-carboxyfluorescein

FAS	Fatty acid synthase
FBS	Fetal bovine serum
G6pase	Glucose 6-phosphatase
Gck	Glucokinase
GCOS	GeneChip® Operating System
Gk	Glucokinase
Gns	Glutamine synthetase
Gpt	Glutamic-pyruvate transaminase
Gpx	Glutathione peroxidase
HBSS	Hank's Balanced Salt solution
HCC	Hepatocellular carcinoma
HCV	Hepatitis C Virus
HDL	High-density lipoprotein
HFD	High-fat diet
HIF-1 $\alpha$	Hypoxia Inducible Factor 1, Alpha Subunit
HIST1H2BC	Histone cluster 1, H2bc
HMGCR	HMGCoA reductase
HRP	Horse radish peroxidase
hsa-miR-1827	<i>Homo sapiens</i> microRNA-1827
IGF1	Insulin-like growth factor 1
IGF1R	Insulin-like growth factor 1 receptor
INSR	Insulin receptor
IRS-2	Insulin receptor substrate-2

IRS-4	Insulin receptor substrate 4
kb	Kilobase
LAP	Liver activator promoter
LDH	Lactate dehydrogenase
Ldlr	Low-density lipoprotein receptor
LOWESS	Locally-weighted Regression
LPL	Lipoprotein lipase
MAPRE1	Microtubule-Associated Protein, RP/EB Family, Member 1
Mb	Megabase
MCS	Multiple cloning site
Mdr1	Multidrug resistance gene 1
Mdr2	Multidrug resistance gene 2
MET	Met Proto-Oncogene
ml	Milliliter
miRISC	miRNA-induced silencing complex
miRNA	microRNA
miR-709	microRNA-709
mmu-miR-709	<i>Mus musculus</i> miRNA-709
Mrp1	Multidrug resistance-associated protein 1
Mrp2	Multidrug resistance-associated protein 2
Mrp3	Multidrug resistance-associated protein 3
Mrp4	Multidrug resistance-associated protein 4
Mrp6	Multidrug resistance-associated protein 6

mTOR	Mammalian Target Of Rapamycin
MVB	Multivesicular bodies
ng	nanogram
nM	nanomolar
N/A	Not available
NAFLD	Non-alcoholic fatty liver disease
NASH	Non-alcoholic steatohepatitis
NDRG3	N-Myc Downstream-Regulated Gene 3
Ntcp	Na/Taurocholate Cotransporting Polypeptide
P450	Cytochrome P450
P-bodies	Processing bodies
P/S	Penicillin/streptomycin
PCA	Principal component analysis
Pck	Phosphoenolpyruvate carboxykinase
PCR	Polymerase chain reaction
Pctp	Phosphatidylcholine transfer protein
Pfkl	Phosphofructokinase liver
Pkl	Pyruvate kinase
PPAR- $\alpha$	Peroxisome proliferator-activated receptor- $\alpha$
pre-miRNA	Precursor miRNA
pri-miRNA	Primary transcript of a miRNA
pri-miR-15a/16-1	Primary transcript of miR-15a and 16-1
QC	Quality control

qRT-PCR	Quantitative real-time polymerase chain reaction
Rab11b	Member RAS oncogene family
RISC	RNA-induced Silencing Complex
RNase	Ribonuclease
RNA	Ribonucleic acid
RNAi	RNA interference
RPS10	40S ribosomal protein S10
RT	Reverse transcription
SD	Standard deviation
SEC	Sinusoidal endothelial cells
siNC	Negative control siRNA
siRab11b	siRNA against Rab11b
siRNA	Silencing RNA
SIRT1	Sirtuin 1
sno-202	Small nucleolar RNA 202
SNP	Single nucleotide polymorphism
SREBP-1	Sterol-regulatory element binding protein 1
SREBP-1c	Sterol-regulatory element binding protein 1c
SREBP-2	Sterol-regulatory element binding protein 2
tTA	Transactivator protein
T2DM	Type 2 diabetes mellitus
TBP	TATA binding protein
TLDA	TaqMan low density array

TRBP	TAR RNA binding protein
TuD	Tough Decoy
UDPGT	UDP glucuronate transferease
VLDL	Very low-density lipoprotein
WAT	White adipose tissue
WT	Whole transcript
XPO5	Exportin 5
XRN1	Exoribonuclease 1

## INTRODUCTION

### A. Role of liver in metabolism

The liver is the largest metabolic organ in the human body<sup>8</sup>. Various metabolic pathways occurring in this tissue, including carbohydrate metabolism (gluconeogenesis, glycolysis, glycogenesis, glycogenolysis), lipid metabolism (cholesterol and triglyceride synthesis and export, fatty acid oxidation, ketogenesis) and protein metabolism (synthesis and degradation), are essential for whole body homeostasis (Figure 1). Finally, the liver produces bile, which is critical for emulsification of lipids and aids in digestion of lipids in the small intestine.

Maintaining blood glucose levels within a narrow range is vital for the body, both in periods of feeding and fasting. This important function of glucose homeostasis is carried out by hepatocytes in the liver. Upon feeding, glucose is broken down into pyruvate through glycolysis to produce energy for the cells. In addition, excess glucose is taken up by the liver and converted into glycogen (glycogenesis). In periods of fasting, the glycogen stores in the liver are used to produce glucose (glycogenolysis); in addition, the liver synthesizes glucose from amino acids, glycerol, and lactate, through the gluconeogenesis pathway.

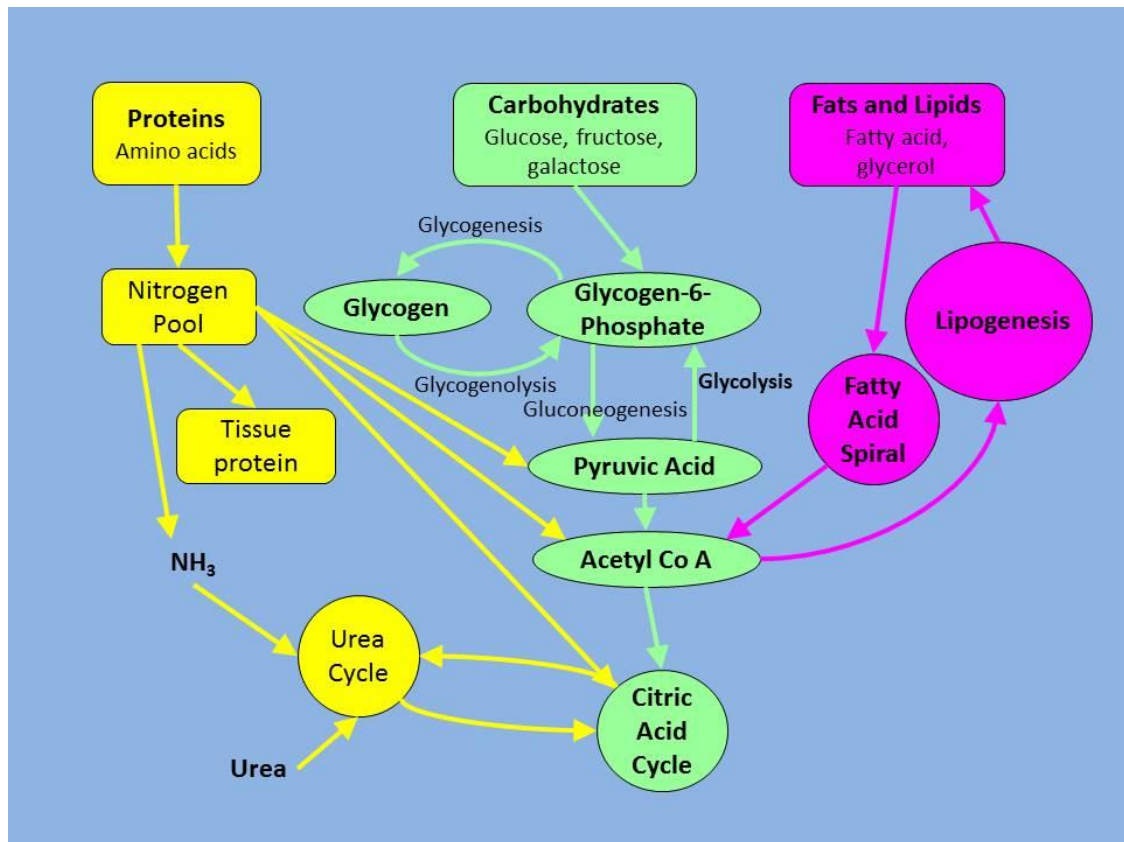
The liver also plays an important role in lipid metabolism. In the fed state, excess glucose is converted into fatty acids (*de novo* lipogenesis) and subsequently esterified into triglycerides, which remain as droplets in the cytoplasm or can be secreted from the

liver into the circulation via very low-density lipoprotein (VLDL) for use by other tissues. In the fasted state, the liver can actively oxidize fatty acids to produce ketone bodies that are exported into circulation, thereby providing an alternate energy source for other organs in the body, in particular for the brain. The liver also synthesizes cholesterol, lipoproteins and phospholipids. Some of the cholesterol is converted into bile salts. In addition to cholesterol, the bile contains organic and inorganic solutes that make up 5% of the bile<sup>9</sup>. The apical membranes of adjacent hepatocytes form a canalicular network through which bile is secreted from the hepatocytes<sup>9</sup>. Bile synthesis is regulated by transport systems localized on the apical membrane of hepatocytes<sup>9</sup>.

Protein metabolism is another important function of the liver. This tissue synthesizes non-essential amino acids and makes most of the plasma proteins such as albumin and clotting factors. The liver is also involved in breakdown of amino acids by deamination and transamination, and removes ammonia from the bloodstream, converting it into urea for excretion.



**Figure 1. Metabolic pathways in liver.** Source: Adapted from image obtained from



<http://www.elmhurst.edu/~chm/vchembook/600glycolysis.html>

## **B. Liver organization**

The liver is a complex organ with at least 15 different cell types<sup>8</sup>. Hepatocytes comprise approximately 60% of the cells and take up 80% of the volume in the liver, while sinusoidal endothelial cells (SEC), Kupffer cells and hepatic stellate cells represent 20%, 15% and 5% of cells, respectively<sup>8</sup>. Each of these four major cellular types has specific functions. Hepatocytes, in particular, play important roles in maintaining lipid and glucose homeostasis.

The liver's blood supply is one of its kind; it receives venous blood from the portal vein, as well as oxygenated blood from the hepatic artery<sup>8</sup>. The blood from these vessels flows through the liver sinusoids, a highly branched discontinuous network of blood vessels, before it is delivered to the hepatocytes<sup>8</sup>. Hepatocytes are arranged into hexagonal lobules, the liver's functional unit (Figure 2 and 3). At the center of the lobule is a central vein. The central veins from multiple lobules combine to form the hepatic vein, which eventually joins the inferior vena cava. At the junction of several lobules is a portal triad, consisting of branches of hepatic artery, hepatic portal vein and interlobular bile ducts. Hepatocytes closer to the entering vascular supply (periportal) receive the most oxygenated blood while hepatocytes close to the central vein (perivenous) receive the least oxygenated blood. This results in a metabolic zonation, wherein the amount of liver enzymes and their activities vary in periportal and perivenous hepatocytes<sup>10</sup>. Periportal hepatocytes are rich in enzymes such as phosphoenolpyruvate carboxykinase (PCK), glucose 6-phosphatase (G6Pase) (carbohydrate metabolism), HMG-CoA reductase (HMGCR) (lipid metabolism) and glutamic-pyruvate transaminase (GPT),

glutathione peroxidase (GPX) (amino acid metabolism)<sup>10</sup>. Periportal hepatocytes are specialized in oxidative functions such as  $\beta$ -oxidation of fatty acids, gluconeogenesis, bile formation and cholesterol synthesis<sup>10</sup>. Also, sub-cellular organelles such as mitochondria and bile canaliculi are more abundant in periportal hepatocytes compared to perivenous hepatocytes<sup>10</sup>. On the other hand, perivenous hepatocytes are abundant in enzymes such as glucokinase (GK), pyruvate kinase (PK<sub>L</sub>) (carbohydrate metabolism), Acetyl-coA carboxylase (ACC), ATP-dependent citrate lysase (ACL), fatty acid synthase (FAS) (lipid metabolism), glutamine synthetase (GNS) (amino acid metabolism) and cytochrome P450 (P450), UDP glucuronate transferease (UDPGT) (xenobiotic metabolism)<sup>10</sup>. These hepatocytes are preferentially involved in glucose uptake for glycogen synthesis, glycolysis, lipogenesis, and detoxification<sup>10</sup>.

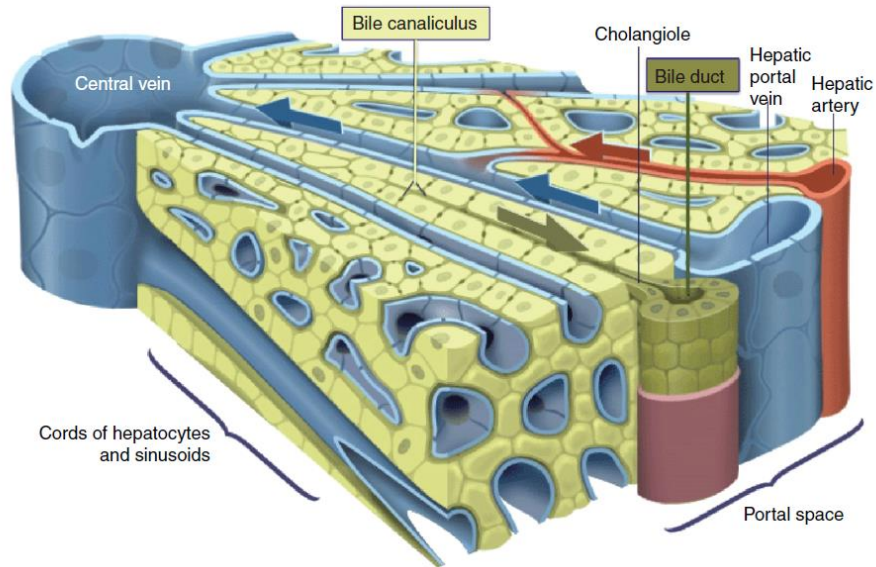


**Figure 2. Liver cross section.** The arrangement of sinusoids, hepatocytes and bile canaliculi is shown. Source: Image from<sup>8</sup>.

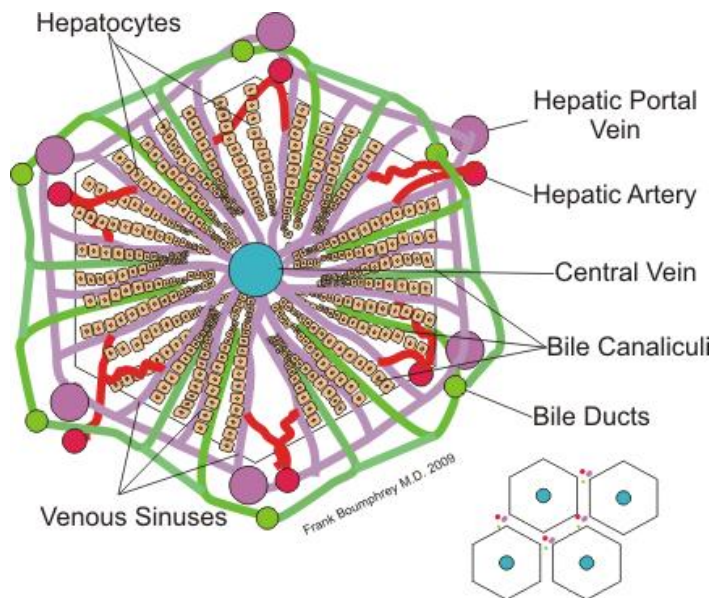


**Figure 3. Liver lobule and portal triad.**

(Source: Image from [http://en.wikipedia.org/wiki/File:Hepatic\\_structure.png](http://en.wikipedia.org/wiki/File:Hepatic_structure.png))

### **C. Hepatocyte polarity and cytoskeletal organization**

The liver is known second after brain for its complexity in structure and function<sup>11</sup>. Hepatocytes are the major cell type in the liver, comprising 80% of the volume<sup>11</sup>. Like all epithelial cells, hepatocytes must be polarized with well-defined apical and basolateral membranes to be functional<sup>12,13</sup>. The apical and basal surfaces are separated by tight junctions<sup>8</sup> (Figure 4). Specific functions are performed depending on the polarity (apical versus basolateral domain) of the hepatocytes<sup>14</sup>. Each of these domains is characterized by specific marker proteins. Hepatic apical or canalicular membrane is characterized by expression of proteins such as Breast Cancer Resistance Protein (Bcrp), Bile Salt Export Pump (Bsep), Multidrug resistance-associated protein 2 (Mrp2), multidrug resistance gene 1 (Mdr1) and multidrug resistance gene 2 (Mdr2) whereas basolateral markers include Multidrug resistance-associated protein 1 (Mrp1), Multidrug resistance-associated protein 3 (Mrp3), Multidrug resistance-associated protein 6 (Mrp6), Multidrug resistance-associated protein 2 (Mrp4) and Na/Taurocholate Cotransporting Polypeptide (Ntcp)<sup>13</sup>. Bile canaliculi are formed on the apical membrane of two adjacent hepatocytes and bile acid transporters are confined to this domain<sup>14,15</sup>. The basolateral surface of hepatocytes is involved in trafficking of metabolites from the bloodstream<sup>14</sup>. Hepatocytes constantly internalize extracellular ligands and other materials by endocytosis<sup>16,17</sup>. The endocytosed products are either recycled back to the cell surface, destined for lysosomal degradation, or undergo transcytosis to the opposite membrane<sup>8,16</sup> (Figure 5). These are mediated by very dynamic and diverse endosomal compartments<sup>17</sup>.

Receptors bound to their ligands at the basolateral membrane are taken up into early endosomes and are separated from their ligand<sup>17,18</sup>. This occurs at the periphery of the cell. The receptor can then recycle back while the ligand destined for degradation has to pass through late endosomes, pre-lysosomes, or multivesicular bodies (MVBs) before being delivered to the lysosomes<sup>17</sup>. Substrates of apical proteins are also endocytosed and transported from the basolateral membrane to the apical membrane of the hepatocyte, and are then released into the bile canaliculi<sup>18</sup>. Many of the apical proteins synthesized in the cell are first sent to the basolateral membrane before being transported to their final destination, the apical membrane<sup>18</sup>. This emphasizes the importance of endocytosis in hepatocytes.

The extracellular matrix (ECM) of the liver plays a vital role in endocytosis. It is primarily made up of type I collagen and is crucial for hepatic function<sup>11</sup>. The ECM comprises many elements such as matrix metalloproteinases; the glycoproteins laminin, fibronectin, vitronectin, undulin, nidogen (entactin); and proteoglycans such as heparan sulfate<sup>11</sup>. Recently, miRNAs have been shown to play a key role in regulating the expression of ECM proteins. miR-29 targets key ECM proteins such as laminin, nidogen and fibrillin and members of miR-29 family have been shown to be downregulated in liver fibrogenesis. miR-199 is upregulated during fibrogenesis and targets matrix metalloproteinases and collagen proteins. This highlights the importance of miRNAs in maintaining the ECM of hepatocytes, which is critical for hepatic polarity.

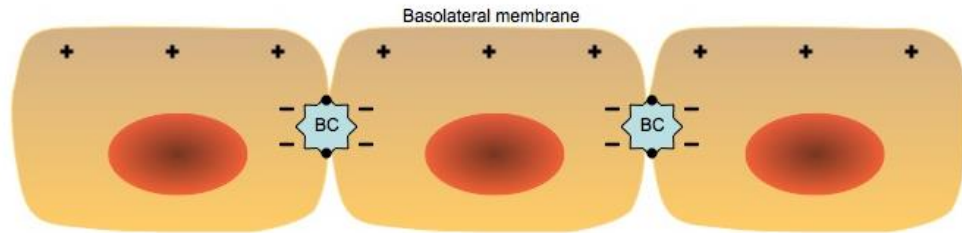


**Figure 4. Hepatocyte polarity.** BC, Bile canaliculi; +++ Basolateral membrane; - - - Apical membrane. (Source: Modified from<sup>13</sup>).

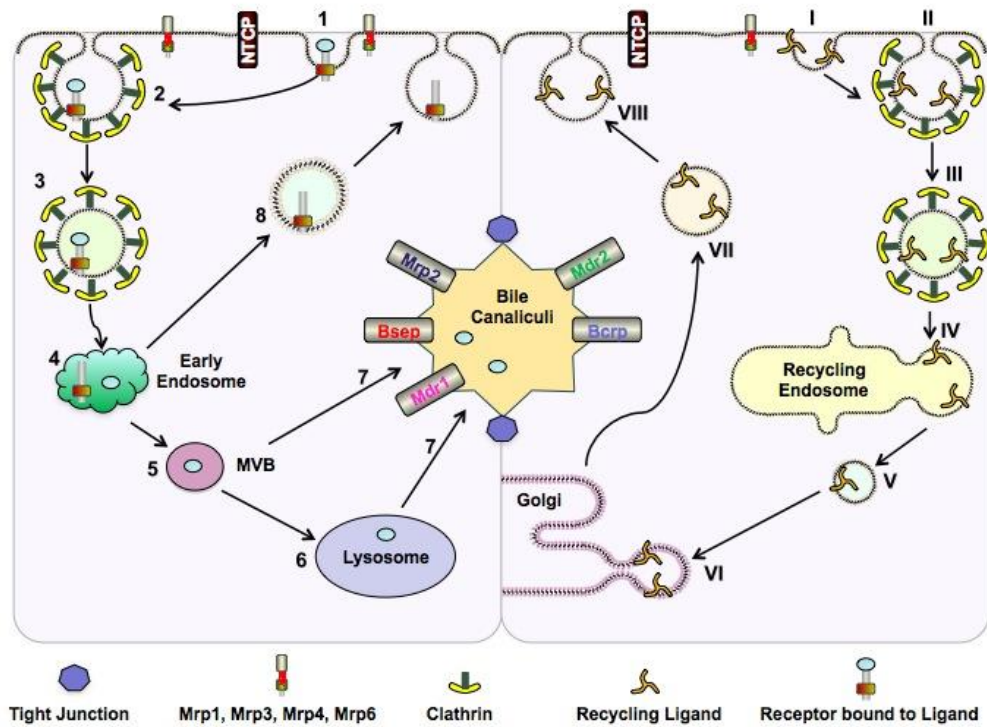


**Figure 5. Endosomal recycling in hepatocytes.** Steps 1, 2, and 3: Receptor mediated endocytosis of receptor bound to ligand. Step 4: Ligand is separated from the receptor in early endosome. 5, 6, and 7: Ligand is either degraded in lysosome or transported into bile canaliculi depending on the final destination of the ligand. Step 8: Receptor is recycled back to the cell surface. Steps I, II, and III: Recycling ligand is endocytosed in clathrin coated vesicles. Steps IV, V, VI, VII, and VIII: The ligand is recycled back to the cell surface.(Source: Adapted from<sup>18</sup>)



## D. MicroRNAs

MicroRNAs (miRNAs) are a class of small non-coding RNAs that are highly conserved<sup>19</sup> and are widely expressed in plants, animals, and some viruses. Mature miRNAs are typically 18-25 nucleotides in length and these regulate gene expression post-transcriptionally<sup>20</sup>. It has been estimated that the human genome encodes over 1,000 miRNAs<sup>21</sup>, which may target about 60% of mammalian genes<sup>22</sup>. Over 1,800 murine mature miRNAs have been identified so far ([www.miRBase.org](http://www.miRBase.org)). miRNAs modulate gene function post-transcriptionally by either specific inhibition of translation or induction of target mRNA cleavage<sup>23</sup>. A single miRNA can target multiple mRNA targets, and each mRNA can be targeted by many miRNAs<sup>20</sup>. This feature allows miRNAs to alter multiple gene expression regulatory networks<sup>20</sup>. Initial studies on miRNA biology indicated that miRNAs regulate their targets mostly at the protein synthesis level and regulate gene expression by mRNA degradation to a lower extent. However, there is increasing evidence that miRNAs target mRNA to a larger extent than initially thought<sup>24</sup>, and most of the miRNA-mediated repression on its targets is caused by mRNA destabilization as opposed to the prior scenario of ‘translational-repression’<sup>24,25</sup>.

*MiRNA processing.* miRNA genes are mostly transcribed by RNA polymerase II, although some are transcribed by RNA polymerase III<sup>26,27</sup>. The primary miRNA transcript (pri-miRNA) is synthesized in the nucleus of cells and is polyadenylated and capped, similar to messenger RNAs<sup>20,28,29</sup>. The pri-miRNA contains regions that are not perfectly complementary, forming a stem-loop structure. In mammals, this pri-miRNA

undergoes further processing by two ribonuclease (RNase) III family members: Drosha and Dicer<sup>28</sup>. The pri-miRNA is cleaved by the complex consisting of Drosha and co-factor DiGeorge syndrome critical region gene 8 (DGCR8), to form precursor miRNA (pre-miRNA)<sup>20,28</sup>. The pre-miRNA, a 60-100 nucleotides long hairpin structure, is then exported from the nucleus into the cytoplasm by the Exportin 5 (XPO5)/Ran-GTP complex<sup>20,28</sup>. In the cytoplasm, Dicer and TAR RNA binding protein (TRBP) then cleave off the loop from the pre-miRNA structure leaving behind an 18-25 nucleotides long dsRNA duplex<sup>20,28</sup>. This duplex is comprised of a guide strand and a passenger strand, each of which has a different purpose in the cell<sup>28</sup>. The guide strand is taken up by Argonaute (AGO) to form the Argonaute-containing miRNA-induced silencing complex (miRISC)<sup>20</sup> while the passenger strand is degraded<sup>28</sup>. miRISC can then bind to the 3' untranslated region (UTR) of target mRNAs by partial base pairing and lead to mRNA degradation or translational repression<sup>20,30-35</sup> (Figure 6).

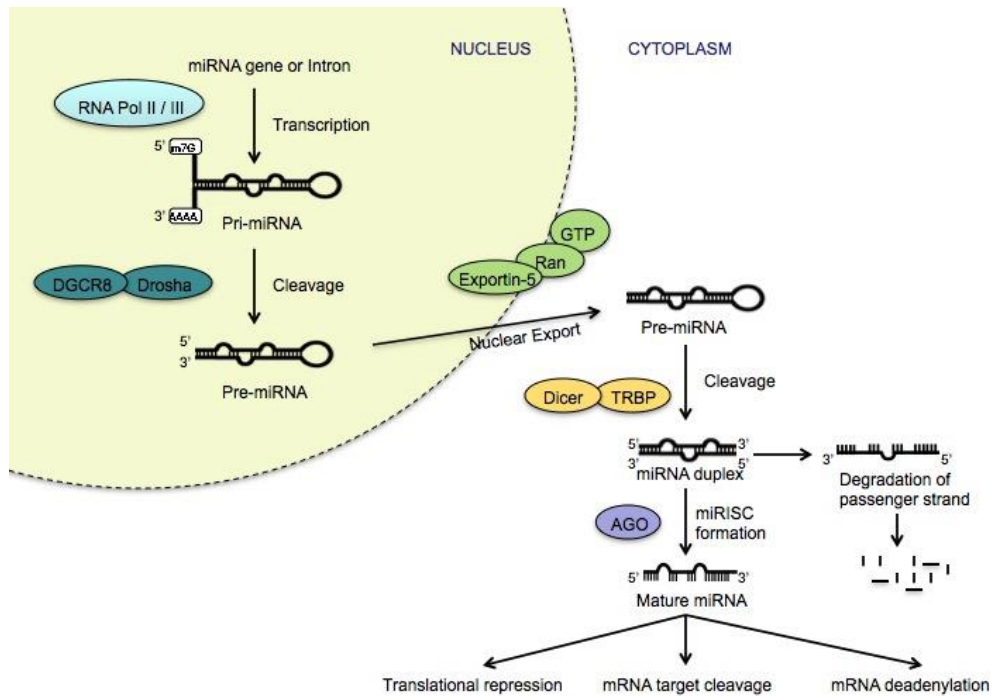


**Figure 6. Processing of miRNA.** The primary miRNA transcript (pri-miRNA) is transcribed by RNA polymerase II or III. The pri-miRNA is then cleaved by the microprocessor complex Drosha – DGCR8 (Pasha) to pre-miRNA in the nucleus. The precursor hairpin, pre-miRNA, is then exported from the nucleus to the cytoplasm by Exportin-5 – Ran-GTP. In the cytoplasm, the RNase Dicer along with the double-stranded RNA-binding protein TRBP cleaves the pre-miRNA hairpin to form a miRNA duplex. The mature strand of the miRNA is then loaded together with Argonaute (Ago) proteins into the RNA-induced silencing complex (RISC), where it guides RISC to silence target mRNAs through mRNA cleavage, translational repression or mRNA deadenylation. The passenger strand from the miRNA duplex is degraded. DGCR8, DiGeorge syndrome critical region gene 8. TRBP, TAR RNA binding protein (Source: Adapted from<sup>36</sup>).

*Repression of gene expression.* The nucleotides in positions 2-8 from the 5' end of the guide strand represent the 'seed' region<sup>20,37</sup> (Figure 7). It is an important feature in miRNA target recognition and mutations in the seed region lead to changes in target specificity and/or disease<sup>38-40</sup>. In plants, perfect pairing of a miRNA with its target mRNA leads to recruitment of deadenylation factors to remove the poly(A) tail of the target mRNA and endonucleolytic cleavage of the mRNA<sup>20,28,41,42</sup>. In mammals, the miRISC mostly induces gene silencing by imperfect matching of nucleotides between the miRNA and its target RNAs, leading to repression of protein synthesis and/or mRNA degradation through deadenylation and decapping<sup>28</sup>. Translational repression occurs through interference with factors required for translation such as eukaryotic translation-initiation factor 4G (eIF4G) and poly(A)-binding protein (PABPC)<sup>43</sup>. After extensive speculation about the stage at which translational repression occurs (initiation versus post-initiation stage), recent data has proved that repression occurs predominantly during initiation of translation<sup>43</sup>. Deadenylation of mRNAs involves the CAF1-CCR4-NOT deadenylase complex, and mRNA-decapping enzyme 2 (DCP2), a decapping enzyme decaps the target mRNA, resulting in mRNA degradation by exoribonuclease 1 (XRN1), the major 5'-to-3' exonuclease in cultured cells<sup>43</sup>. However, this is not true in cellular extracts. In cell extracts, deadenylated mRNAs are thought to remain undegraded in a deadenylated, translationally repressed state<sup>43</sup>. Irrespective of the mode of action of the miRNA, the miRISC complexes along with the bound target mRNAs are found enriched in processing bodies (P-bodies or GW-bodies), cytoplasmic structures containing mRNA degrading enzymes and are implicated in the storage and degradation of the target mRNAs<sup>23</sup>.

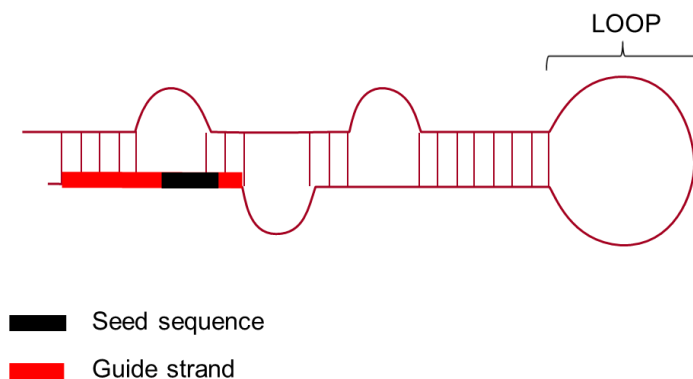


**Figure 7. Structural components of a pre-miRNA.** The pre-miRNA is composed of a stem-loop structure comprising the guide strand, passenger strand, additional sequences, and the loop. The guide strand is shown in red and the seed sequence is highlighted in black.

Gene regulation by miRNAs is also controlled by RNA binding proteins. RNA binding proteins interacting with the 3' UTR of miRNA target mRNAs can reverse or augment the inhibition by certain miRNAs<sup>23</sup>. Under stress conditions, inhibition of CAT-1 mRNA by miR-122 is relieved by the protein HuR, which translocates from the nucleus to the cytoplasm and binds to the 3' UTR of the CAT-1 mRNA, causing the CAT-1 mRNA to leave the P-body and bind to polysomes<sup>23,44</sup>.

Several groups have recently reported that miRNAs can also activate gene expression of its targets, in addition to inhibit expression<sup>23</sup>. One example is miR-122, which has been shown to upregulate the levels of Hepatitis C Virus (HCV) RNA through binding to its 5' UTR<sup>23</sup>. Also, miR-10a has been shown to increase translation of mRNAs

with 5' TOP motifs by binding to the 5' UTR downstream of the 5' TOP motif<sup>23,45</sup>. Recent data shows that translational activation by miRNAs may be mediated through AGO2-containing complexes under serum starvation conditions and during cell cycle arrest<sup>45</sup>.

## **E. Role of miRNAs in liver**

Given that miRNAs are largely transcribed by RNA polymerase II, their expression is subject to transcriptional regulation in a similar manner to protein-encoding genes. Thus, the metabolic state of a cell can influence the expression of a single or multiple miRNAs, and miRNA expression profiles have been found to be altered in various metabolic disorders such as diabetes and obesity<sup>28</sup>. In a study comparing miRNA expression profiles between skeletal muscle of normal and diabetic rats, 4 miRNAs were found up-regulated and 11 miRNAs were found down-regulated<sup>46</sup>. This may suggest that miRNAs play a key role in metabolism and can in fact be potential diagnostic and prognostic markers<sup>28,47</sup>.

Dicer1, the only RNase III family member in mammals for processing dsRNA into both miRNAs and siRNAs<sup>48</sup>, is critical for miRNA maturation from early postnatal liver, and its deletion results in profound hepatocyte apoptosis, steatosis and mild hypoglycemia<sup>37</sup>. This implies that miRNAs have critical roles in normal liver development and physiology. It is now widely accepted that miRNAs have important regulatory roles in various cellular processes. Recent work has implicated miRNAs in pancreas development and insulin secretion<sup>49</sup>, as well as insulin sensitivity in liver<sup>50</sup>. It has also been shown that miRNAs play a role in various hepatic metabolic functions such as fatty acid and cholesterol metabolism, insulin signaling and glucose metabolism.

**miRNA-10b** (miR-10b) was identified in L02 cells, a human model of hepatic steatosis<sup>28,51</sup>. Overexpression of miR-10b resulted in triglyceride and lipid accumulation

in these cells by directly targeting peroxisome proliferator-activated receptor- $\alpha$  (PPAR- $\alpha$ ), a nuclear receptor involved in lipid metabolism<sup>28,51</sup>. This study provided a novel mechanism by which miR-10b regulated hepatic steatosis in the context of non-alcoholic fatty liver disease (NAFLD).

**miRNA-122** (miR-122) is the most abundant liver-specific miRNA and has been implicated in various metabolic processes important for hepatic function and liver pathology<sup>52</sup>. miR-122 is almost solely expressed in hepatocytes<sup>53</sup> and represents roughly 70% of the total miRNAs expressed in the adult liver<sup>54</sup>. miR-122 is expressed in mouse and human livers, primary hepatocytes and liver-derived cell lines such as Hepa1-6 and Huh7 cells<sup>54</sup>. miR-122 has been shown to bind to the 3' UTR of cationic amino acid transporter-1 (CAT-1) mRNA<sup>44,54,55</sup>. miR-122 has been shown to play roles in fatty acid metabolism and cholesterol metabolism<sup>52</sup> through downregulation of 1-Acylglycerol-3-Phosphate O-Acyltransferase 1 (AGPAT1) and Cell Death-Inducing DFFA-Like Effector C (CIDEC). Silencing miR-122 in mice fed a high-fat diet resulted in a significant reduction of hepatic steatosis<sup>56</sup>. This was also seen with a notable decrease in serum cholesterol levels<sup>54,56</sup>.

miR-122 has also been involved in the pathophysiology of hepatocellular carcinoma (HCC). It acts as a tumor suppressor and is downregulated in 70% of HCC cases<sup>57</sup>. This is mediated by upregulation of miR-122 targets such as Cut-like homeobox 1 (CUTL1), A disintegrin and metalloprotease family 17 (ADAM17) and cyclin G1<sup>57</sup>. Other targets of miR-122 involved in hepatocarcinogenesis that have been recently found



are: A disintegrin and metalloprotease family 10 (ADAM10)<sup>52</sup>, insulin-like growth factor 1 receptor (IGF1R)<sup>52</sup>, N-Myc Downstream-Regulated Gene 3 (NDRG3)<sup>58</sup> and Microtubule-Associated Protein, RP/EB Family, Member 1 (MAPRE1)<sup>59</sup>. Overall, this suggests that miR-122 and its targets have an integral role in liver development and function<sup>52</sup> (Figure 8).

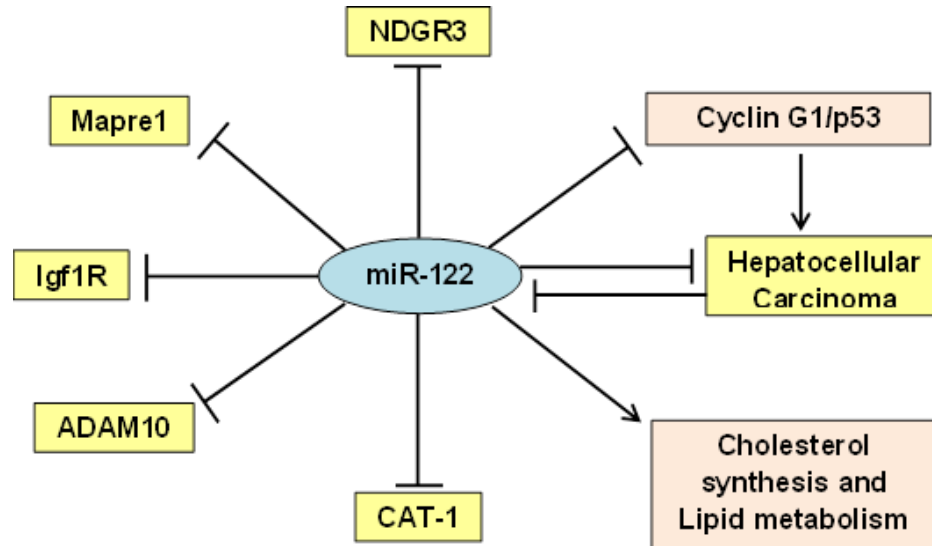


**Figure 8. Role of miR-122 in liver<sup>52</sup>.** The figure illustrates the role of miR-122 in the liver. miR-122 inhibits expression of CAT-1, ADAM10, Igf1R, Mapre1, NDGR3 and is found downregulated in hepatocellular carcinoma. miR-122 prevents hepatocellular carcinoma through inhibiting cyclin G1 and preventing the association of cyclin G1 with p53. miR-122 has also been shown to play a role in cholesterol and lipid metabolism.

**miRNA-216** (miR-216) and **miRNA-302a** (miR-302a) were found downregulated in livers of hypercholesterolemic low-density lipoprotein receptor (LDLR) knockout mice that were fed a high-fat diet compared to those that were fed a chow diet<sup>28,60</sup>. Also, this study found an inverse correlation between the levels of miR-

302a and its target genes ABCA1 transporter and ELOVL fatty acid elongase 6 (ELOVL6), a microsomal enzyme involved in the formation of long-chain FA<sup>28,60</sup>. This suggests a role for miR-302a in fatty acid, cholesterol and glucose metabolism<sup>60</sup>.

**miRNA-33a/b** (miR-33a/b) are the best example of intronic miRNAs that work together with their host genes to regulate cholesterol and fatty acid metabolism. miR-33a is co-transcribed with sterol-regulatory element binding protein 2 (SREBP-2) gene<sup>61</sup>, a transcription factor important in *de novo* cholesterol synthesis and uptake<sup>62</sup>, while miR-33b is co-transcribed with sterol-regulatory element binding protein 1 (SREBP-1), a transcription factor involved in fatty acid synthesis<sup>61,63,64</sup>. *In vivo* studies in mice and non-human primates have both shown that inhibition of miR-33a/b using different approaches resulted in increased hepatic expression of miR-33 target gene, adenosine triphosphate-binding cassette (ABC) transporter member 1 (ABCA1), a transporter that reduces cholesterol efflux to high-density lipoprotein (HDL)<sup>65,66</sup>. This increase in expression of ABCA1 resulted in elevated HDL levels in mouse and non-human primate animal models<sup>65,66</sup>. Other cholesterol metabolism genes targeted by miR-33a are ATP-binding cassette sub-family G member 1 (ABCG1) and Niemann-Pick disease, type C1 (NPC1)<sup>67</sup>. miR-33b has been shown to target genes involved in fatty acid metabolism such as carnitine palmitoyltransferase 1a (CPT1a), carnitine O-octaniltransferase (CROT), hydroxyacyl-CoA-dehydrogenase (HADHB), AMP kinase subunit- $\alpha$  (AMPK1 $\alpha$ ) and reduce fatty acid oxidation<sup>67</sup>.

In addition, miR-33 has also been shown to have a negative role in regulating insulin signaling by acting on insulin receptor substrate-2 (IRS-2) and reducing downstream signaling<sup>28,67</sup> in human hepatocellular carcinoma cell lines HepG2 and Huh7.

**miRNA-34a** (miR-34a) was found upregulated in livers of patients with nonalcoholic steatohepatitis (NASH)<sup>28,68</sup>. miR-34a directly inhibits sirtuin 1 (SIRT)-1, leading to downstream activation of HMGCoA reductase (HMGCR) which, in turn results in elevated levels of cholesterol in these patients<sup>28,69</sup>.

**miRNA-335** (miR-335) was found upregulated in livers and white adipose tissues (WAT) of three animal models of obesity – db/db, ob/ob and KKAY mice<sup>70</sup>. This was associated with elevated hepatic triglyceride and cholesterol levels suggesting that miR-335 may represent a biomarker for hepatic lipid accumulation in mice<sup>47,70</sup>.

**miRNA-370** (miR-370) has been shown to be a potent regulator of lipid metabolism in HepG2 cells<sup>71</sup>. miR-370 regulates genes involved in fatty acid and triglyceride synthesis such as transcription factor sterol-regulatory element binding protein 1c (SREBP-1c), diacylglycerol acyltransferase-2 (DGAT2), fatty acid synthase (FAS), and acyl-CoA carboxylase 1 (ACC1) through upregulating miR-122<sup>28,71</sup>. miR-370 directly targets the 3' UTR of carnitine palmitoyl transferase 1a (Cpt1a), a mitochondrial enzyme involved in shuttling fatty acids into mitochondria for  $\beta$ -oxidation<sup>28,71</sup>. This implies that miR-370 may be implicated in the accumulation of triglycerides in the liver by increasing

the expression of miR-122 (thereby increasing *de novo* lipogenesis) and by reducing  $\beta$ -oxidation<sup>71</sup>.

**miRNA-467b** (miR-467b) was shown to be downregulated in livers of mice fed a high-fat diet and in steatotic hepatocytes<sup>72</sup>. miR-467b was found to regulate the expression of hepatic lipoprotein lipase (LPL), an enzyme that hydrolyzes triglycerides<sup>28,72</sup>. This interaction between miR-467b and LPL has been associated with insulin resistance and plays an important role in the spectrum of NAFLD.

In addition to miR-122 (see page 18), other miRNAs have been consistently found downregulated in hepatocellular carcinoma (HCC). MicroRNAs miR-199a-1, miR-199a-2 and miR-199b have been shown to be downregulated in HCC, which results in upregulation of targets such as MET (Met Proto-Oncogene), mTOR (Mammalian Target Of Rapamycin), CD44 (CD44 Molecule) and HIF-1 $\alpha$  (Hypoxia Inducible Factor 1, Alpha Subunit)<sup>57</sup>. This causes HCC to be highly proliferative, invasive and resistant to radiation. On the other hand, miR-221 is upregulated in HCC and results in downregulation of genes involved in cell cycle inhibition, negative regulation of the mTOR pathway, pro-apoptosis, as well as inhibition of metalloproteases<sup>57</sup>.

Overall, these studies highlight the possibility that pharmacological inhibition of miRNAs may become a therapeutic strategy for the treatment of hepatic diseases. Identification of miRNA targets therefore becomes an important aspect of developing new miRNA-based therapeutic products. Despite the emerging role of miRNAs at

controlling genes important in liver metabolism, the mechanisms by which miRNA regulate physiological responses is still poorly understood.

## **F. Thesis hypothesis and research aims**

The liver is an important organ regulating many metabolic processes and is responsible for various critical functions in the body. In recent years, differential expression of miRNAs has been observed in many disease states. Thus, the development of molecules to inhibit miRNAs that are found upregulated in particular diseases can be exploited for therapeutic purposes. Likewise, targeting deleterious genes with miRNAs represents an attractive therapeutic strategy. Thus, understanding the mechanisms by which miRNAs govern hepatic functions is key for developing novel therapeutic agents. I proposed to identify miRNAs differentially expressed in murine liver under pathological or nutritionally distinct conditions, to understand the role of miRNA in the pathophysiology of type 2 diabetes, and on vital hepatic functions. My central hypothesis was that miRNA that are dysregulated may affect expression of target genes, and contribute to the development of that disorder. Using primary hepatocytes as a cellular model, my central hypothesis was tested by pursuing the following specific aims: (i) To identify miRNAs dysregulated in livers of an animal model of type 2 diabetes, and in the transition from the fasted to refeed state; (ii) To identify gene targets of *mmu-miR-709* (miR-709); (iii) To determine the biological role of miR-709 in murine liver.

**Specific Aim 1: To identify miRNAs dysregulated in livers of an animal model of type 2 diabetes, and in the transition from the fasted to refeed state.**

The working hypothesis for Aim 1 was that expression of hepatic miRNAs are altered in metabolic disorders such as diabetes. Also, miRNAs are largely transcribed by RNA polymerase II and therefore, may be transcriptionally regulated like protein-encoding

genes. Identifying these miRNA and understanding their function in the liver will help understand the mechanisms that lead to hepatic disorders and developing novel therapies. This hypothesis was tested by conducting miRNA microarrays on liver tissues from normal and db/db mice, and from fasted and refed animals.

**Specific Aim 2: To identify gene targets of miR-709.** The working hypothesis for Aim 2 was that mRNAs directly regulated by a miRNA should be downregulated upon transient transfection of miRNA mimics. I checked mRNA profiles of primary hepatocytes transfected with miR-709 and confirmed the expression of its targets at protein level. Identifying the targets of miR-709 enabled the characterization of the pathways regulated by miR-709 in the murine liver.

**Specific Aim 3: To determine the biological role of miR-709 in murine liver.** The abundance of miR-709 in murine liver, its predicted and confirmed targets, suggested an important role for miR-709 in cell proliferation. This hypothesis was tested by analyzing miR-709 in animal models of liver regeneration and liver cancer and by studying the impact of depleting miR-709 during cell division.

## MATERIALS AND METHODS

### A. MATERIALS

**A.1. Plasmids.** psiCHECK<sup>TM</sup>-2 Luciferase vector (Promega, Madison, WI) was used to generate p.miR-709-3p, p.miR-709-5p, p.Rab11b, p.Ces1g, p.Pctp, p.NC-Rab11b, p.NC-Ces1g and p.NC-Pctp constructs. pBluescript II SK(+) vector (Stratagene, CA, USA) was used to generate plasmid p.pri-Cel-239b.

### A.2. Primers

**Table 1. Oligonucleotides used to generate luciferase constructs and primers used for qRT-PCR (5' → 3').**

Oligonucleotides	
<b>Pctp</b>	TATGCACTCGAGCATCTGGATTTTTTCCTTTCCC ATCAGGCGGCCGCGGTGGTACACGCCTTTAATC
<b>NC- Pctp</b>	TATGCACTCGAGTCAGGCTTCAAAGATGGCTTG AATCAGGCGGCCGCCTGAGTTCGAGGCTAACCTG
<b>Ces1g</b>	TATGCACTCGAGTCAATCGTCTGACACCAGTG AATCAGGCGGCCGCTTCTAAGGGAATGTATTTGTGA T
<b>NC-Ces1g</b>	TATGCACTCGAGGAGCCAAGGAAACAGCAGAG ATCAGGCGGCCGCTCCAGGAAAGCCAGGACTAC
<b>Rab11b</b>	ATGCACTCGAGCAGGGTTTCTCTGTGTAGC TCAGGCGGCCGCGAGGGGCAAGGGTGTCTT
<b>NC-Rab11b</b>	ATGCACTCGAGCCAGGAAGAGCAGGAGTCC ATCAGGCGGCCGCGAGTTTGGGATGAGGATACAG
<b>Cel-239b primary transcript</b>	CCAGTGTCCCACAGAGTAATTAGTGTGTAGCGACTA AACACATCAACTCAGAAGTGCTCTA AGCTTAGAACTGTCCAGTTTGAGCAGCACTGGTTGA TGTGTTTAGTCGCTATTGTCTTTTGTATATTGACTT ATGCTGCA
Primers used for qRT-PCR	
<b>CD36</b>	GGCAAAGAACAGCAGCAAATC TGAAGGCTCAAAGATGGCTCC
<b>Gck</b>	CACTGCGGAGATGCTCTTTGAC CCACGATGTTGTTCCCTTCTGC
<b>Acox2</b>	GAATAACAGTTGGGGACATAGG



<b>Pfkl</b>	CTGGAGGGTGGGTAGGAATC GCAAGGTATGAATGCTGCTGTC
<b>Pctp</b>	TGGAAACGCTGAGCCAGTTGG CAAGAAGGGGAGCAGAGAATGG
<b>Rab11b</b>	TGGTGTAGCACAGCCAGAGATG CAAAGTGGTGCTTATTGGGGAC
<b>Ces1g</b>	CTGAGCCTTGATGGTCTTGCC TGTA AAACCACCACCTCCGCTG
<b>TBP</b>	TCTCTGGGGTCTCCAAGAAAATC TATCACTCCTGCCACACCAG CATGATGACTGCAGCAAATCG

**A.3. Mice.** Animals were purchased from The Jackson Laboratory (Bar Harbor, ME). Animal studies were performed in compliance with Indiana University School of Medicine Institutional Animal Care and Use Committee guidelines.

**A.3.1. Liver miRNA analysis:** Four 12-week old, male C57BLKS/J and *db/db* mice (an obese animal model of type 2 diabetes lacking a functional leptin receptor), were used to study hepatic miRNA expression profiles under fed conditions (see section B.6.a).

**A.3.2. Primary hepatocyte isolation:** Male C57BL/6J mice (11 to 12 weeks old, 24 to 30g) were used for isolation of primary hepatocytes. Mice were fed rodent chow *ad libitum* and allowed free access of water. A standard 12 h light/12 h dark cycle (7 AM/7 PM) was maintained throughout the experiments. Mice were allowed to acclimate for at least a week before experimentation.

**A.3.3. miRNA profiles under fed, fasted, refed conditions:** Fifteen 14-week old, male C57BL/6J mice were used for studying the expression of miRNAs under different nutritional status (see section B.6.b).

**A.3.4. Relative expression of pre-miR-709 vs mature miR-709:** Livers from normal LapMyc mice (5 male and 2 female) and tumor LapMyc mice (5 male) were obtained from Dr. Janaiah Kota (Department of Medical and Molecular Genetics, Indiana

University School of Medicine)<sup>59</sup>. Livers from normal C57BL/6 male mice before hepatectomy, and 24, 36 and 44 hours post-hepatectomy (3 animals per group) were provided by Dr. Guoli Dai (Department of Biology, Purdue University School of Science)<sup>73</sup>.

#### A.4. Antibodies

<b>Table 2. Antibodies used for Western blotting.</b>		
<b>Antibody</b>	<b>Manufacturer</b>	<b>Dilution factor</b>
Rab11b	Cell Signaling, Boston, MA	1:1,000
DYNC1LI1	GeneTex, San Antonio, TX	1:1,000
Glucokinase (N-term)	Abgent, San Diego, CA	1:500
Insulin receptor- $\alpha$	Santa Cruz Biotechnology, Dallas, TX	1:500
LDLR	Abcam, Cambridge, MA	1:3000
FATP1	Santa Cruz Biotechnology, Dallas, TX	1:500
Timp3	Santa Cruz Biotechnology, Dallas, TX	1:1000
Cyclophilin 40	Abcam, Cambridge, MA	1:1000
Tubulin- $\alpha$ Ab-2 (Clone DM1A)	Thermo Scientific, Rockford, IL	1:10,000
$\beta$ -actin (C4)	Santa Cruz Biotechnology, Dallas, TX	1:500
Anti-rabbit IgG, HRP-linked	Cell Signaling, Boston, MA	1:3,000 - 1:5,000

#### A.5. Other reagents

**A.5.a. Plasmid isolation.** Plasmid mini kit (Qiagen, Valencia, CA) and plasmid maxi kit (Qiagen, Valencia, CA) was used for small scale (~3 ml LB broth) and large scale (~200 ml LB broth) plasmid isolation, respectively.

**A.5.b. RNA isolation.** Total RNA Isolation from cells and tissues for RT-PCR: RNAeasy mini/midi kit (Qiagen, Valencia, CA), RNase free-DNase I (Qiagen,

Valencia, CA) and  $\beta$ -mercaptoethanol were used to isolate total RNA. Total RNA Isolation from cells and tissues for Taqman miRNA assay and Northern blot of miRNAs: the long (>200 bp) and miRNA-enriched (<200 bp) RNA fractions were isolated using mirVana<sup>TM</sup> miRNA Isolation kit (Ambion, Life Technologies, Grand Island, NY).

**A.5.c. Protein isolation.** RIPA buffer (25 mM Tris•HCl pH 7.6, 150 mM NaCl, 1% NP-40, 1% sodium deoxycholate, 0.1% SDS; Thermo Scientific, Rockford, IL) containing protease and phosphatase inhibitors (Roche, Indianapolis, IN) was used to lyse cells and isolate proteins.

**A.5.d. DNA gel extraction.** QIAEX II Gel Extraction Kit (Qiagen, Valencia, CA) was used to isolate PCR product fragments from agarose gels.

**A.5.e. Ligation.** T4 DNA ligase (New England Biolabs, Ipswich, MA) was used to ligate PCR products into psiCHECK<sup>TM</sup>-2 Luciferase vector according to manufacturer's instructions.

**A.5.f. PCR.** High Capacity cDNA reverse transcription kit (Applied Biosystems, Life Technologies, Grand Island, NY) was used to generate cDNA from mouse liver.

**A.5.g. qRT-PCR.** QuantiTect SYBR Green RT-PCR kit (Qiagen, Valencia, CA) was used, following the manufacturer's recommendations. Reactions were set up in 96-well Optical reaction plates covered with optical caps (Applied Biosystem, Foster City, CA). Real time PCR was performed using an ABI Prism 7500 instrument (Applied Biosystem, Foster City, CA).

**A.5.h. TaqMan miRNA assay.** TaqMan miRNA Reverse Transcription Kit (Applied Biosystems, Foster City, CA) was used to generate cDNA, followed by PCR with TaqMan miRNA Assays (Applied Biosystems) specific for miR-709 and sno-202.

**A.5.i. Protein quantification.** Pierce® BCA Protein Assay Kit (Thermo Scientific, Hanover Park, IL) was used to quantify proteins.

**A.5.j. Western Blot detection.** Pierce® ECL Western Blotting Substrate (Thermo Scientific, Hanover Park, IL) was used to detect proteins.

**A.5.k. LDH assay.** Cytotoxicity LDH Detection Kit (Clontech, Mountain View, CA) was used for detection of lactate dehydrogenase (LDH).

**A.5.l. Transfection.** METAFECTENE® PRO (Biontex, Germany) was used as transfection reagent at lipid:DNA ratios described in the cell transfection section.

**A.5.m. LB broth.** Luria-Bertani (LB) broth (Sigma, St. Louis, MO) was used to grow *E. coli* (*Escherichia coli*) bacteria.

**A.5.n. Bacteria for subcloning.** XL1-Blue Subcloning grade competent cells (Agilent, Santa Clara, CA) were used for transformation of plasmids.

**A.5.o. Cell lines.** The mouse hepatoma cell line Hepa-1c1c7 and human embryonic kidney cell line HEK293 were obtained from American Type Culture Collection (ATCC).

## B. METHODS

**B.1. Plasmid cloning.** p.miR-709-3p and p.miR-709-5p constructs were generated by cloning an oligonucleotide with a sequence perfectly complementary to either the 3' or the 5' strand of miR-709 (based on the sequence published in TargetScan), downstream of the renilla luciferase gene in plasmid psiCHECK<sup>TM</sup>-2 Luciferase vector (Promega, Madison, WI) (Figure 9). Oligonucleotides (Invitrogen, Life Technologies, Grand Island, NY) were inserted into the NotI – XhoI site using Quick ligation kit (New England Biolabs, Ipswich, MA). These plasmids were used to determine whether the 3' or 5' strand is the guide strand of miR-709.

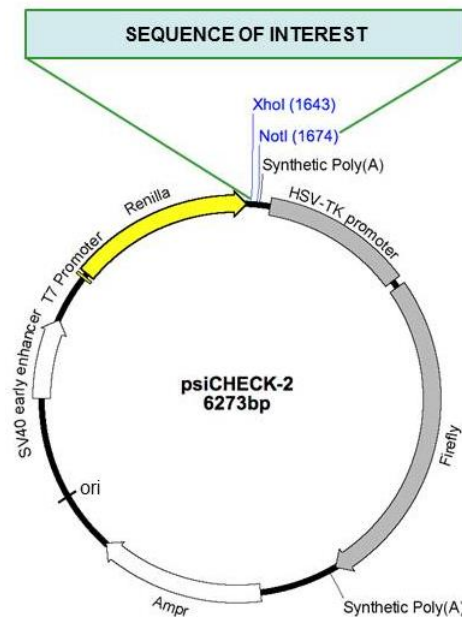


**Figure 9. Schematic representation of the psiCHECK<sup>TM</sup>-2 plasmid used for generating constructs for luciferase reporter assays.** All sequences were cloned using Not I and Xho I sites into the 3' UTR of the Renilla luciferase cDNA.

Tough decoys (TuDs) to reduce cellular levels of miR-709 and miR-122, were generated by cloning 8 copies of the sequence complementary to the 3p strand of miR-709 or the 5p strand of miR-122, downstream from the luciferase gene in psiCHECK<sup>TM</sup>-2. The sequence inserted was chemically synthesized (GenScript, NJ, and Genewiz, NJ) with XhoI and NotI sites at the ends to facilitate cloning.

To confirm that Rab11b, Ces1g and Pctp are direct targets of miR-709, 220-720 base-pair (bp) fragments of the 3' UTR containing the putative binding sites (microrna.org<sup>74</sup>), were cloned in the NotI – XhoI site of psiCHECK<sup>TM</sup>-2 vector. Total mRNA from mouse liver was used to generate the cDNA (High Capacity cDNA reverse transcription kit, Applied Biosystems, Life Technologies, Grand Island, NY) and the corresponding portion of the 3' UTR of Rab11b, Ces1g and Pctp was amplified by PCR using primers with restriction sites for NotI – XhoI (Table 1). The PCR products were digested with XhoI and NotI, gel purified with QIAEX II Gel Extraction Kit (Qiagen, Valencia, CA) and cloned into psiCHECK<sup>TM</sup>-2, generating plasmids p.Rab11b, p.Ces1g and p.Pctp. In addition, a portion of the 3' UTR of these mRNAs without miR-709 binding sites was cloned into psiCHECK<sup>TM</sup>-2 and used as negative controls (p.NC-Rab11b, p.NC-Ces1g and p.NC-Pctp). Clones were sequenced prior to using them in luciferase assays.

A plasmid expressing the primary transcript of miR-709 (p.pri-miR-709) was purchased from OriGene (Rockville, MD, USA). p.pri-miR-709 is composed of pre-miR-709 (88 nt) and 250-300 nt flanking genomic sequence (Figure 10A). The flanking

sequence is required for correct pri-miR expression and processing by the microprocessor complex (Drosha). As control, p.pri-Cel-239b was cloned into pBluescript II SK(+) vector (Stratagene, CA, USA) in 4 steps (Figure 10B). The promoter, polyA signal and 300 bp flanker regions were obtained by PCR amplification from the p.pri-miR-709 plasmid and thus, have the same sequence. The pre-Cel-239b sequence was chemically synthesized as 4 oligonucleotides that anneal to form the appropriate restriction enzyme sites on either end. All clones were sequenced prior to using them in experiments.

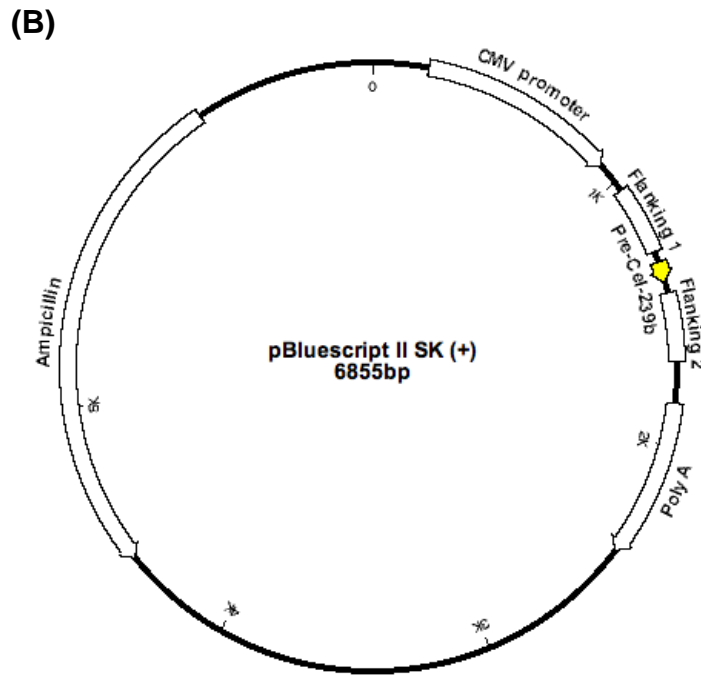
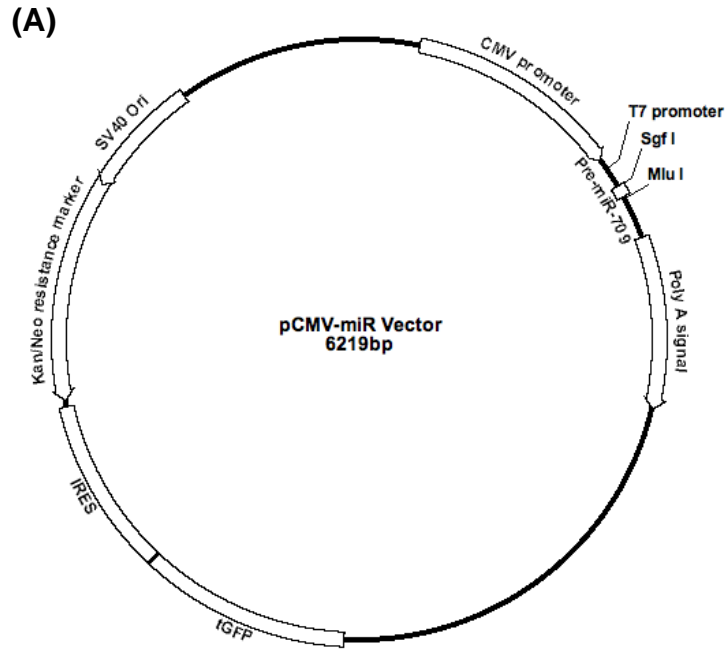


**Figure 10. Schematic representation of plasmids expressing pri-miR-709 and pri-Cel-239b.** (A) Plasmid expressing pri-miR-709 (OriGene). (B) Plasmid expressing pri-Cel-239b miRNA was generated as described in the text.



**B.2. Primary hepatocyte isolation.** Primary hepatocytes were isolated using a two-step collagenase procedure, as previously described<sup>75</sup>. Briefly, mice were anesthetized with pentobarbital (90 mg/kg body weight i.p.) and the liver was perfused with Ca<sup>2+</sup> and Mg<sup>2+</sup> free Hank's Balanced Salt solution (HBSS) containing 5 mM ethylene glycol tetraacetic acid (EGTA) and 0.05 M HEPES. This was followed by perfusion with 0.075% collagenase solution in DMEM. After perfusion, the liver was cut out and liver cells were dispersed in 15 ml collagenase solution using forceps. Cells were filtered through a 70- $\mu$ m nylon mesh and centrifuged at 100xg for 5 min to pellet hepatocytes. The cell pellet was washed in 20 ml DMEM with 10% FBS and centrifuged again. To enrich for live cells, the cell pellet was resuspended in 25 ml DMEM (without FBS) plus 24 ml 90% Percoll solution<sup>76</sup>. Cell viability was assessed by trypan blue staining exclusion (>80% viability). Cells were seeded at a density of 4-6x10<sup>5</sup> cells per well or 35-mm dish in 2 ml DMEM supplemented with 10% (v/v) fetal bovine serum (FBS), 100 I.U./ml penicillin, 100  $\mu$ g/ml streptomycin, 3 nM insulin and 1 nM dexamethasone. Cells were incubated at 37°C, 5% CO<sub>2</sub> in a humidified incubator and allowed to attach for 4 hours. Media was then replaced with fresh media.

**B.2.a. Primary hepatocyte sandwich<sup>77</sup> experiments.** For primary hepatocyte sandwich experiments, 6x10<sup>5</sup> cells were plated on collagen-coated glass-bottom 35-mm dishes (MatTek, Ashland, MA). Media was replaced 4 hours post-plating and cells were transfected with 34 nM of miR-709 or the control miRNA Cel-239b (Dharmacon, Pittsburgh, PA). The next day, primary hepatocytes were overlaid with BD Matrigel<sup>TM</sup> (BD Biosciences, San Jose, CA) at a final concentration of 0.25 mg/ml in cold DMEM

supplemented with 10% (v/v) fetal bovine serum, 100 I.U./ml penicillin, 100 µg/ml streptomycin and 100 nM dexamethasone. Cells were cultured for 3-5 days to allow the formation of bile canalicular networks between cells. Media was replaced every day.

**B.2.b. Sodium fluorescein assay.** Four hours after plating, mouse primary hepatocytes were transfected with 34 nM miR-709 or Cel-239b (Dharmacon, Lafayette, CO), siRab11b-1 and siRab11b-2, or siNC (Invitrogen, Life Technologies). Cells treated with siRab11b-1 and siRab11b-2 received equimolar concentrations of siRab11b-1 and siRab11b-2 for a final concentration of 30 nM. Next morning, media was aspirated and 2 ml of 0.25 mg/ml Matrigel<sup>TM</sup> (BD Biosciences, San Jose, CA, USA) in DMEM supplemented with 10% FBS, 100 I.U./ml penicillin, 100 µg/ml streptomycin and 100 nM dexamethasone was added to all wells. Twenty-four hours later, media was replaced. Seventy-two hours post-transfection, cells were washed twice with media I (150 mM NaCl, 20 mM HEPES, 1 mM CaCl<sub>2</sub>, 5 mM KCl, 1 mM MgCl<sub>2</sub>, and 10 mM glucose) and sodium fluorescein was added at 4 µM in media I. Cells were then incubated at 37°C in incubator for 10 min. The cells were washed twice with media I and 2 ml of DMEM supplemented 10% FBS, 100 I.U./ml penicillin, 100 µg/ml streptomycin and 100 nM dexamethasone, was added. Cells were again incubated for 10 min at 37°C in a CO<sub>2</sub> incubator. Images were taken at specified time points.

**B.2.c. Imaging of labeled miR-709 in primary hepatocytes.** For imaging experiments,  $6 \times 10^5$  cells were plated on collagen-coated glass-bottom 35-mm dishes (MatTek, Ashland, MA). Media was replaced 4 hours post-plating. Next day, cells were transfected

with 34 nM of 3' FAM labeled miR-709 or the control miRNA Cel-67 labeled with Dy547 (Dharmacon, Pittsburgh, PA). Twenty-four hours later, media was replaced and 4 drops of Hoechst 33342 (NucBlue® Live ReadyProbes® Reagent; Molecular probes) was added to each well and incubated at 37°C in a 5% CO<sub>2</sub> incubator for 20 mins. Samples were then imaged by confocal fluorescence microscopy on an inverted microscope fitted with an FV1000 MPE using a 60x 1.2 NA water immersion objective lens (Olympus). Imaging was performed sequentially with excitation provided by solid state lasers at 405 and 559 nm and an Argon-ion laser at 488 nm; emission was collected with spectral filtration from 425-475 nm, 500-545 nm or filter based from 575-675 nm, respectively. Confocal slices were taken at 0.49 micron intervals with voxel dimensions of 0.265 x 0.265 microns. All post-acquisition analysis was performed in Fiji v1.48p<sup>78</sup> and figure generation was performed in Photoshop (Adobe).

**B.3. Cell culture.** Mouse hepatoma Hepa1c1c7 cells were cultured in MEM- $\alpha$  supplemented with 10% FBS and 100 I.U./ml penicillin, 100  $\mu$ g/ml streptomycin and were plated in 6-well plates at a cell density of  $1.5 \times 10^5$  cells/well in 2 ml media.

Human embryonic kidney HEK293 cells were cultured in MEM- $\alpha$  supplemented with 10% FBS and 100 I.U./ml penicillin, 100  $\mu$ g/ml streptomycin and were plated in 6-well plates at a cell density of  $6 \times 10^5$  cells/well in 2 ml media.

**B.3.a. Imaging of labeled miR-709 in Hepa1c1c cells.** For imaging experiments,  $4 \times 10^5$  cells were plated on collagen-coated glass-bottom 35-mm dishes (MatTek, Ashland, MA). Media was replaced 5 hours post-plating and cells were transfected with 34 nM of

miR-709 or the control miRNA Cel-67 (Dharmacon, Pittsburgh, PA). Next day, media was replaced and samples were imaged by confocal fluorescence microscopy on an inverted Olympus microscope fitted with an FV1000 MPE using a 60 x 1.2 NA water immersion objective lens (Olympus). A second set of samples was imaged 24 hours after culturing them in media without FBS and glucose (metabolic stress conditions). Imaging was performed sequentially with excitation provided by solid state lasers at 405 and 559 nm and an Argon-ion laser at 488 nm; emission was collected with spectral filtration from 425-475 nm, 500-545 nm or filter based from 575-675 nm, respectively. Confocal slices were taken at 0.49 micron intervals with voxel dimensions of 0.265 x 0.265 microns. All post-acquisition analysis was performed in Fiji v1.48p<sup>78</sup> and figure generation was performed in Photoshop (Adobe).

**B.3.b. LDH assay in Hepa1c1c cells.** For lactate dehydrogenase (LDH) release experiments,  $4.5 \times 10^5$  cells were plated on 6-well plates. Media was replaced 16 hours post-plating and cells were transfected with 25 nM or 50 nM of anti-miR-709 or anti-control-miR. The next day, media was replaced. One-hundred  $\mu$ ls of media was collected before and 24, 48 and 72 hours post-transfection, and LDH release was quantified.

#### **B.4. Cell transfection**

**B.4.a. Using plasmids and miRNA:** Mouse primary hepatocytes or Hepa1c1c7 cells were transfected with plasmids (1.5  $\mu$ g) together with 34 nM of miR-709 or the control miRNA Cel-239b (Dharmacon). Transfection was performed at a nucleic acid:lipid ratio of 1:6. Cells were incubated at 37°C in a 5% CO<sub>2</sub> incubator. After overnight incubation,

media was replaced with fresh media. Cells were harvested 24 hours later and analyzed for luciferase activity using the dual-luciferase® reporter assay system (Promega) and a luminometer (Centro LB 960 microplate luminometer, Berthold Technologies). Renilla luciferase activity was normalized to firefly luciferase expressed from the same psiCHECK™-2 plasmid.

**B.4.b. Using plasmids:** HEK293 cells or Hepa1c1c7 cells were transfected with 1.5 µg plasmids expressing pri-miR-709 or pri-Cel-239b. Transfection was performed at a nucleic acid:lipid ratio of 1:4. Cells were incubated at 37°C in a 5% CO<sub>2</sub> incubator. After overnight incubation, media was replaced with fresh media. Cells were harvested 24 hours later and RNA was isolated for analyzing miR-709 expression.

**B.4.c. Using miRNA/siRNA/antagomiRs/anti-miRs:** Four hours or the next morning after plating, mouse primary hepatocytes were transfected with 34 nM miR-709 (Dharmacon, Lafayette, CO), Cel-239b, siRab11b-1 (MSS208343), siRab11b-2 (MSS208345), siRab11b-1 and siRab11b-2, control siRNA (siNC, 12935-300, Invitrogen, Life Technologies) using Metafectene Pro (1:6 ratio). Cells treated with siRab11b-1 and siRab11b-2 received equimolar concentrations of siRab11b-1 and siRab11b-2 for a final concentration of 30 nM. Media was replaced 24 hours later and cells were harvested 48 hours post-transfection to analyze protein expression. For antagomiRs/anti-miRs, mouse primary hepatocytes or Hepa1c1c cells were transfected with 10, 17, 25, 34 or 50 nM of anti-miR-709, or anti-control-miR using Metafectene Pro (1:6 ratio). Media was replaced 24 hours later and cells were harvested 24 hours post-

transfection to analyze mRNA or miR-709 expression or were maintained in culture upto 72 hours for LDH assay.

**B.5. miRNA target predictions.** Multiple databases (miRanda<sup>74</sup>, miRDB<sup>79,80</sup>, miRWalk<sup>81</sup>, TargetScan<sup>82</sup>, DIANA-T<sup>83,84</sup>, miRBase<sup>85-91</sup>, PICTAR5<sup>92</sup> and RNA22<sup>93</sup>) were used to predict targets of mmu-miR-709 (*Mus musculus* miRNA-709).

## **B.6. Array analyses.**

**B.6.a. miRNA microarray:** miRNA chip analysis was conducted by LC Sciences (Houston, TX). Four animals per group (normal and *db/db*) were used. The RNA of two mice from one group was labeled with Cy3 and the RNA from the other two animals was labeled with Cy5. One wild type and one *db/db* sample was used to hybridize each of four chips. Background was determined using a regression-based background mapping method. The regression was performed on 5% to 25% of the lowest intensity data points excluding blank spots. Raw data matrix was then subtracted from the background matrix. Normalization was carried out using a LOWESS (Locally-weighted Regression) method on the background-subtracted data. Transcripts were considered detectable if they met at least two conditions: signal intensity higher than 3x background standard deviation; and spot CV <0.5. CV was calculated by standard deviation (SD)/signal intensity. A transcript was listed as detectable only if the signals from at least 50% of the repeating probes were above detection level. Data adjustment included data filtering, log<sub>2</sub> transformation, and gene centering and normalization. The data filtering removed miRNAs with (normalized) intensity values below a threshold value of 32 across all

samples. The log<sub>2</sub> transformation converts intensity values into log<sub>2</sub> scale. Gene centering and normalization transform the log<sub>2</sub> values using the mean and the standard deviation of individual genes across all samples. A t-test was performed between normal and diabetic sample groups. T-values were calculated for each miRNA, and p-values were computed from the theoretical t-distribution. miRNAs with p-values below 0.01 were selected for cluster analysis. The clustering was done using a hierarchical method and was performed with average linkage and Euclidean distance metric.

**B.6.b. mRNA Affymetrix analysis:** Four replicates for miR-709 and three replicates for Cel-239b were used. The quality of RNA was determined by Agilent 600 Nanobioanalyzer. mRNA microarray hybridization was performed by the Center for Medical Genomics, at Indiana University School of Medicine. Affymetrix mouse gene 1.0 ST arrays were used to compare expression of about 28,850 genes using one chip per replicate. Briefly, samples were labeled using the standard Affymetrix protocol for the WT Target Labeling and Control Reagents kit according to the Affymetrix user manual: GeneChip® Whole Transcript (WT) Sense Target Labeling Assay GeneChip. Individual labeled samples were hybridized to the Mouse Gene 1.0 ST GeneChips® for 17 hours, then washed, stained and scanned with the standard protocol using Affymetrix GCOS (GeneChip® Operating System). GCOS was used to generate data (CEL files). The CEL file stores the results of the intensity calculations on the pixel values of the DAT file. This includes an intensity value, standard deviation of the intensity, the number of pixels used to calculate the intensity value, a flag to indicate an outlier as calculated by the algorithm and a user defined flag indicating the feature should be excluded from future

analysis ([www.Affymetrix.com](http://www.Affymetrix.com)). Arrays were visually scanned for abnormalities or defects.

CEL files were imported into Partek Genomics Suite (Partek, Inc., St. Louis, Mo). RMA signals were generated for the core probe sets using the RMA background correction, Quantile normalization and summarization by Median Polish. Summarized signals for each probe set were log<sub>2</sub> transformed. These log transformed signals were used for Principal Components Analysis, hierarchical clustering and signal histograms to determine if there were any outlier arrays. Untransformed RMA signals were used for fold change calculations. Data was analyzed using a 1-way Anova (analysis of variance) using log<sub>2</sub>-transformed signals with treatment as factor and all possible contrasts made. Fold changes were calculated using the untransformed RMA signals. Principal component analysis (PCA) and hierarchical clustering of the top 100 genes was done.

**B.6.c. Taqman Low Density Array.** The ABI Taqman® microRNA Low Density Arrays for rodents (TLDA, Applied Biosystems, Foster City, CA) was used to analyze the expression of miRNAs between fasted and refed liver samples. The rodent TLDA consists of 2 arrays: TLDA A array and TLDA B array for 518 mouse-specific microRNAs. Each array/panel includes three endogenous controls including the mammalian U6 (MammU6) assay that is repeated four times on each card as a positive control as well as an assay unrelated to mammalian species, ath-miR159a, as negative control. Total RNA is first converted to cDNA using Megaplex™ RT primer pools (Stem-loop RT primers for A and B arrays) and TaqMan® Universal PCR Master Mix is



simply combined with each reaction. One-hundred  $\mu$ l of this mix is then loaded onto each port of the TLDA array card. The TLDA plate was centrifuged with 9 up and down ramp rates at 1,200 rpm for 1 min and loaded into the 7900 HT Sequence Detection System using the 384-well TaqMan Low Density Array default thermal-cycling conditions. The ABI TaqMan SDS v2.3 software was utilized to obtain raw  $C_t$  values. To review results, the raw  $C_t$  data (SDS file format) were exported from the Plate Centric View into the ABI TaqMan RQ manager software. Automatic baseline and manual  $C_t$  were set to 0.2 for all samples. All the data was normalized to U87 expression. Delta  $C_t$  ( $\Delta C_t$ ) values of miRNAs was calculated by subtracting the U87  $C_t$  values from target miRNA  $C_t$  values. Delta delta  $C_t$  ( $\Delta\Delta C_t$ ) values were obtained by taking a difference of the  $\Delta C_t$  of a miRNA between fasted and refed groups.  $\Delta\Delta C_t$  values were then converted into fold-change by using the formula  $2^{-\Delta\Delta C_t}$ . Anova analysis was performed to get differentially expressed miRNAs from  $2^{-\Delta\Delta C_t}$  data.

**B.7. Western blotting.** Primary hepatocytes were lysed in RIPA buffer (25 mM Tris-HCl pH 7.6, 150 mM NaCl, 1% NP-40, 1% sodium deoxycholate, 0.1% SDS; Thermo Scientific, Rockford, IL) containing protease and phosphatase inhibitors (Roche, Indianapolis, IN). Cell extracts were centrifuged at 13,000 rpm, the fat layer carefully aspirated, and the supernatant was collected. Protein concentration was determined using the BCA kit from Pierce (Rockford, IL). Proteins (20-30  $\mu$ g) were separated in 10% Tris-HCl SDS PAGE Criterion gel (Bio-Rad, Hercules, CA) and transferred to 0.2-mm PVDF membrane (Bio-Rad, Hercules, CA). Antibodies to detect Rab11b,  $\alpha$ -tubulin, LDLR, Timp3, FATP1, Cyc-40, IR-  $\beta$ ,  $\beta$ -actin, Dync11i1 and Gck were used at the dilution

factors shown in Table 2. The secondary antibody horse radish peroxidase (HRP)-conjugated anti-rabbit IgG (Cell Signaling, Boston, MA), was added and incubated at room temperature for 1 hour at a 1:3,000 - 1:5,000 dilution. Blots were developed with Pierce ECL kit (Thermo Scientific, Rockford, IL), and exposed to enhanced chemiluminescence (ECL) film (GE Healthcare, Piscataway, NJ).

**B.8. Northern blotting.** miRNA-enriched (200 bp) RNA fractions were isolated from ~100 mg of liver using mirVana RNA isolation kit according to the manufacturer's instructions (Ambion, Austin, TX). Four  $\mu$ g of miRNA-enriched RNA was separated on 15% TBE urea gels (Bio-Rad), transferred to Hybond-N membranes (GE Healthcare), and then UV-cross-linked using a Stratalinker 2400 (Stratagene). For miR-122 and 5s, DNA oligonucleotide probes were used. Probes (100 pmol) were labeled with DIG using a 2<sup>nd</sup> generation DIG oligonucleotide tailing kit (Roche, Indianapolis, IN). Probes were hybridized to membranes at 25°C overnight in a hybridization oven after 2 hours of pre-hybridization at 60°C. Three 2X SSC, 0.1% SDS washes were carried out for 10 min at room temperature followed by blocking and incubating with antibody against DIG. The signal was developed using CSPD (Roche, Indianapolis, IN) according to the manufacturer's instructions. Probes used were as follows: miR-122: ACAACACCATTTGTCACACTCCA, 5s: TTAGCTTCCGAGATCA, miR-709: TCCTCCTGCCTCTGCCTCC and ATCCTCCTGCCTCTGCCTCCCC. In addition, to confirm the data, a 5'-DIG labeled miRCURY LNA Detection probe for miR-709 was used (TCCTCCTGCCTCTGCCTCC) (Exiqon, Woburn, MA, USA). For the miRCURY LNA probe, the protocol was followed as described<sup>94</sup>.

**B.9. LDH assay.** LDH measurements were performed on medium collected from Hepa1c1c cells transfected with miR-709 or Cel-239b, using the LDH Cytotoxicity Detection Kit (Clontech, CA, USA). At each timepoint, 100  $\mu$ l of media from each well was collected and stored at -20°C. For analysis, the medium from each well was diluted 1:4 in medium without FBS and glucose, and the company's recommendations were followed. Absorbance was measured at 490 nm using a microplate reader.

### **B.10. qPCR analysis**

**B.10.a. qRT-PCR:** qRT-PCR was performed for the following genes: Cluster of Differentiation 36 (*Cd36*), acyl-CoA oxidase 2 (*Acox2*), glucokinase (*Gck*), phosphofructokinase liver (*Pfkl*), member RAS oncogene family (*Rab11b*), carboxylesterase 1G (*Ces1g*), phosphatidylcholine transfer protein (*Pctp*) and TATA binding protein (*Tbp*), using the primer pairs shown in Table 1. qRT-PCR was performed using an ABI PRISM 7500 instrument (ABI, Foster City, CA) and the SYBR Green Qiagen One-Step reverse transcription-PCR kit (Qiagen, Valencia, CA), following the manufacturer's recommendations. A standard curve was generated with serial dilutions of an RNA sample from cells treated with the control miRNA (Cel-239b) (200 ng to 1.6 ng). Quantification of mRNA was measured by analyzing 50 ng of RNA, in duplicate, in a 50- $\mu$ l reaction volume and using 0.5 mM of each primer.  $C_t$  values were compared to those of the standard curve. The *Tbp* gene was used as loading control. Fold-changes are expressed relative to Cel-239b transfected cells.

**B.10.b. TaqMan assay to quantify mature miRNAs:** To quantify the level of mature miR-709, cDNA was generated from 10 ng of total RNA sample using the TaqMan miRNA Reverse Transcription Kit (Applied Biosystems, Foster City, CA). Quantitative PCR was performed with TaqMan miRNA Assays (Applied Biosystems) specific for miR-709 (P/N 001644). As endogenous control, sno-202 was used (TaqMan miRNA Assay P/N 001232).

**B.11. Statistical analysis.** All experimental conditions were done at least in duplicate and repeated in at least two separate hepatocyte isolations. Data are presented as the arithmetic mean  $\pm$  standard deviation. Statistical differences were calculated using the unpaired two-tailed Student's t-test. A p-value of less than 0.05 was considered statistically significant.

## RESULTS

### A. Hepatic murine miRNA expression

The importance of miRNAs regulating liver function was demonstrated recently in mice lacking Dicer in this tissue<sup>95,96</sup>. The hepatocytes in the knock-out mice displayed prominent steatosis and depleted glycogen stores<sup>95,96</sup>, and these mice were severely hypoglycemic after a short period of fasting. Recent work has also implicated miRNAs in other processes, including hepatic insulin sensitivity<sup>50</sup>. Given that miRNA expression profiles are tissue-specific and can be altered by developmental stage, cell cycle, or metabolic processes, the role of miRNA in liver needs to be established under specific conditions that are relevant to its function.

#### A.1. Identification of miRNAs expressed in livers of normal and *db/db* mice

To identify miRNAs dysregulated in livers of an animal model of type 2 diabetes relative to normal mice, the small RNA fraction of four C57BLKS/J and four *db/db* mice fed *ad libitum*, were obtained. Expression of 617 murine miRNAs was tested using chip miRNA microarrays (LC Sciences, Houston, TX). Of all the miRNAs expressed in the liver, miR-122 was the most abundant (Table 3). As described in the Introduction, miR-122 has been well characterized and shown to be involved in various cellular processes such as fatty acid metabolism, amongst others<sup>52,56</sup>. Of all the differentially expressed miRNA (total of 22), those with a p-value < 0.01 were selected. These included miRNA-709, miR-574-5p and miR-676, which were found significantly upregulated, and miR-805 and miR-23a, which were significantly downregulated in *db/db* livers (Figure 11). A

published study showed that hepatic miR-709 expression increased 7.6-fold with ageing in mice<sup>97</sup>, suggesting a connection with metabolism. In addition, its abundance relative to other miRNAs made it particularly attractive to study, given the existing evidence that only the most abundant miRNAs suppress their targets, and that about 60% of the miRNAs are not active<sup>98</sup>. Predicted targets across multiple databases such as miRDB, TargetScan, and miRBase indicated a possible role in regulating genes important for cell adhesion/extracellular matrix (actin binding proteins, myosin proteins). Thus, we chose to further characterize the function of miR-709, based on its high abundance and potential role in controlling metabolic processes.

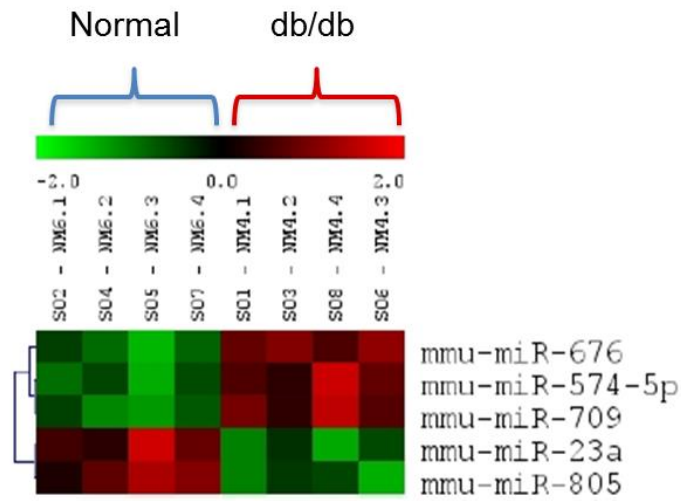


**Figure 11. Hierarchical clustering analysis of miRNAs with p-value < 0.01.** The clustering was done using a hierarchical method and was performed with average linkage and Euclidean distance metric. Red indicates higher expression and green indicates lower expression.

**Table 3. miRNAs expressed in liver of normal C57BLKS/J mice.**

<b>miRNA</b>	<b>Mean miRNA signal</b>	<b>S.D.</b>
<b>mmu-miR-122</b>	50,406	15,046
<b>mmu-miR-709</b>	14,482	2,168
<b>mmu-let-7a</b>	6,797	1,504
<b>mmu-let-7f</b>	6,096	1,436
<b>mmu-let-7c</b>	6,086	811
<b>mmu-let-7d</b>	4,780	623
<b>mmu-let-7b</b>	4,103	369
<b>mmu-miR-466f-3p</b>	2,614	742
<b>mmu-miR-26a</b>	2,346	288
<b>mmu-miR-467b*</b>	1,842	499
<b>mmu-let-7g</b>	1,520	351
<b>mmu-miR-192</b>	1,463	227
<b>mmu-miR-689</b>	1,159	617
<b>mmu-miR-23b</b>	838	242
<b>mmu-miR-466i</b>	782	240
<b>mmu-miR-720</b>	778	455
<b>mmu-miR-467f</b>	774	253
<b>mmu-miR-467a*</b>	718	242
<b>mmu-miR-466g</b>	554	154
<b>mmu-miR-574-5p</b>	487	72
<b>mmu-miR-669f</b>	463	161
<b>mmu-miR-191</b>	456	170
<b>mmu-miR-483</b>	451	91
<b>mmu-miR-705</b>	378	132
<b>mmu-let-7i</b>	370	107
<b>mmu-miR-690</b>	369	48
<b>mmu-let-7e</b>	369	169
<b>mmu-miR-21</b>	355	355
<b>mmu-miR-805</b>	352	131
<b>mmu-miR-24</b>	350	125
<b>mmu-miR-1895</b>	343	66
<b>mmu-miR-22</b>	308	30
<b>mmu-miR-762</b>	301	107
<b>mmu-miR-126-3p</b>	293	120
<b>mmu-miR-26b</b>	283	245
<b>mmu-miR-1224</b>	262	72
<b>mmu-miR-23a</b>	258	52
<b>mmu-miR-16</b>	235	74
<b>mmu-miR-125b-5p</b>	231	80
<b>mmu-miR-103</b>	222	57
<b>mmu-miR-1187</b>	210	39



<b>mmu-miR-194</b>	209	47
<b>mmu-miR-455</b>	205	66
<b>mmu-miR-107</b>	197	45
<b>mmu-miR-320</b>	196	66
<b>mmu-miR-29a</b>	190	119
<b>mmu-miR-574-3p</b>	190	46
<b>mmu-miR-214</b>	175	74
<b>mmu-miR-145</b>	164	64
<b>mmu-miR-31</b>	157	59
<b>mmu-miR-30c</b>	155	49
<b>mmu-miR-378</b>	153	34
<b>mmu-miR-1196</b>	144	65
<b>mmu-miR-27b</b>	140	46
<b>mmu-miR-151-5p</b>	139	50
<b>mmu-miR-30d</b>	117	16
<b>mmu-miR-92a</b>	110	29
<b>mmu-miR-423-5p</b>	108	32
<b>mmu-miR-361</b>	105	34
<b>mmu-miR-1892</b>	91	35
<b>mmu-miR-185</b>	90	27
<b>mmu-miR-568</b>	84	47
<b>mmu-miR-143</b>	83	22
<b>mmu-miR-1897-5p</b>	80	18
<b>mmu-miR-148a</b>	69	71
<b>mmu-miR-681</b>	68	63
<b>mmu-miR-669c</b>	64	36
<b>mmu-miR-489</b>	64	64
<b>mmu-miR-222</b>	64	19
<b>mmu-miR-25</b>	58	10
<b>mmu-miR-15b</b>	57	28
<b>mmu-miR-30a</b>	56	13
<b>mmu-miR-181a</b>	52	9
<b>mmu-miR-188-5p</b>	49	9
<b>mmu-miR-140*</b>	49	22
<b>mmu-miR-27a</b>	42	13
<b>mmu-miR-485*</b>	42	7
<b>mmu-miR-221</b>	40	13
<b>mmu-miR-680</b>	39	30
<b>mmu-miR-92b</b>	37	4
<b>mmu-miR-290-5p</b>	37	23
<b>mmu-miR-30b</b>	36	17
<b>mmu-miR-369-5p</b>	35	53
<b>mmu-miR-101b</b>	34	12
<b>mmu-miR-146a</b>	33	16
<b>mmu-miR-199a-3p</b>	33	4
<b>mmu-miR-20a</b>	33	8

<b>mmu-miR-99b</b>	32	12
<b>mmu-miR-674</b>	32	11
<b>mmu-miR-193</b>	32	11

## **A.2 Differential expression of hepatic miRNAs in the fasted and refed state**

The transition from fasting to the refed state requires significant changes in hepatic mRNA profiles<sup>99,100</sup>. Most of the genes are implicated in lipid metabolism, cholesterol synthesis, gluconeogenesis and ketogenesis<sup>99,100</sup>, as expected from the established role of the liver at regulating these pathways in response to changes in levels of glucose and insulin. MicroRNAs are largely transcribed by RNA polymerase II and therefore, can be transcriptionally regulated like protein-encoding genes to change levels of genes needed for the metabolic switch between the fed and fasted periods. To determine whether miR-709 levels are influenced by nutritional/hormonal status, and to gain an insight on other miRNAs that could be regulated in such manner, we generated miRNA profiles in mice under fasted or refed conditions.

Total RNA from 14-week old, male C57BL/6J mice (5 mice per group) was used in the study. Mice under fed conditions had free access to food throughout the study. Mice were fasted for 16 hours (fasted group) or fasted for 16 hours and refed for 5 hours (refed group) (Table 4). TaqMan Low Density Array (TLDA) cards A and B for rodents were used to analyze miRNA expression in four animals from the fasted versus the refed group. These two groups were used because we anticipated that if miRNA play a role at regulating metabolic genes, the largest differences in miRNA expression would occur between the fasted and refed periods, when genes involved in fatty acid oxidation, ketogenesis and gluconeogenesis need to be shutdown, while genes involved in

glycolysis and lipogenesis need to be upregulated. The A and B array cards together can detect 518 miRNAs specific to rodents. We have identified 39 miRNAs from the ‘A’ card and 22 miRNAs from the ‘B’ card that are differently expressed under fasting/refed conditions, with a fold-level of expression ranging from 1.5 to 32.4 (Table 5). It was striking to note that all miRNAs except one (mmu-miR-21\*) were downregulated under refed relative to fasting conditions, suggesting that miRNA control metabolic pathways mostly by inhibiting expression of gene targets during fasting conditions.

<b>Table 4. Blood glucose and body weight.</b>			
	<b>Fed</b>	<b>Fasted</b>	<b>Refed</b>
<b>Glucose (mg/dl)</b>	140.8±19.1	71.0±9.1	148.0±11.0
<b>Body weight (g)</b>	29.0±2.4	26.4±1.1	28.2±2.2

**Table 5. miRNAs differentially expressed between fasted and refed groups.**

<b>'A' Array</b>		
<b>miRNA</b>	<b>Fold Change (Fasted/Refed)</b>	<b>p-value</b>
mmu-miR-455	27.05	0.022
mmu-miR-214	3.88	0.025
mmu-miR-23b	2.93	0.013
mmu-miR-676	2.90	0.023
snoRNA202	2.87	0.018
mmu-miR-25	2.86	0.005
mmu-miR-99a	2.82	0.012
mmu-miR-425	2.79	0.013
mmu-miR-652	2.69	0.002
mmu-miR-221	2.67	0.004
mmu-miR-340-3p	2.58	0.019
mmu-let-7g	2.50	0.017
mmu-miR-181a	2.47	0.035
mmu-miR-335-5p	2.33	0.021
mmu-miR-145	2.17	0.026
mmu-miR-125b-5p	2.17	0.006
mmu-miR-532-5p	2.16	0.009
mmu-miR-30c	2.12	0.017
mmu-miR-199a-3p	2.03	0.000
mmu-miR-381	1.98	0.020
mmu-miR-590-5p	1.95	0.045
mmu-let-7d	1.93	0.042
mmu-miR-328	1.89	0.023
mmu-miR-27a	1.86	0.033
mmu-let-7b	1.85	0.003
mmu-miR-146b	1.83	0.027
mmu-miR-93	1.82	0.017
mmu-let-7i	1.82	0.022
mmu-miR-18a	1.80	0.047
mmu-miR-152	1.80	0.022
mmu-miR-365	1.74	0.031
mmu-miR-26a	1.73	0.004
mmu-miR-143	1.73	0.023
mmu-let-7c	1.72	0.033
mmu-miR-30b	1.72	0.028
mmu-miR-195	1.68	0.039
mmu-miR-122	1.54	0.021
mmu-miR-148a	1.53	0.019

mmu-miR-103	1.52	0.008
<b>'B' Array</b>		
<b>miRNA</b>	<b>Fold Change (Fasted/Refed)</b>	<b>p-value</b>
mmu-miR-29b*	32.42	0.008
mmu-miR-744*	15.79	0.003
mmu-miR-28*	5.11	0.016
mmu-miR-15b*	4.80	0.010
mmu-miR-674*	4.11	0.040
mmu-let-7a*	3.87	0.022
mmu-miR-760	3.65	0.033
mmu-miR-29c*	3.38	0.025
mmu-miR-22*	2.79	0.006
mmu-miR-214*	2.75	0.030
mmu-miR-872*	2.56	0.020
mmu-miR-193*	2.49	0.009
mmu-miR-720	2.48	0.025
mmu-miR-22*	2.34	0.015
mmu-miR-22	1.98	0.026
mmu-miR-706	1.92	0.045
mmu-miR-31*	1.88	0.023
mmu-miR-22	1.67	0.024
mmu-miR-30a*	1.64	0.034
mmu-miR-378	1.54	0.032
mmu-miR-378	1.52	0.027
mmu-miR-21*	-29.52	0.025

The predicted targets of the 10 genes with >3-fold decrease/increase were identified using the DIANA-microT-CDS v5.0 database. This was followed by analysis using DIANA-miRPath v2.0 to perform hierarchical clustering of miRNAs and to identify pathways based on their interaction levels (Table 6). Several of these pathways were relevant to metabolic functions, including the PI3K-Akt and mTOR signaling pathways. By the time this thesis project started, the role of these miRNAs was unknown. Nevertheless, a recent literature search (at the end of this thesis project) on these miRNAs has shown that several of them have roles in hepatocellular carcinoma (miR-22<sup>101-103</sup>, miR-378<sup>104</sup>, miR-214<sup>105</sup>, miR-99a<sup>106</sup>, miR-195<sup>107</sup>, miR-27a<sup>108</sup>, miR-199a-3p<sup>109</sup>, let-7g<sup>110</sup>, let-7c<sup>111</sup>, miR-122<sup>112</sup>, miR-181a<sup>113</sup>, miR-145<sup>114</sup>, miR-148a<sup>115</sup>, miR-221<sup>116</sup>, miR-125b-5p<sup>117</sup>, miR-590-5p<sup>118</sup>, miR-18a<sup>119</sup>, miR-93<sup>120</sup>, miR-25<sup>121</sup>), liver regeneration (miR-23b<sup>122,123</sup>), liver cirrhosis (miR-652<sup>124</sup>, miR-181a<sup>113</sup>), liver fibrosis (miR-199a-3p<sup>125</sup>) and insulin sensitivity (miR-103<sup>50</sup>, miR-99a<sup>126</sup>, miR-145<sup>127</sup>, miR-143<sup>128</sup>).

The results of the TaqMan Low Density Array showed that miR-709 was a highly expressed miRNA, confirming the microarray chip results (Table 3 and data not shown). However, the data indicated that miR-709 expression does not change significantly between the fasted to refed state. Thus, it is unlikely that this miRNA is needed to regulate pathways in response to insulin and/or metabolites that are generated during fasting or refeeding. Nevertheless, given that it was significantly upregulated in *db/db* animals, we questioned how miR-709 might contribute to the pathophysiology of type 2 diabetes. Analysis of predicted targets using the databases miRanda and miRWalk, suggested a potential role on cell proliferation. Hepatic steatosis is a hallmark of type 2 diabetes, and is associated with inflammatory processes and increased apoptosis, which

leads to cell repair and regeneration. Thus, we hypothesized that miR-709 would play a role in this response and proceeded with identifying its targets.

**Table 6. Predicted pathway regulation by miRNAs.**

<b>Pathway/gene cluster</b>	<b>miRNA</b>
PI3K-Akt signaling pathway	let-7b, miR-199a, miR-25
Focal adhesion	miR-25, miR-199a
Transcriptional misregulation in cancer	let-7b, miR-199a
Renin-Angiotensin system	miR-26a, miR-193
ECM-receptor interaction	let-7b, miR-25
Protein processing in endoplasmic reticulum	miR-26a, miR-125b
Pathways in cancer	miR-103, miR-532
Protein digestion and absorption	let-7b, miR-26a
Hypertrophic cardiomyopathy (HCM)	miR-25, miR-26a
mTOR signaling pathway	miR-26a
ErbB signaling pathway	miR-199a
Hedgehog signaling pathway	miR-103
N-Glycan Biosynthesis	miR-26a
Ubiquitin mediated proteolysis	miR-125b
Mucin type O-Glycan biosynthesis	miR-125b
Arrhythmogenic right ventricular cardiomyopathy	miR-25

## **B. Targets of miR-709 in murine liver**

### **B.1. miR-709-3p is the mature strand of miRNA-709**

To determine which strand of the miRNA is loaded into the RNA-induced Silencing Complex (RISC), and therefore available for knockdown of its target genes, luciferase reporter constructs were generated containing the sequence complementary to the 5' or 3' strand of miR-709 (Figure 9). Primary hepatocytes were transfected with these plasmids and miR-709 mimic or control miRNA (Cel-239b). A 22.4-fold downregulation was seen specifically for the miR-709-3p construct, compared to control constructs (Figure 12). No effect was seen in cells transfected with miRNA-805, confirming the specificity of the binding. The plasmid specific for the miR-709-3p strand was also significantly downregulated in the Hepa1c1c cell line (Figure 13).

Furthermore, primary hepatocytes transfected with a tough decoy (TuD) containing 8 copies of the sequence complementary to the 3' strand showed a significant downregulation of luciferase expression relative to cells transfected with a plasmid without the sites (psiCHECK<sup>TM</sup>-2), indicating that the 3p is used as the guide strand for the endogenous miR-709 (Figure 14). Altogether, these data indicate that the 5p strand is not used by RISC and confirms that the 3p is used as the guide strand of miR-709 in murine liver.



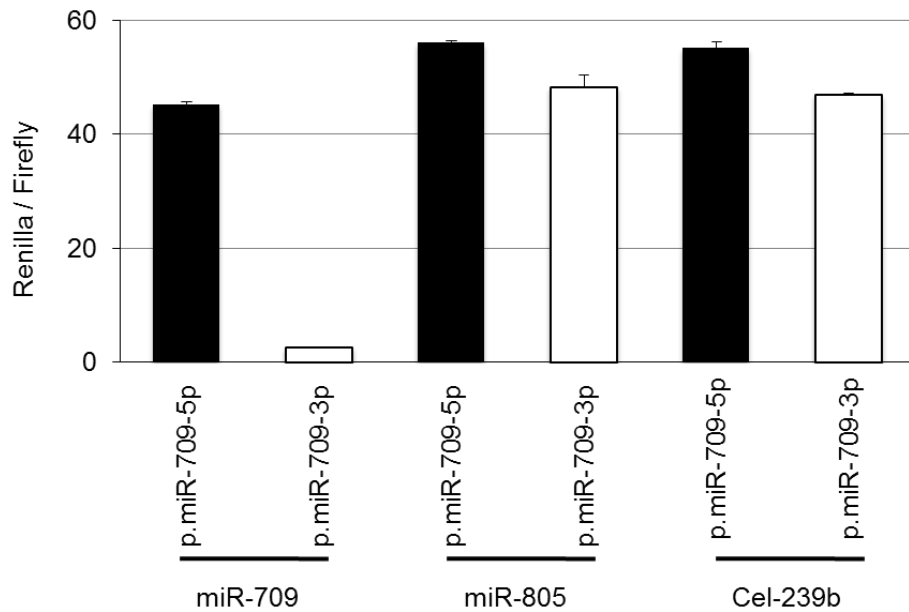


**Figure 12. miR-709 strand selection in primary hepatocytes.** Primary hepatocytes were plated on 6-well plates at  $4 \times 10^5$  cells/well and transfected with 34 nM miR-709, miR-805 or Cel-239b, and 1.5  $\mu$ g of plasmid p.miR-709-5p or p.miR-709-3p. Dual-luciferase assays were performed on extracts prepared 24 hours later. Renilla luciferase activity was normalized to firefly luciferase expressed from the same plasmid. Cel-239b and miR-805 serve as negative control miRNAs. The results are representative of two independent experiments. Error bars represent the standard deviation.

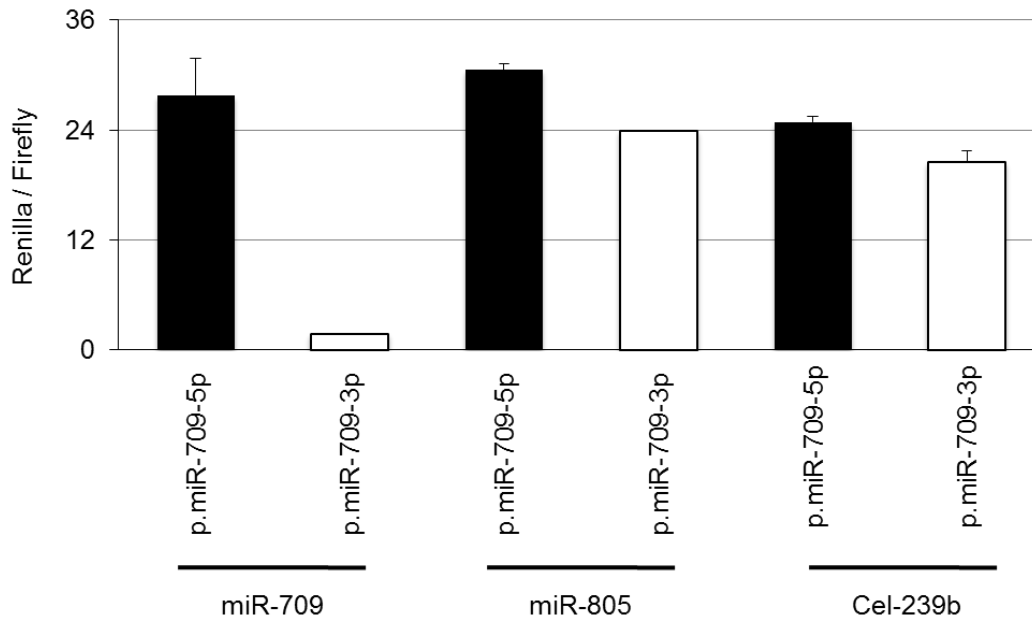


**Figure 13. miR-709 strand selection in the Hepa1c1c7 cell line.** Hepa1c1c7 cells were plated on 6-well plates at  $1 \times 10^5$  cells/well and transfected with miR-709, miR-805 or Cel-239b, as described in Figure 12. Dual-luciferase assays were performed on extracts prepared 24 hours later. Renilla luciferase activity was normalized to firefly luciferase expressed from the same plasmid. Cel-239b and miR-805 serve as negative control miRNAs. The results are representative of two independent experiments. Error bars represent the standard deviation.

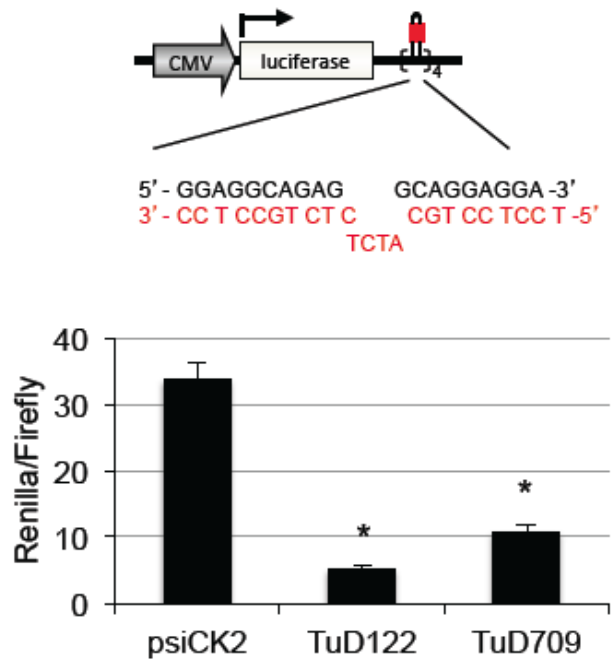


**Figure 14. Strand selection of endogenous miR-709 in primary hepatocytes.** Tough decoys were generated by cloning 8 copies of the sequence complementary to the 3p strand of miR-709 or the 5p strand of miR-122. Primary hepatocytes were plated on 6-well plates at  $4 \times 10^5$  cells/well and transfected with 2  $\mu$ g of TuD122, TuD709 or psiCHECK<sup>TM</sup>-2 (psiCK2) using Metafectene-Pro at 1:4 ratio. Dual-luciferase assays were performed on extracts prepared 40 hours later. Renilla luciferase activity was normalized to firefly luciferase expressed from the same plasmid. TuD122 was used as positive control, and psiCHECK<sup>TM</sup>-2 as reference for luciferase expression. n = 3, with error bars representing the standard deviation. \*p < 0.05 TuD vs psiCHECK<sup>TM</sup>-2. The same data was obtained from two independent experiments.

## **B.2. miR-709-regulated transcriptome**

To identify gene targets of miR-709, mouse primary hepatocytes were transfected with miR-709 mimic or Cel-239b. Increased levels of miR-709 (3.8-fold) were confirmed by TaqMan miRNA assay in cells harvested 24 hours post-transfection (Figure 15). Gene expression profiles were then generated using murine-specific Affymetrix mRNA microarrays (n = 3-4). The short time frame (24 hours) allowed identifying direct targets of miR-709, reducing the possibility of detecting changes in mRNA levels due to secondary effects.

Close to 570 genes were seen downregulated in miR-709-treated cells, compared to Cel-239b. Hierarchical cluster of the top 100 genes was done by ANOVA, arrays Euclidean distance, genes Pearson's dissimilarity and average linkage (Figure 16). Of the 28,850 genes on the microarray, 36 genes were significantly downregulated >2-fold and 10 genes were downregulated >3-fold in the miR-709 group compared to control Cel-239b-treated cells (Table 7; p-value <0.01). The list of downregulated genes was further analyzed using bioinformatic analysis resource DAVID (Database for Annotation, Visualization and Integrated Discovery)<sup>129,130</sup> and GENEGO Databases using pathway analysis and metabolic maps. The results of this analysis suggested a role for this miRNA at controlling cellular processes involved in lipid synthesis and transport (Ces1g, Pctp, Daglb), cytoskeleton organization (Rab11b, Dync1li1, Acta2, M6prbp1, Myo1d) and cell adhesion (Timp3, Nid1, Thbs1, Krt19).

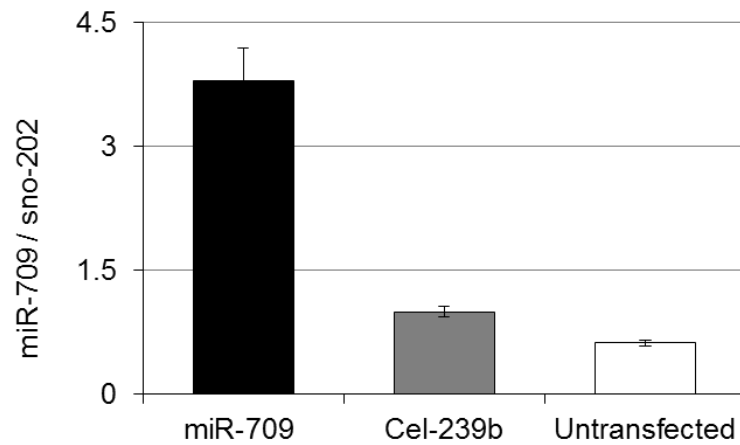


**Figure 15. miR-709 quantification in primary hepatocytes transfected with mimic.**

Primary hepatocytes were plated on 6-well plates at  $5 \times 10^5$  cells/well and transfected with 34 nM of miR-709 or Cel-239b using Metafectene-Pro at 1:6 ratio. Cells were harvested 24 hours later and mature miR-709 was quantified by TaqMan assay. A 3.8-fold increase was observed relative to Cel-239b-treated cells. snoRNA-202 was used as normalizer.

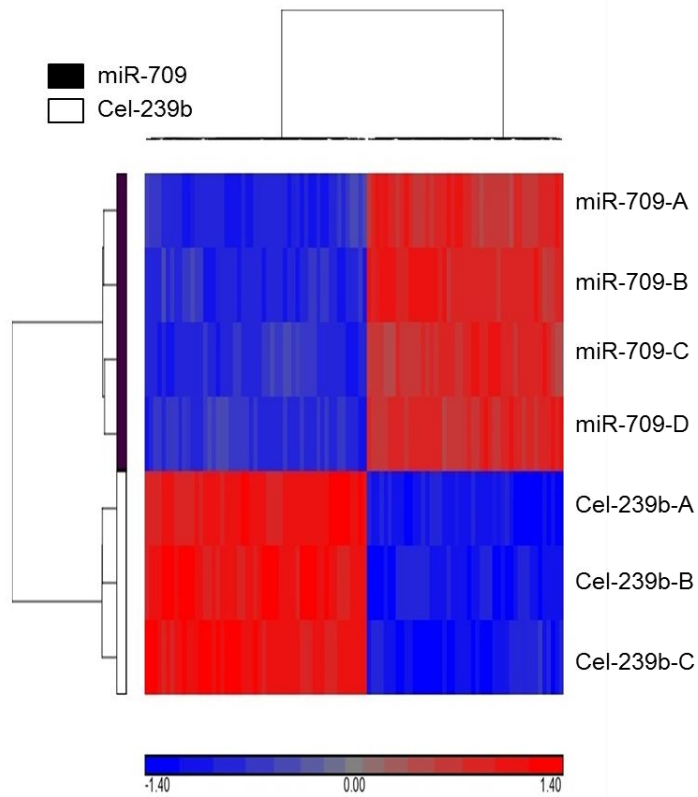


**Figure 16. Hierarchical cluster of top 100 genes.** Analysis was done by ANOVA arrays Euclidean distance, genes Pearson’s dissimilarity, and average linkage. The top dendrogram separates genes by their expression pattern. Blue indicates lower and red indicates higher signals. The dendrogram on the left separates the two treatment groups – miR-709 and Cel-239b.

**Table 7. Genes significantly downregulated >2-fold in miR-709-treated compared to Cel-239-treated primary hepatocytes.**

<b>Gene symbol</b>	<b>Gene name</b>	<b>Fold change</b>	<b>p-value</b>
<b>Tspan31</b>	Tetraspanin 31	-5.27	1.8E-06
<b>Rab11b</b>	Ras-related protein	-4.18	6.5E-06
<b>Cyp20a1</b>	Cytochrome P450, Family 20, Subfamily A, Polypeptide 1	-3.76	1.2E-07
<b>Dync1li1</b>	dynein, cytoplasmic 1, light intermediate chain 1	-3.40	2.3E-07
<b>Bpnt1</b>	3'(2'), 5'-bisphosphate nucleotidase 1	-3.28	9.3E-09
<b>Mmachc</b>	methylmalonic aciduria (cobalamin deficiency) cblC type, with homocystinuria	-3.27	1.5E-05
<b>Ces1</b>	carboxylesterase 1	-3.22	1.7E-06
<b>Timp3</b>	Tissue Inhibitor Of Metalloproteinases 3	-3.20	4.6E-05
<b>Pctp</b>	phosphatidylcholine transfer protein	-3.19	6.2E-07
<b>Nid1</b>	nidogen 1	-3.03	2.7E-06
<b>Slc35e1</b>	solute carrier family 35, member E1	-2.95	3.7E-09
<b>Mare</b>	alpha globin regulatory element containing gene	-2.75	7.0E-08
<b>D13Wsu177e</b>	DNA segment, Chr 13, Wayne State University 177, expe	-2.71	1.7E-08
<b>Thbs1</b>	thrombospondin 1	-2.67	2.1E-06
<b>Lrrc58</b>	leucine rich repeat containing 58	-2.53	6.2E-07
<b>Acta2</b>	actin, alpha 2, smooth muscle, aorta	-2.52	1.4E-05
<b>M6prbp1</b>	mannose-6-phosphate receptor binding protein 1	-2.50	1.7E-06
<b>Atrn</b>	attractin	-2.46	4.7E-06
<b>Mpzl2</b>	myelin protein zero-like 2	-2.41	4.1E-06
<b>Tagln</b>	transgelin	-2.36	6.6E-06
<b>Cnn1</b>	calponin 1	-2.36	4.0E-05
<b>Krt19</b>	keratin 19	-2.35	2.9E-03
<b>Myo1d</b>	myosin ID	-2.31	1.5E-07
<b>Cyb5d2</b>	cytochrome b5 domain containing 2	-2.29	1.1E-06
<b>Actc1</b>	actin, alpha, cardiac muscle 1	-2.29	1.3E-05
<b>Pfas</b>	phosphoribosylformylglycinamide synthase	-2.27	1.1E-08
<b>Ggcx</b>	gamma-glutamyl carboxylase	-2.20	7.5E-05
<b>Ccnyl1</b>	cyclin Y-like 1	-2.17	1.0E-05
<b>Amt</b>	aminomethyltransferase	-2.16	2.0E-04
<b>BC057893</b>	cDNA sequence BC057893	-2.12	3.3E-06
<b>Gpr155</b>	G protein-coupled receptor 155	-2.05	1.7E-04
<b>Daglb</b>	diacylglycerol lipase, beta	-2.05	2.7E-06
<b>Sema6a</b>	sema domain, transmembrane domain	-2.04	9.4E-05

	(TM), and cytoplasmic		
<b>Fnip2</b>	folliculin interacting protein 2	-2.01	3.9E-04
<b>Slc7a1</b>	solute carrier family 7 (cationic amino acid transporter	-2.01	1.6E-06
<b>Mobkl2a</b>	MOB1, Mps One Binder kinase activator-like 2A (yeast)	-2.00	2.3E-05



To validate the microarray results, CD36, Acox2, Gck, Pfkf1, Rab11b, Ces1g and Pctp were analyzed by quantitative real time PCR. Identical trends to those observed in the microarray analysis were observed (Figure 17). Interestingly, Rab11b, Pctp and Ces1g showed more than 5-fold downregulation upon validation, which was greater than what was observed in the microarray analysis. The decrease in gene expression was maintained for at least 4 days (Figure 18). Changes were confirmed at protein level for several genes, including Rab11b, Dync1li1 and Timp3 (Figure 19). The low-density lipoprotein receptor (Ldlr) was 1.2-fold downregulated in the microarray ( $p=0.004$ ), but remained unaltered at protein level, suggesting that small changes in mRNA levels had no impact at protein level (Figure 19). Remarkably, levels of Rab11b, Dync1li1 and Timp3 were lower in primary hepatocytes within 48 hours of transfection with miR-709 (Figure 19). miR-709 induced a 90% decrease in Rab11b protein levels and a 70% decrease in Dync1li1 protein expression. Consistent with these data, Rab11b protein levels were also significantly reduced in Hepalclc cells transfected with miR-709 mimics (Figure 20).

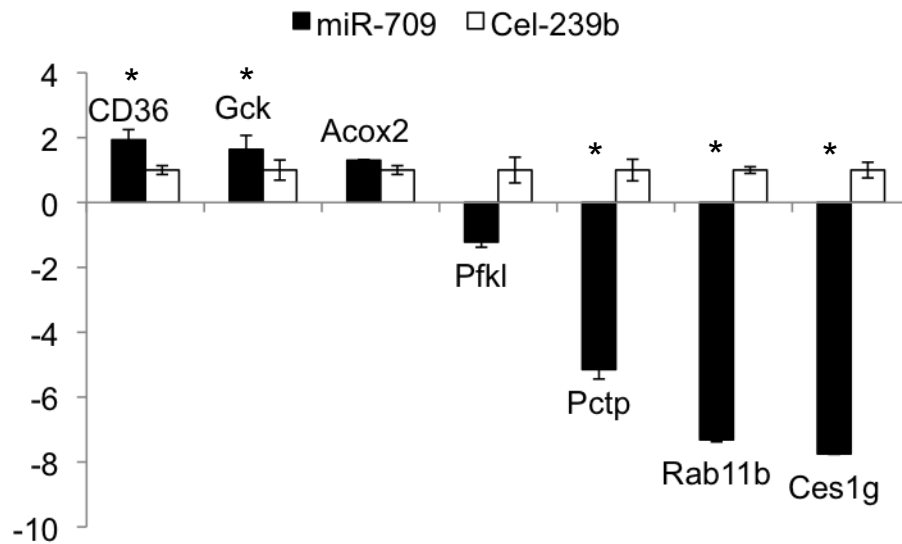


**Figure 17. Real time RT-PCR analysis of miR-709 targets.** Cluster of Differentiation 36 (CD36), Acyl-CoA oxidase 2 (Acox2), Ras-related protein (Rab11b), phosphofructokinase, liver (Pfkf), phosphatidylcholine transfer protein (Pctp), glucokinase (Gck) and carboxylesterase 1g (Ces1g) were analyzed by qPCR. Mouse primary hepatocytes were plated on 6-well plates at  $1 \times 10^6$  cells/well and transfected with 34 nM miR-709 or Cel-239b using Metafectene-Pro at 1:6 ratio. Cells were harvested 24 hours later (n = 4; error bars represent the standard deviation). TATA Binding protein (*Tbp*) was used as normalizer gene. \* $p < 0.05$  relative to Cel-239b-treated. The fold-change for each gene relative to Cel-239b-treated is plotted.

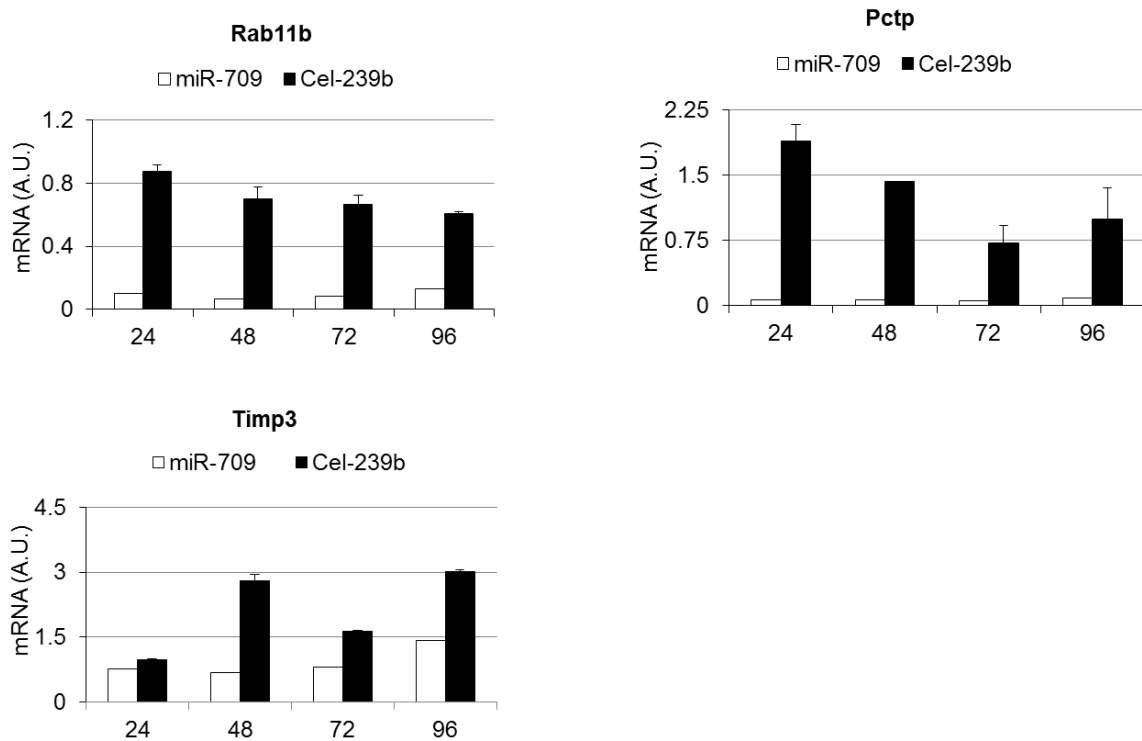


**Figure 18. Prolonged downregulation of miR-709 targets over time.** Real time RT-PCR analysis of Ras-related protein (Rab11b), phosphatidylcholine transfer protein (Pctp) and tissue inhibitor of metalloproteinases 3 (Timp3). Mouse primary hepatocytes were plated on 6-well plates at  $4 \times 10^5$  cells/well and transfected with 34 nM miR-709 or Cel-239b using Metafectene-Pro at 1:6 ratio. Cells were harvested at 24, 48, 72 and 96 hours post-transfection (error bars represent standard deviation). TATA binding protein (*Tbp*) was used as normalizer gene. The mRNA expression for each gene is plotted.

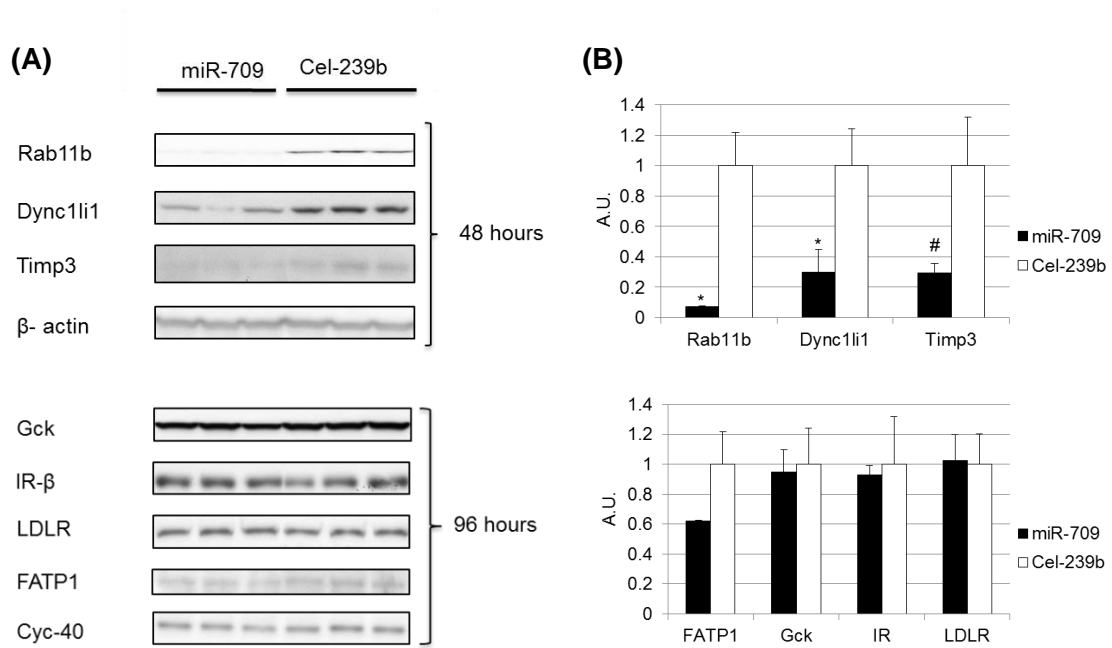


**Figure 19. miR-709 on Rab11b, Timp3 and Dync11i1 protein levels.** (A) Primary hepatocytes were plated on 6-well plates at  $4 \times 10^5$  cells/well and transfected with miR-709 or Cel-239b using Metafectene Pro. Media was replaced 24 hours post-transfection and cells were harvested 48 hours or 96 hours later. Rab11b, Dync11i1, Timp3, Ldlr, IR- $\beta$ , Fatp1 and Gck protein expression was analyzed by Western blot. Cyclophilin-40 and  $\beta$ -actin are normalizers. Data are representative of at least 3 independent experiments with at least 4 replicates for each group. (B) Bands on blot were quantified by densitometry and results were normalized to  $\beta$ -actin or cyclophilin-40. \*p<0.01 relative to Cel-239b, #p<0.06 relative to Cel-239b.

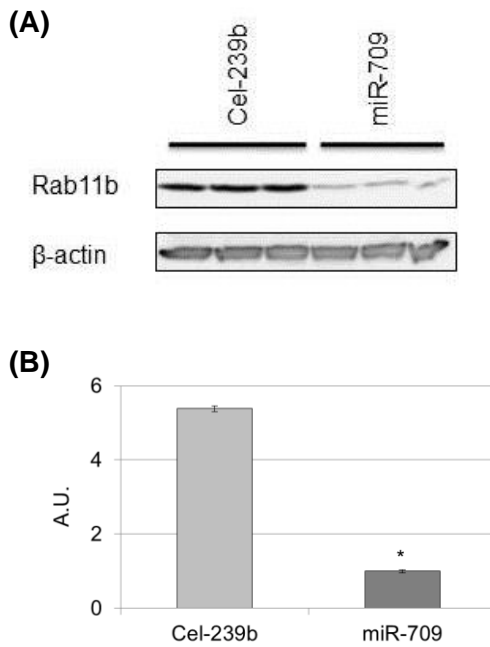


**Figure 20. miR-709 decreases Rab11b in Hepa1c1c cells.** Hepa1c1c cells were plated on 6-well plates at  $4 \times 10^5$  cells/well and transfected with 34 nM of miR-709 or Cel-239b. Media was replaced 24 hours post-transfection and cells were harvested 72 hours later. Rab11b protein expression was analyzed by Western blot.  $\beta$ -actin acts as normalizer. Data are representative of 3 replicates for each group. **(B)** Bands on blot were quantified by densitometry and results were normalized to  $\beta$ -actin. \* $p < 0.01$  relative to Cel-239b.

### **B.3. Ces1g, Rab11b and Pctp are direct targets of miR-709**

miRNAs act on their target genes mostly by binding to the 3' untranslated region (UTR) of their mRNAs. We have shown that miR-709 downregulates Rab11b, Pctp, and Ces1g. To confirm that these are direct gene targets, we used the miRanda database to identify predicted binding sites for miR-709 on the 3' UTR of these genes. Rab11b, Pctp and Ces1g had 3, 2 and 1 predicted binding sites, respectively. Using PCR, we amplified the 3' UTR of Rab11b, Ces1g and Pctp containing at least one of the miR-709 binding sites (Figure 21), and cloned them in plasmid psiCHECK<sup>TM</sup>-2 (Figure 9). As negative control for each gene, a fragment of the 3' UTR without miR-709 binding sites was amplified and cloned in psiCHECK<sup>TM</sup>-2. Primary hepatocytes were transfected with these constructs together with miR-709 mimic or Cel-239b, and harvested 24 hours later. Lower levels of Renilla luciferase were observed in the constructs containing binding sites for miR-709 (p.Rab11b, p.Pctp and p.Ces1g), compared to constructs that had a fragment of the 3' UTR without the miR-709 target sequence (p.NC-Rab11b, p.NC-Pctp and p.NC-Ces1g) (Figure 22). These data confirm that Rab11b, Pctp and Ces1g are direct targets of miR-709.

### Pctp

Fwd Primer miR-709 binding site NC Fwd Primer  
...GCCCA**CATCTGGATTTTCTTTCCATCCAC****TGAGAAATAGCTGCCTCT**ACCT...AAGCC**TCAGGCTTCAAAGATGGCTTGC**GA...  
NC Rev Primer miR-709 binding site Rev Primer  
...TAGAC**CAGGTTAGCCTCGAACTCAGAAA****TCCACCTGCCTCTGCCTCT**CGAGTGCTGG**GATTAAGGCGTG**TACCACC**ACTG**...

### Ces1g

NC Fwd Primer Fwd Primer NC Rev Primer  
...GCTCA**GAGCCAAGGAAACAGCAGAG**AGGT...AAA**ATCAATCGTCTGACCCAGTGGACA** ...CCTGT**GTAGTCCTGGCTTTCCTGGA**ACT...  
miR-709 binding site Rev Primer  
...AGAC**CCACCTGCCTCTGCC**TCCAAGTT...TGAC**ATCACAAATACATTCCCTTAGAA**ATCAAACCAGAGTCTCTG...

### Rab11b

Fwd Primer miR-709 binding site NC Fwd Primer  
...GAGAC**GAGGTTTCTGTGTAGCCT**...AAA**TCCACCTGCCTCTGCCTCC**CAA...GGC**CCAGGAAGAGCAGGAGTCC**AGTGG...  
NC Rev Primer miR-709 binding site Rev Primer  
...GGCC**TGTATCCTCATCCAAACT**TCTCT...GGTGGAC**ATTCTGGGCTCTGCCTCC**TGCC...GGGAG**AAGACACCCTTGCCCTCTCC**...

## Figure 21. miR-709 putative binding sites in the 3' UTR of Rab11b, Ces1g and Pctp.

The primers (shown in green) were designed such that they flanked the putative miR-709 binding site (shown in red) for each gene. The 3' UTR fragment used as negative control (NC) was amplified using primers that bind outside of the miR-709 binding sites (shown in blue). The size of the 3' UTR amplified by PCR for Rab11b, NC-Rab11b, Ces1g, NC-Ces1g, PCTP and NC-PCTP are 712, 261, 253, 236, 365 and 237 bp respectively.

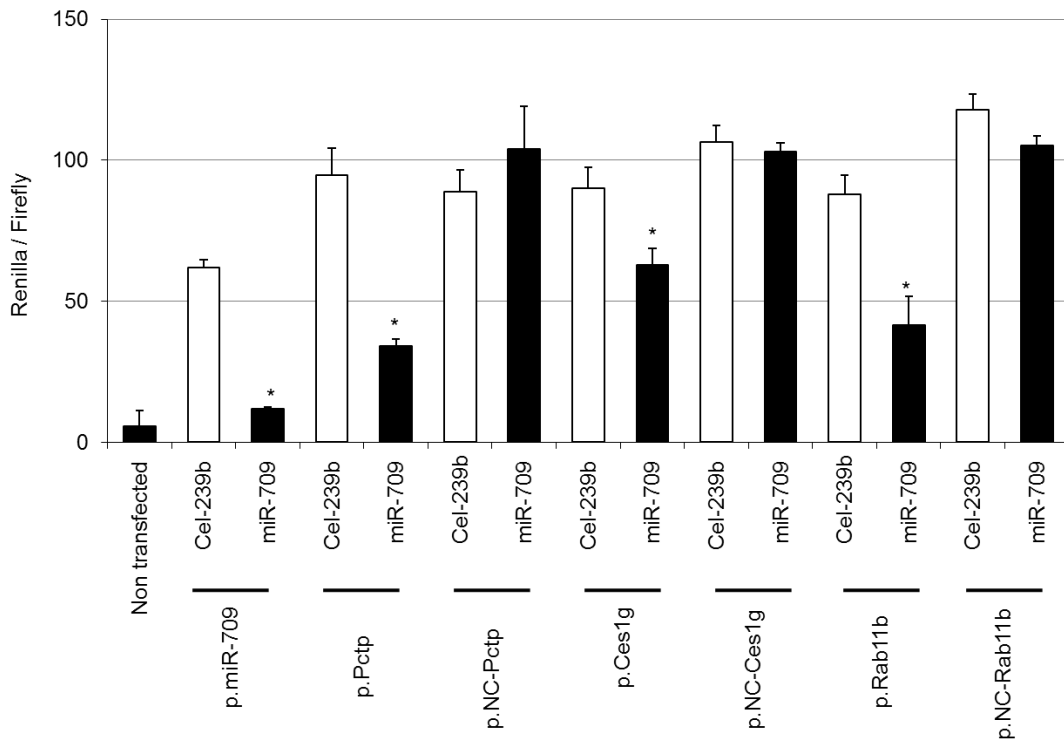


**Figure 22. Rab11b, Pctp and Ces1g are direct targets of miR-709.** Primary hepatocytes were plated on 6-well plates at  $4 \times 10^5$  cells/well and transfected with 34 nM miR-709 or Cel-239b, and 1.5  $\mu$ g of plasmids containing the 3' UTR of Rab11b, Pctp and Ces1g. Twenty-four hours later, dual-luciferase assays were performed. Renilla luciferase activity was normalized to firefly luciferase expressed from the same plasmid (n=3). Error bars represent the standard deviation. The experiment was performed in two independent experiments with identical results. p-values (\*p < 0.01) are relative to cells treated with the same plasmid using Cel-239b miRNA. p.miR-709, plasmid containing the sequence perfectly complementary to miR-709-3p strand; p.Pctp, p.Ces1g and p.Rab11b, plasmids containing a fragment of the 3' UTR with miR-709 binding sites; p.NC-Pctp, p.NC-Ces1g and p.NC-Rab11b, plasmids with a fragment of the 3' UTR without miR-709 binding sites.



#### **B.4. Database gene predictions**

Multiple databases are available to identify predicted targets of miRNA. To determine the accuracy of these predictions, we compared the list of the genes downregulated at least 2-fold, with target predictions from seven databases, including miRanda<sup>74</sup>, miRDB<sup>79,80</sup>, miRWalk<sup>81</sup>, TargetScan<sup>82</sup>, DIANAmt<sup>83,84</sup>, miRBase<sup>85-91</sup>, PICTAR5<sup>92</sup> and RNA22<sup>93</sup> (Table 8). The predictions were based on presence of the miR-709 putative binding site in the 3' UTR of the mRNAs. This analysis revealed that miRanda, miRWalk, DIANAmt and PICTAR5 are the best database predictors of miRNA targets, with 60-70% of gene predictions, while miRDB, TargetScan and RNA22 predicted less than 22% of the genes that were found downregulated. Only one gene was predicted by all databases (Myo1d) (Table 8) and 22% of genes were not predicted by any of them.

miR-709 is not a conserved miRNA, and the human ortholog is hsa-miR-1827, which shares the same seed sequence (UGAGGCAGUAGAUUGAAU). Analysis of predicted hsa-miR-1827 targets using the miRWalk database, indicates that similar genes and pathways are regulated by both miRNA (Table 9). Overall, approximately 61% of miR-709 target genes are also predicted targets of miR-1827. Given that the miRWalk database only predicted 69% of the actual miR-709 targets, it is likely that the number of commonly targeted genes is higher.

**Table 8. Predicted versus observed miR-709 target genes.**

Gene	FL	Database						
		mR	mD	mW	TS	DT	PT5	R22
Tspan31	-5.3	*	*	*		*	*	
Rab11b	-4.2	*	*	*		*	*	
Cyp20a1	-3.8							
Dync1li1	-3.4	*		*		*	*	*
Bpnt1	-3.3	*		*		*	*	
Mmachc	-3.3							
Ces1	-3.2	*		*		*	*	
Timp3	-3.2	*		*	*	*	*	
Pctp	-3.2	*		*	*	*	*	
Nid1	-3.0					*	*	
Slc35e1	-3.0	*	*	*		*	*	
Mare	-2.8	*		*		*	*	*
D13Wsu177e	-2.7	*		*		*	*	
Thbs1	-2.7	*	*	*		*	*	
Lrrc58	-2.5	*		*		*	*	
Acta2	-2.5	*		*	*			*
M6prbp1	-2.5	*		*		*	*	
Atrn	-2.5	*	*	*	*	*	*	
Mpzl2	-2.4	*		*		*	*	
Tagln	-2.4	*	*		*	*	*	
Cnn1	-2.4						*	
Krt19	-2.4							
Myo1d	-2.3	*	*	*	*	*	*	*
Cyb5d2	-2.3							
Actc1	-2.3							*
Pfas	-2.3							
Ggcx	-2.2	*		*		*	*	*
Ccnyl1	-2.2							
Amt	-2.2							
BC057893	-2.1	*		*		*	*	
Gpr155	-2.1	*				*		
Daglb	-2.1	*		*		*	*	
Sema6a	-2.1	*			*		*	
Fnip2	-2.0							
Slc7a1	-2.0	*		*	*	*	*	
Mobkl2a	-2.0	*		*		*	*	
TOTAL PREDICTED:		25	7	22	8	24	25	6
(%):		(69)	(20)	(61)	(20)	(67)	(69)	(17)
TOTAL UNPREDICTED:		11	29	14	28	12	11	30
(%):		(31)	(80)	(39)	(80)	(33)	(31)	(83)

FL, fold-level; mR, miRanda; mD, miRDB; mW, miRWalk; TS, Targetscan; DT, DIANAmT; PT5, PICTAR5; R22, RNA22; \* predicted.

**Table 9. Overlap between mmu-miR-709 target genes and hsa-miR-1827 predicted targets.**

<b>miR-709</b>	<b>miR-1827</b>
Tspan31	TSPAN32
Rab11b	RAB11FIP5
Cyp20a1	CYP19A1
Dync1li1	DYNLL2
Bpnt1	BPNT1
Mmachc	MMACHC
Timp3	TIMP4
Pctp	STARD3
Slc35e1	SLC35C1, SLC35E4
Mare	NPR3
Thbs1	THBS1
Lrrc58	LRRC58
Tagln	TAGLN
Cnn1	CNN3
Krt19	Many KRT proteins
Myo1d	Many MYO proteins
Cyb5d2	CYB561D2
Pfas	PFAS
Gpr155	Many GPR proteins
Sema6a	SEMA6A
Fnip2	FNIP1
Slc7a1	SLC7A60S

## **C. Biological role of miR-709 in liver**

### **C.1. miR-709 gene targets do not regulate hepatocyte polarity**

A coordinated role between Rab11 and Dync1li1 in membrane trafficking has been described in A431 cells, a human epidermal carcinoma cell line<sup>131</sup>. However, the role of these proteins in hepatic function is unknown. The Rab family of proteins is a group of small GTPases that regulate various facets of endosomal trafficking<sup>16,132</sup>. Rab proteins participate in vesicle formation, trafficking and fusion and are often associated with cytoskeletal motor proteins<sup>133</sup>. Rab11b is one of the widely studied members of the Rab11 family and is ubiquitously expressed<sup>133</sup>. It localizes to apical vesicles separated from the Rab11a compartment in MDCK and gastric parietal cells<sup>132,134,135</sup>. Rab11b plays a critical role in apical recycling of epithelial sodium channel (ENaC) in mpkCCD cells<sup>133</sup> and has been shown to interact with its effector protein Rip11 in insulin granule exocytosis<sup>136</sup>. Cytoskeletal motor proteins are accountable for the trafficking of endocytosed material between the surface of the cell and intracellular compartments<sup>137</sup>. Dynein cytoplasmic light chain 1 (Dync1li1) is a component of the Dynein-1 complex, a minus-end-directed microtubule-based motor protein<sup>131,138-142</sup>. Rab11 along with its effector protein FIP3 acts together with Dync1li1 and guides membrane trafficking from peripheral sorting endosomes to the endosomal recycling compartment (ERC)<sup>131</sup>. Given that Rab11b and Dync1li1 were among the top downregulated genes, we hypothesized whether a role of miR-709 is to regulate hepatocyte polarization and trafficking.

To study if miR-709 affected the capacity of primary hepatocytes to maintain polarity and form bile caniculi, a sandwich cell culture model was established to enable

adjacent hepatocytes to form bile canaliculi and mimic the 3D arrangement of the murine liver (Figure 4). Primary hepatocytes were cultured on collagen-I coated glass coverslip bottom 6-cm dishes, and the next day, cells were washed and overlaid with Matrigel™ (see Methods: Primary hepatocyte isolation)<sup>77</sup>. Bile canaliculi were apparent 24 hours later and maintained for several days (Figure 23). Unlike primary hepatocytes cultured in a conventional monolayer, which lose hepatocyte-specific functions as the result of dedifferentiation, the sandwich model enables hepatocytes to form intact bile canaliculi closed by tight junctions, retaining their function for several weeks<sup>12,143</sup>. Cells cultured under these conditions secrete albumin, urea, transferrin, fibrinogen, and bile acids<sup>144</sup>. Next, we tested the capacity of these bile canaliculi to transport sodium fluorescein, a substrate for Multidrug resistance-associated protein 2 (Mrp2), a protein found on the membrane of the bile canaliculi. Within 30 minutes, sodium fluorescein disappeared from the cytoplasm of cells and became visible in the bile canaliculi (Figure 24).

To study if the alterations in gene expression affected the capacity of the hepatocytes to maintain polarity and form bile canaliculi, primary hepatocytes were transfected with miR-709 or Cel-239b, 4 hours after plating. The next day, cells were covered with Matrigel™ to allow contact between adjacent cells. miR-709 and Cel-239b transfected cells could form bile canaliculi between cells within 24 hours that were maintained for at least 4 days, without a noticeable difference between the two groups. Furthermore, uptake and transport of sodium fluorescein into the bile canaliculi was similar for both miR-709 and Cel-239b-treated hepatocytes (Figure 25). These data indicate that miR-709 does not influence the establishment and maintenance of

hepatocyte polarity, the formation of bile canaliculi, and the intracellular transport of Mrp2 substrates. Given that Rab11b was one of the highest downregulated genes, and its function in liver is unknown, we tested whether knocking it down with siRNA would lead to abnormal transport of sodium fluorescein. Similar results were obtained in sandwich cultures of primary hepatocytes transfected with a combination of two siRNAs against Rab11b (siRab11b-1 and siRab11b-2), or control siRNA (siNC) (Figure 26 and Figure 27). Therefore, we concluded that Rab11b was not essential for the ability of primary hepatocytes to be polarized nor did it alter the apical transport of an Mrp2 substrate.

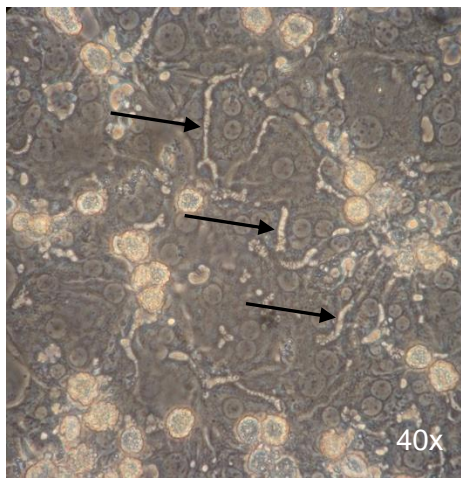
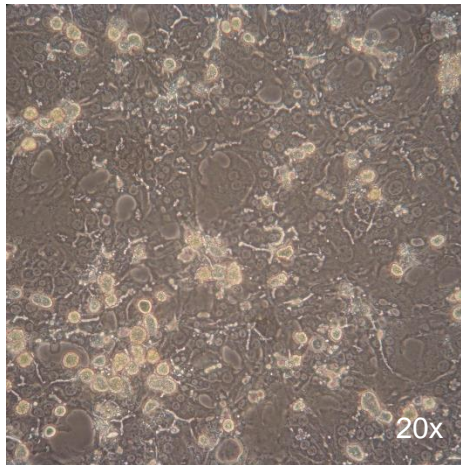


**Figure 23. Formation of bile canaliculi between primary hepatocytes cultured in a sandwich configuration.** Primary hepatocytes were plated on 35-mm glass bottom collagen-coated dishes at  $6 \times 10^5$  cells/well. The following day, Matrigel<sup>TM</sup> was added on top of the cells. Images were acquired with a Nikon TE 2000 U inverted microscope 96 hours post-addition of Matrigel<sup>TM</sup>. Images were acquired with a 20x or 40x Air EL WD Plan Fluor 0.60NA Differential interference contrast objective (Melville, NY) and a Sony DSCW170 16.1 MP digital camera. Arrows point at bile canaliculi.

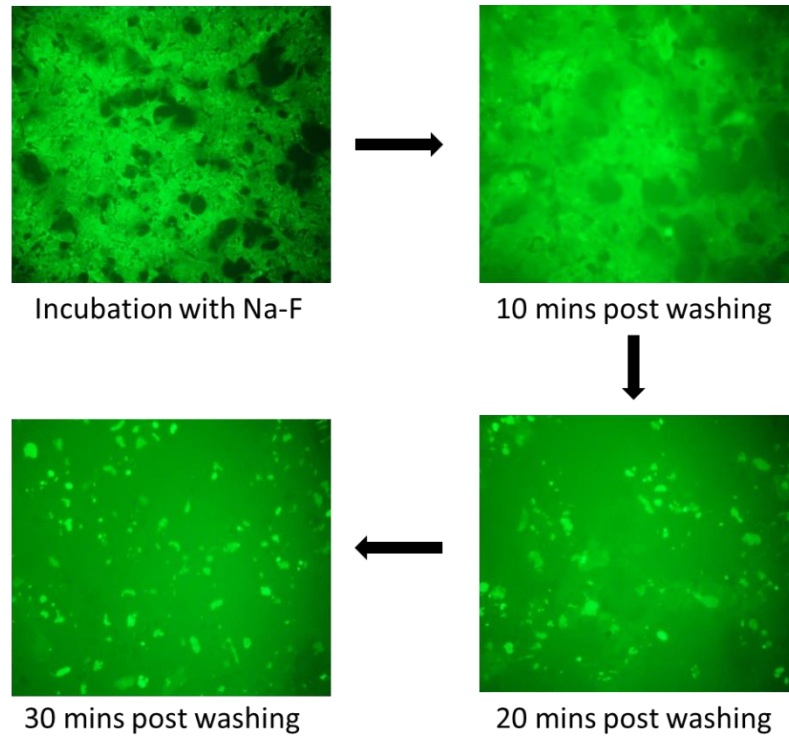


**Figure 24. Uptake and secretion of sodium fluorescein.** Primary hepatocytes were plated on 35-mm glass bottom collagen-coated dishes at  $6 \times 10^5$  cells/well. Matrigel<sup>TM</sup> was added to cells the following day. Cells were assayed for sodium fluorescein transport 96 hours post Matrigel<sup>TM</sup> overlay. Na-F, sodium fluorescein.



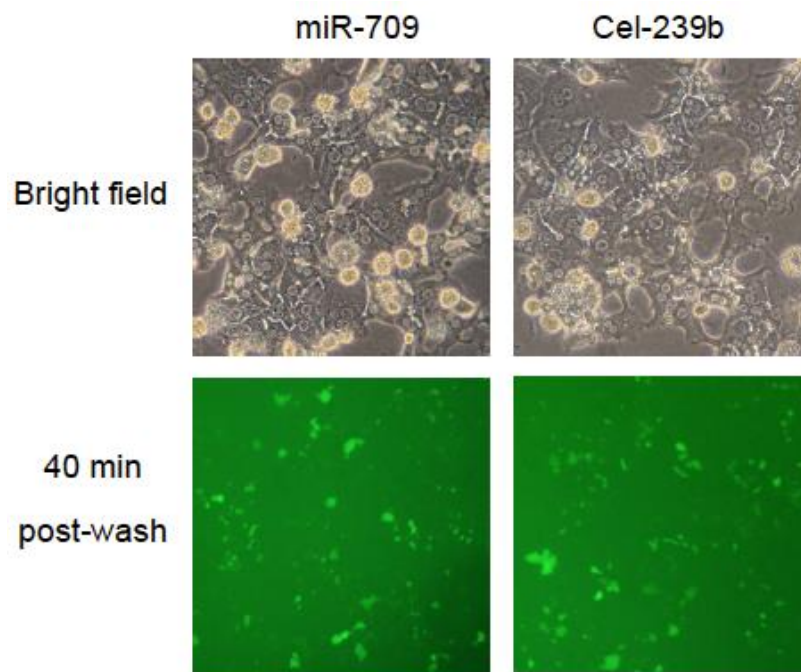


**Figure 25. Sodium fluorescein transport in primary hepatocytes transfected with miR-709 or Cel-239b.** Primary hepatocytes were plated on 35-mm glass bottom collagen coated dishes at  $6 \times 10^5$  cells/well and transfected with 34 nM miR-709 or Cel-239b. Matrigel<sup>TM</sup> was added to cells the following day. Cells were assayed for sodium fluorescein transport 72 hours post-transfection.

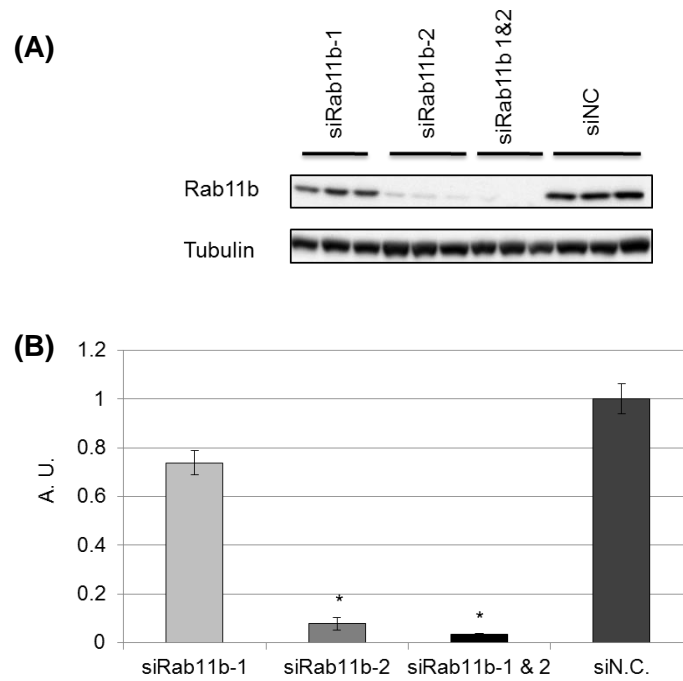


**Figure 26. Rab11b silencing in mouse primary hepatocytes.** (A) Primary hepatocytes were plated on 6-well plates at  $6 \times 10^5$  cells/well and transfected with 30 nM of siRNAs to knockdown Rab11b (siRab11b-1, siRab11b-2) or negative control siRNA (siNC) or a 1:1 complex of both siRab11b-1 and siRab11b-2. Media was replaced 24 hours post-transfection and cells were harvested 24 hours later. Rab11b was quantified by Western blot. Tubulin was used as normalizer (n=3). (B) Densitometry analysis of Western blot; Rab11b expression was normalized to tubulin. \* p-value <0.001.

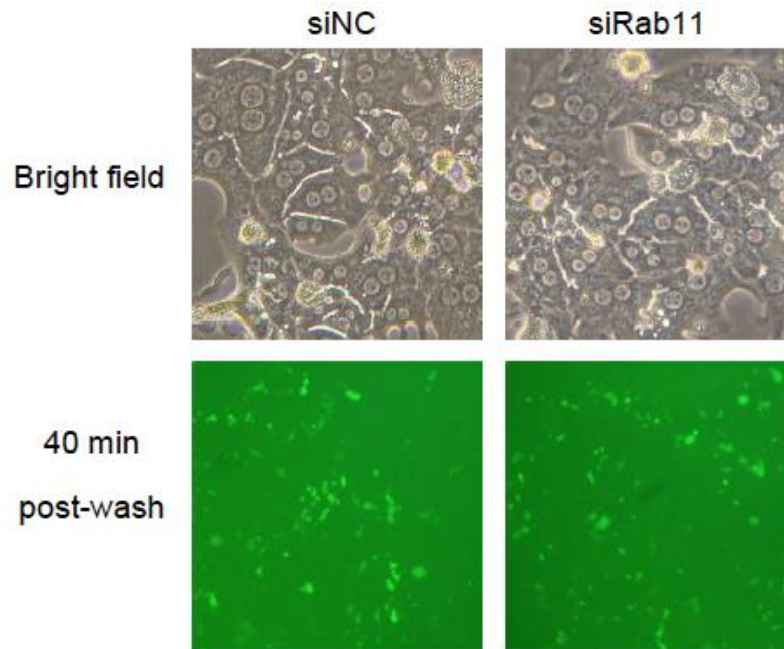


**Figure 27. Sodium fluorescein transport in primary hepatocytes treated with siRab11b.** Primary hepatocytes were plated on 35-mm glass bottom collagen-coated dishes at  $6 \times 10^5$  cells/well and transfected with 30 nM of a combination of siRab11b-1 and siRab11b-2 (1:1 ratio) or negative control siRNA (siNC). Matrigel<sup>TM</sup> was added to cells the following day. Cells were assayed for sodium fluorescein transport 72 hours post-transfection.

## C.2. Intracellular localization of miR-709

Recently, miR-709 has been shown to regulate the processing of a miRNA cluster in the nucleus of fibroblast cells<sup>145</sup>. miR-709 binds to a miR-709 binding element in the primary transcript of miR-15a/16-1 and prevents further processing into precursor or pre-miR-15a/16-1<sup>145</sup>. The same group reported that miR-709 was mostly localized in the nucleus<sup>145</sup>. In fibroblasts, apoptosis-inducing stimuli such as serum starvation, elicited miR-709 translocation to the cytoplasm, without altering the total levels of the miRNA in the cell<sup>145</sup>. This change in localization resulted in loss of inhibition of miR-15a/16-1 processing and led to downregulation of a well-characterized miR-15a/16-1 target, B-cell lymphoma 2 (Bcl-2)<sup>145</sup>. Bcl-2 is an anti-apoptotic gene that prevents cell death by blocking activation of caspases, downstream activators of apoptosis<sup>146</sup>. The authors concluded that miR-709 was sensitive to apoptotic stimuli and it indirectly affected apoptosis through regulation of Bcl-2 levels<sup>145</sup>.

To study the cellular localization of miR-709, primary hepatocytes were co-transfected with a 3'-FAM-labeled miR-709 or Dy547-labeled miRIDIAN miRNA Mimic Transfection Control (Thermo Fisher, CO). This control miRNA is cytoplasmic, like the majority of mature miRNAs. Both, miR-709 and the control miRNA were found localized only in the cytoplasm of primary hepatocytes (Figure 28). To determine whether the intracellular localization of miR-709 depends on cell division, Hepa1c1c cells were co-transfected with the two miRNA. Similar to what was observed in primary hepatocytes, both miRNAs were located in the cytoplasm of Hepa1c1c cells (Figure 29). Next, we tested if serum and glucose starvation would have an impact on the cellular

distribution of miR-709. For this, Hepa1c1c cells transfected with 3'-FAM-labeled miR-709 and Dy547-labeled miRIDIAN microRNA Mimic Transfection Control were subjected to serum and glucose starvation and observed 24 hours later. Both miRNAs were seen only in the cytoplasm, co-localizing in the same area (Figure 29). Single transfection of 3'-FAM-labeled miR-709 gave the same result, discarding the possibility that the control miRNA influences the localization of miR-709 (Figure 30). Thus, in normal liver cells and in hepatoma cells, mature miR-709 is only localized in the cytoplasm of the cells. Also, cellular stress such as starvation did not result in change in localization of miR-709 in hepatoma cells.

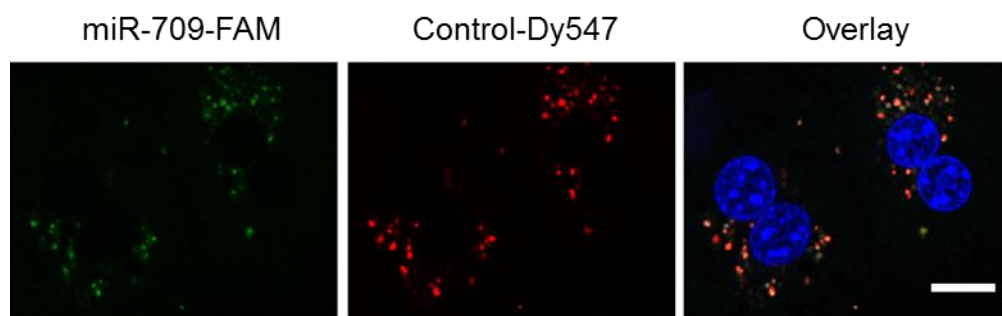


**Figure 28. Intracellular localization of miR-709 in primary hepatocytes.** Primary hepatocytes were plated on 35-mm glass bottom collagen-coated dishes at  $6 \times 10^5$  cells/well and co-transfected with 17 nM of 3'-FAM-labeled miR-709 and 17 nM of Dy547-labeled miRIDIAN microRNA Mimic Transfection Control. Next day, media was replaced and cells were imaged using confocal fluorescence microscopy. Nuclei were stained with Hoechst 33342. Scale bar, 15  $\mu\text{m}$ .

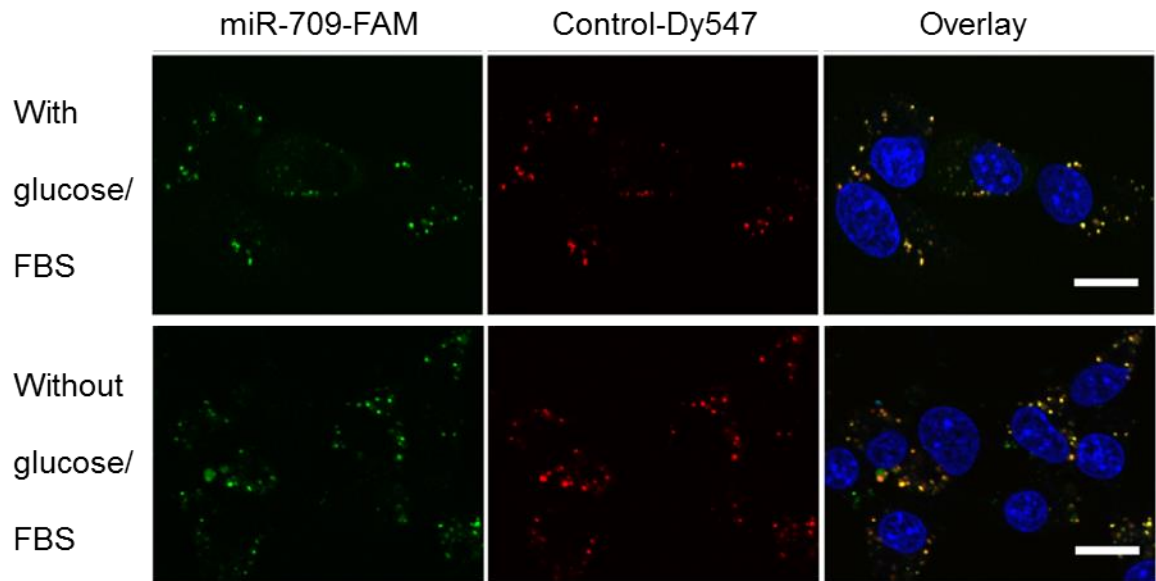


**Figure 29. Intracellular localization of miR-709 in Hepa1c1c cells.** Hepa1c1c cells were plated on 35-mm glass bottom collagen coated dishes at  $4 \times 10^5$  cells/well and co-transfected with 17 nM of 3'-FAM-labeled miR-709 and 17 nM of Dy547-labeled miRIDIAN microRNA Mimic Transfection Control. Next day, media was replaced with medium with/without glucose and FBS. Twenty-four hours later, cells were imaged using confocal fluorescence microscopy. Nuclei were stained with Hoechst 33342. Scale bar, 15  $\mu$ m.

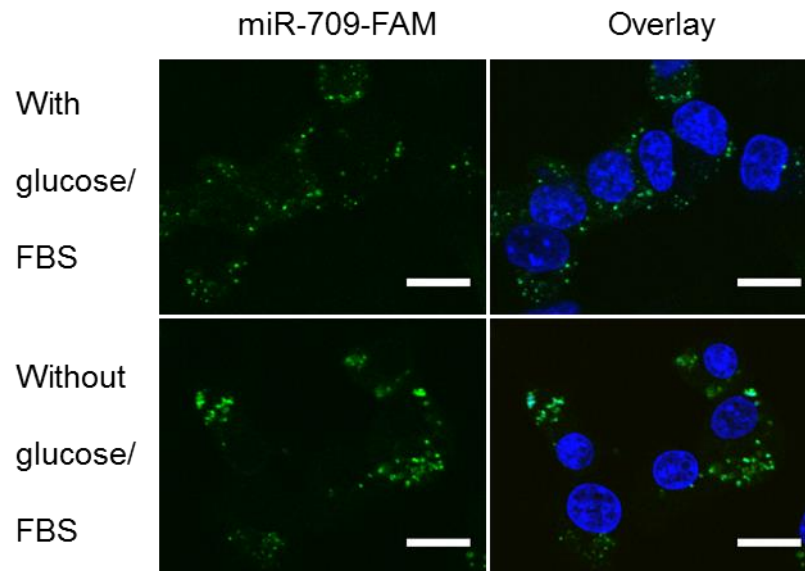


**Figure 30. Cytoplasmic miRNA localization in Hepa1c1c cells transfected with miRNA-709.** Hepa1c1c cells were plated on 35-mm glass bottom collagen coated dishes at  $4 \times 10^5$  cells/well and transfected with 34 nM 3'-FAM-labeled miR-709. Next day, media was replaced with medium with/without glucose and FBS. Twenty-four hours later, cells were imaged using confocal fluorescence microscopy. Nuclei were stained with Hoechst 33342. Scale bar, 15  $\mu$ m



### C.3. Pre-miR-709 accumulates in liver

To further gain an insight on the relative abundance of precursor and mature form of miR-709, levels were analyzed by Northern blot. Remarkably, in normal liver, the precursor miR-709 was present at high levels, while the mature form was scarce, contrary to what is typically seen for most miRNAs<sup>147</sup>, including miR-122 (Figure 31 and Figure 32). This suggested the possibility that pre-miR-709 is the major form of miR-709, and only in the presence of appropriate signals, it is transported to the cytoplasm for Dicer processing and production of the mature form. Consistently with these data, when HEK293 and Hepa1c1c cells were transfected with plasmids expressing miR-709 primary transcript (p.pri-miR-709), there was no increase in levels of mature miR-709 (Figure 33). This suggests that the majority of primary transcript expressed is not processed to mature miR-709.

Given the nature of the gene targets of miR-709 (*Tspan31*, *Rab11*, *Thbs1*, *Timp3*, *Tagln*, *Cnn1*, *Krt19*), we questioned whether this miRNA might be needed in liver cells actively dividing. Thus, we tested the relative abundance of pre-miR-709 and mature miR-709 in a mouse model of hepatocellular carcinoma, and in a model of liver regeneration after partial hepatectomy<sup>148</sup>. Cell proliferation, mitosis and expression of cell cycle proteins in the model of partial hepatectomy peaks at 36 and 44 hrs<sup>148</sup>. Hence, these timepoints were used for this study. Remarkably, we found that the levels of mature miR-709 were significantly increased in liver tumor and regenerating livers (Figures 31 and 34). Taqman real-time PCR was used to confirm the increase in levels of mature miR-709 (Figure 35).

Several lines of evidence suggest that the half-life of a miRNA can be regulated at the biosynthesis as well as decay level. Some miRNA are inherently unstable and have short half-lives<sup>149</sup>. In others, the stage of the cell cycle as well as the presence of growth factors, influences miRNA stability without affecting transcription of the primary transcript<sup>150</sup>. MiR-709 is localized in intron 8 of the *Rfx1* gene, which encodes for a transcription factor with a function not well characterized in liver. Rfx1 inhibits c-Myc and Proliferating Cell Nuclear Antigen (PCNA), both critical genes for cell proliferation<sup>151-153</sup>. To determine whether the increase of miR-709 is the result of increased expression of Rfx1, its mRNA was analyzed by qPCR. Levels of Rfx-1 were found 5.2-fold upregulated in tumor samples (Figure 35), indicating that the increased levels of mature miR-709 are likely the result of increased transcription of the host gene. These data link Rfx1 to liver cell proliferation.

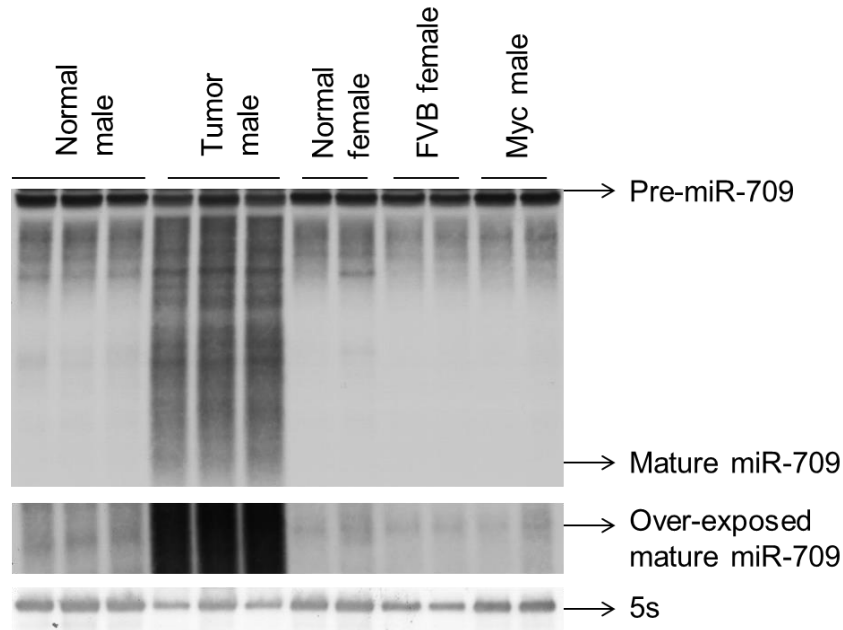


**Figure 31. Relative abundance of miR-709 in an animal model of hepatocellular carcinoma.** Northern blot analysis using 4  $\mu$ g of small RNA fraction. A DIG-labeled miR-709 LNA probe was used for detection of miR-709. LapMyc male (tumor and adjacent normal tissue; n=5), LapMyc female (n=2), FVB female and Myc male mouse liver RNA was used to probe for miR-709 by Northern blotting. The ribosomal RNA 5s was used as loading control. The LapMyc mice are bi-transgenic. *c-Myc* oncogene expression is conditionally regulated via Tet-Off system. The tetracycline-transactivator (tTA) protein is driven by the liver-specific promoter, Liver Activator Protein (LAP), and the *c-Myc* gene (in the Y chromosome) has a tetracycline response element. In the absence of doxycycline, tTA can bind to the response element and cause *c-Myc* expression in male mice. This causes the male mouse livers to develop spontaneous tumors. *c-Myc* expression was induced at 4 weeks of age and animals were sacrificed at 14 weeks of age. LapMyc females are control mice that received doxycycline (and did

not express c-Myc). FVB are wild type female mice. Myc male mice are parents of LapMyc mice. LapMyc female, FVB and Myc mice are negative controls.

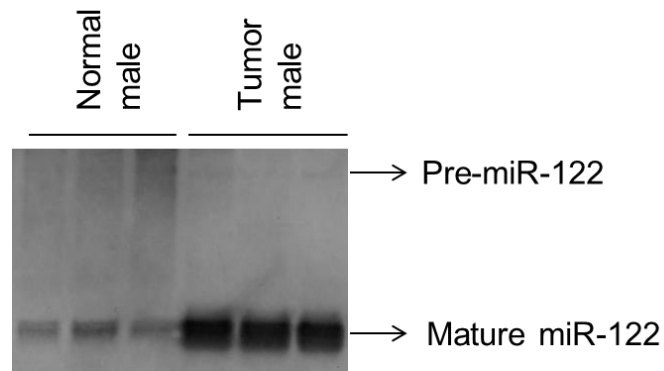


**Figure 32. Relative abundance of miR-122 in an animal model of hepatocellular carcinoma.** Northern blot analysis using 4  $\mu$ g of the small RNA fraction. An oligonucleotide probe was used for detection of miR-122. LapMyc male mouse liver (tumor and adjacent normal tissue; n=5) RNA was used to probe for miR-122. The ribosomal RNA 5s was used as loading control. For miR-122, the mature form is more abundant than the pre-miR-122 in normal liver.

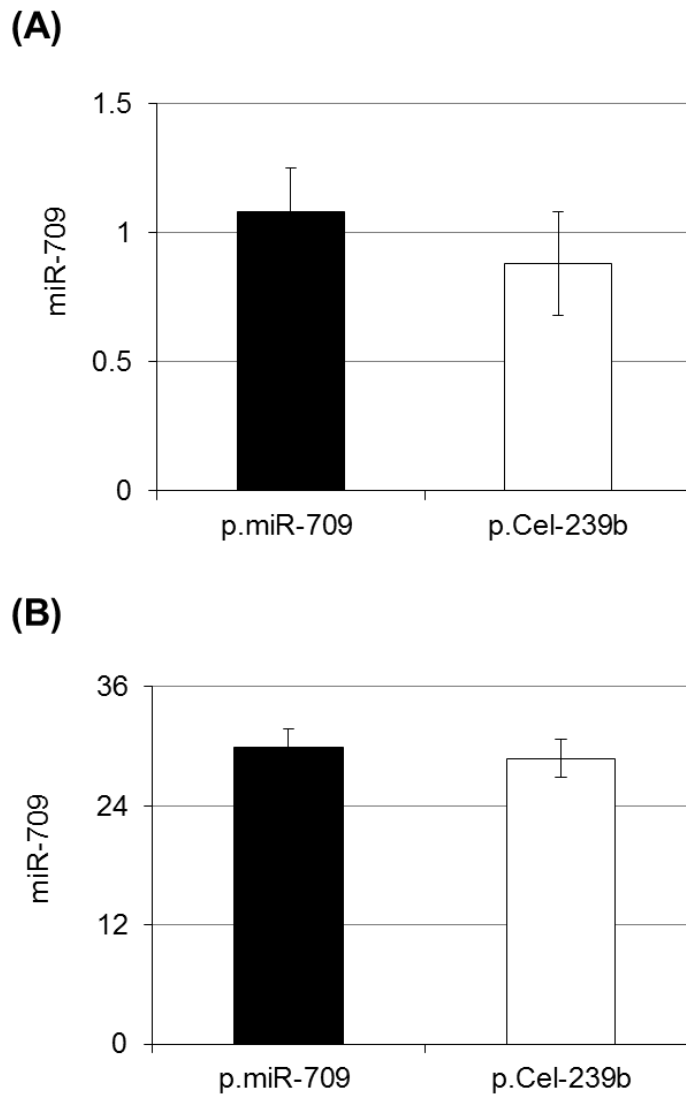


**Figure 33. Levels of mature miR-709 in HEK293 and Hepa1c1c cells upon transfection with plasmids expressing pri-miR-709 or pri-Cel-239b.** HEK293 (A) or Hepa1c1c (B) cells were transfected with 2  $\mu$ g of p.pri-miR-709 or p.pri-Cel-239b and harvested 24 later. Mature miR-709 was quantified by TaqMan assay (n = 3).

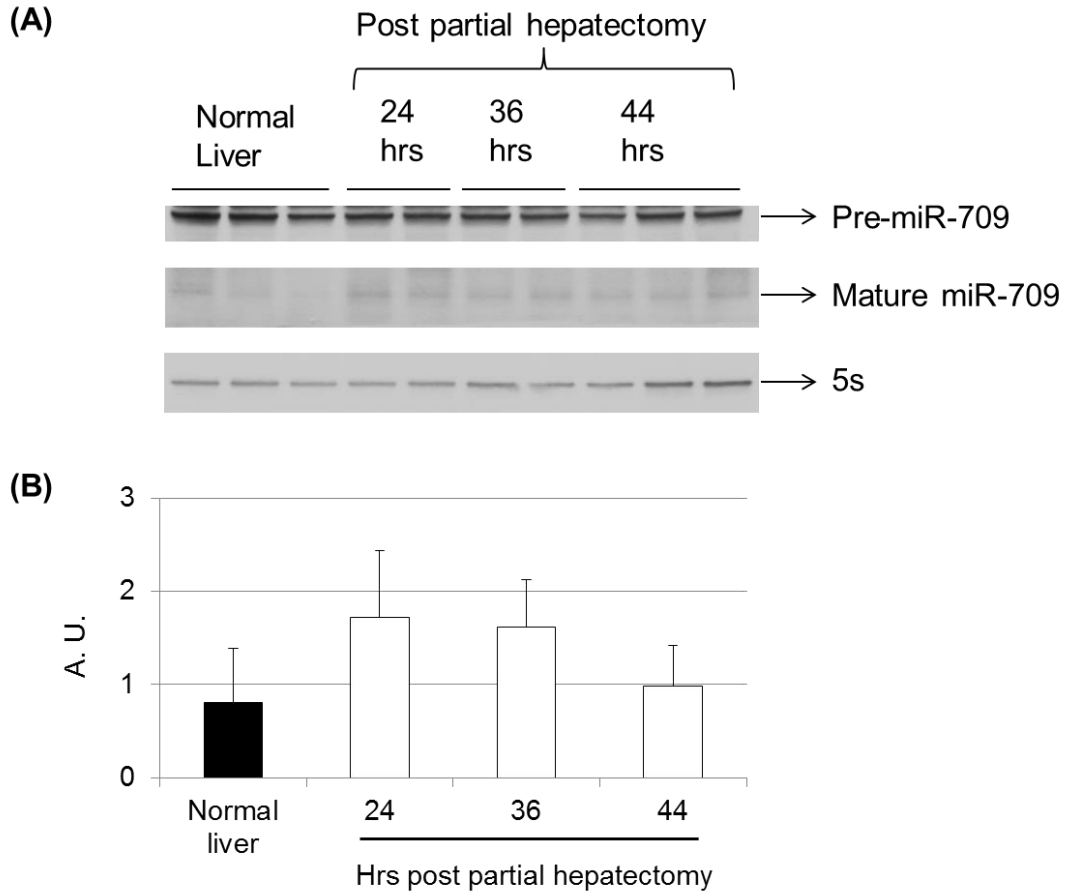


**Figure 34. Relative abundance of miR-709 in an animal model of liver regeneration.**

(A) Livers from normal animals and mice that underwent partial hepatectomy (24, 36 and 44 hours post-hepatectomy) were used to probe for miR-709 by Northern blotting using an LNA probe. The ribosomal RNA 5s was used as loading control. (B) miR-709 bands on blot were quantified by densitometry and results were normalized to 5s.

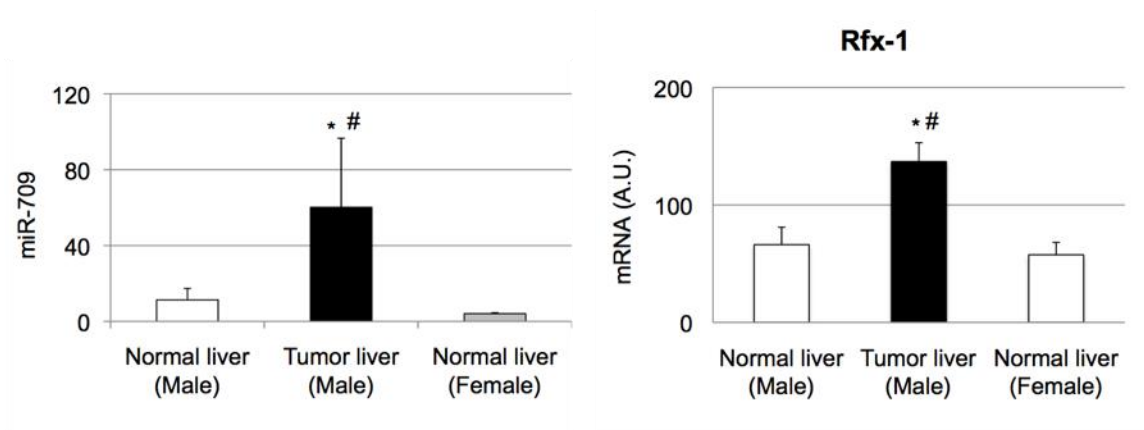


**Figure 35. qPCR analysis of miR-709 and Rfx1 in an animal model of hepatocellular carcinoma.** LapMyc male (tumor and adjacent normal; n=5) and LapMyc female mouse (n=2) livers (see legend of Figure 31 for details on genotype) were used to quantify mature miR-709 by TaqMan assay (left). Rfx-1 mRNA was analyzed on the same samples by qRT-PCR. \*p<0.01 relative to normal male liver; #p<0.01 relative to normal female liver.

#### **C.4. miR-709 inhibition elicits cell death**

Overall, the results suggested a role for miR-709 in cell proliferation. We questioned what would be the impact of inhibiting miR-709 function in quiescent versus actively dividing cells. The use of oligonucleotides complementary to the mature miRNA sequence (antagomiR or anti-miRs) has been a useful tool to downregulate miRNA activity and perform functional analysis. Thus, primary hepatocytes and Hepa1c1c cells were transfected with miR-709 inhibitors.

Primary hepatocytes were transfected with 10, 17 and 25 nM miRIDIAN miR-709 hairpin inhibitor or a control miRNA Cel-239b (Dharmacon). Neither antagomiR was toxic to cells, based on microscopic observation. Cells were harvested 24 hours later, and total RNA was isolated for analysis of miR-709 targets. Interestingly, levels of Rab11b and Ces1g barely increased even at the 25 nM dose (Figure 36). To confirm the data, a second anti-miR-709 from a different company (Ambion) was tested. Cells were transfected with 10 or 34 nM antagomiR, and RNA was isolated from cells 24 hours post-transfection. Levels of miR-709 and snoRNA-202 (normalizer miRNA) were quantified using TaqMan assays. Surprisingly, the mirVana miRNA inhibitor against miR-709 induced higher levels of miR-709 at a dose that was not toxic in cells that received the equivalent amount of Cel-239b (Figure 36). Levels of targets followed a similar pattern to those observed with the miRIDIAN inhibitor (data not shown). These data suggest that miR-709 has an important role in normal hepatocyte function and it cannot be downregulated.



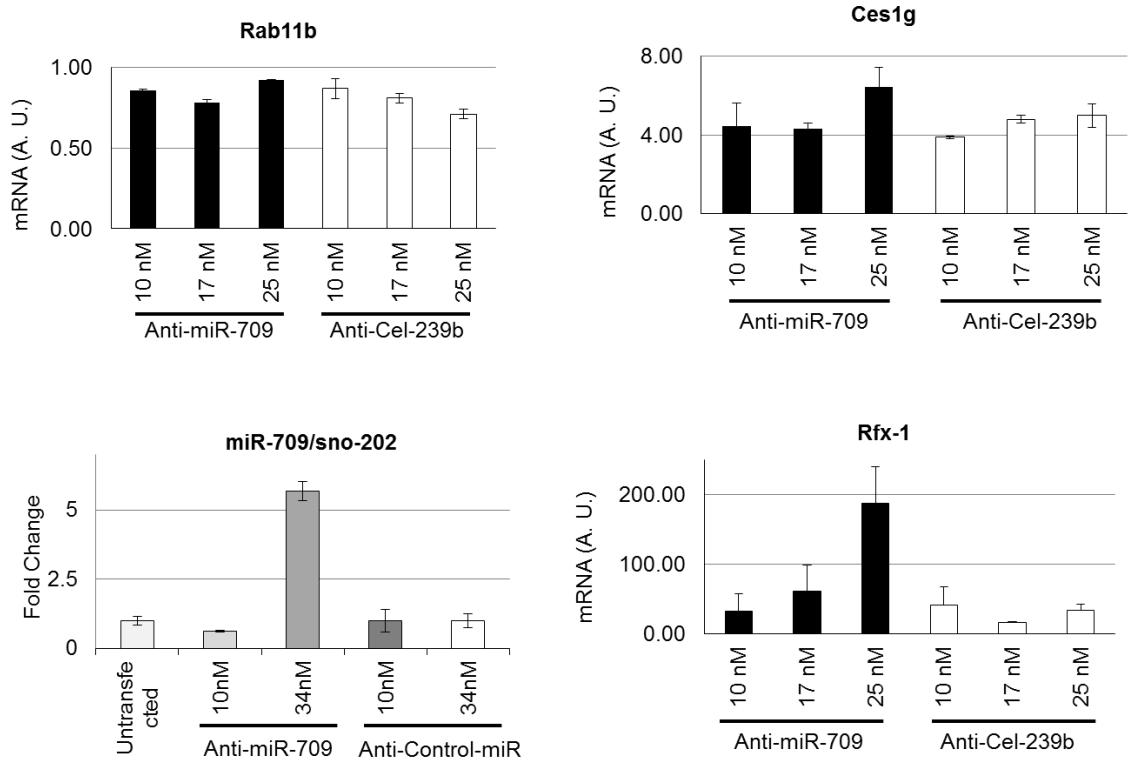


**Figure 36. miR-709, Rab11b, Ces1g and Rfx-1 expression in primary hepatocytes transfected with anti-miR-709.** Primary hepatocytes were transfected with 10, 17 or 25 nM of miRIDIAN miRNA inhibitor against miR-709 or control inhibitor, and harvested 24 hours post-transfection (n=2; error bars represent standard deviation). Real time RT-PCR analysis of Rab11b, Ces1g and Rfx-1. Cyclophilin A was used as normalizer gene. Primary hepatocytes were transfected with 10 or 34 nM of mirVana miRNA inhibitor against miR-709 or control inhibitor, and harvested 24 hours later. Mature miR-709 was quantified by TaqMan miRNA assay. Small nucleolar RNA 202 (snoRNA-202) was used as normalizer.

We then analyzed the impact of inhibiting miR-709 in actively dividing cells. Hepal1c1c cells were transfected with amounts of antagomiR that were not toxic: 25 and

50 nM. Cell viability was then tested over time using an LDH assay. Inhibition of miR-709 in hepatoma cells resulted in reduced viable cells at 50 nM concentration 72 hours post-transfection (Figure 37). As shown for quiescent cells, these data suggest that miR-709 cannot be downregulated in actively dividing cells.

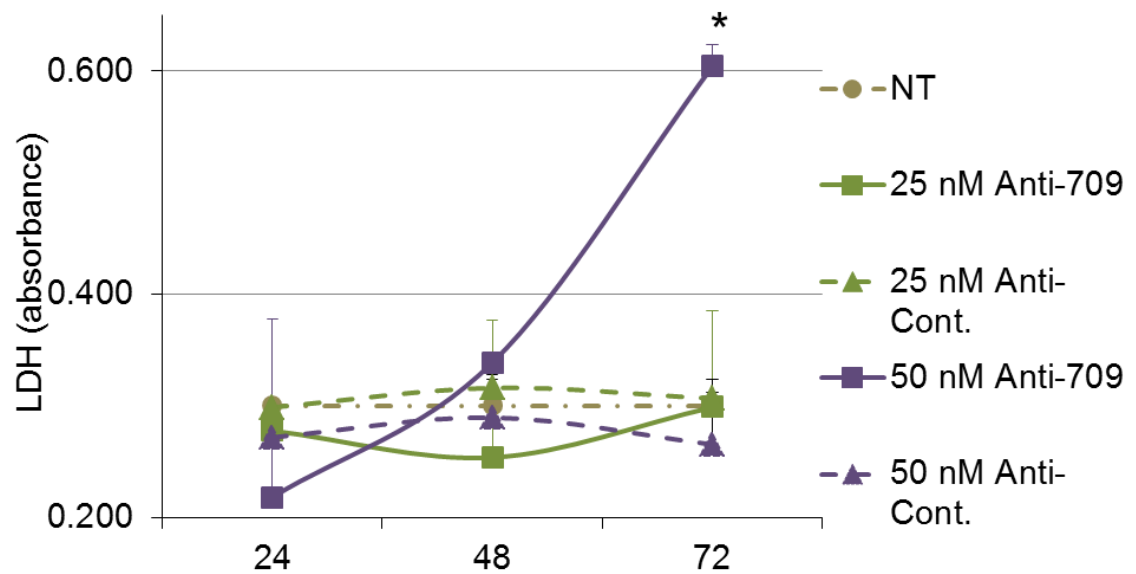


**Figure 37. Cell viability assay in Hepa1c1c cells transfected with miR-709 inhibitor.**

Hepa1c1c cells were transfected with 25 or 50 nM of mirVana miRNA inhibitor against miR-709 or control inhibitor, and media was replaced 24 hours post-transfection. One-hundred  $\mu$ l of media was collected 24, 48 and 72 hours post-transfection for LDH analysis. (n=3; error bars represent standard deviation). NT, not transfected.

### C.5. Mature levels of miR-709 do not increase in *db/db* livers

We have shown that miR-709 is upregulated in an animal model of type 2 diabetes (Figure 11). To validate the microarray data and determine whether the increase in miR-709 is the mature form, Taqman assays were performed using total RNA. Figure 38 shows that no difference was observed between *db/db* and normal mice, indicating that the increase in miR-709 detected in the chip array is likely to be precursor.

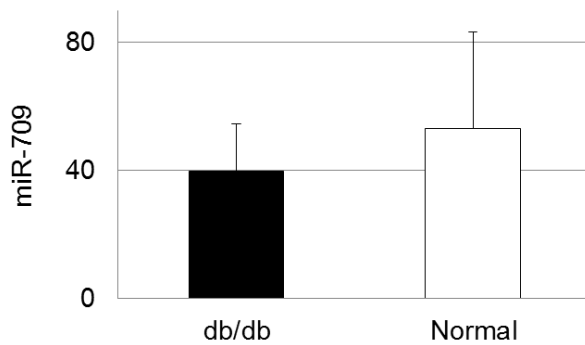


**Figure 38. Levels of mature miR-709 in livers of *db/db* mice.** Normal and *db/db* livers were used to quantify mature miR-709 by TaqMan assay (n=4).

## DISCUSSION

miRNAs play an important role in various cellular processes such as metabolism, development and apoptosis<sup>154</sup>. miRNAs are variably expressed across different tissues<sup>155</sup>, and the presence of abnormal profiles has been associated with various human disorders<sup>154</sup>. Despite emerging evidence of the role of miRNAs at regulating tissue function, there is a scarcity of information on their role at controlling the complex processes that take place in the liver. Therefore, we sought to identify miRNAs expressed in this tissue. By miRNA profiling between normal and *db/db* mice, we found that miR-709 was upregulated in livers of diabetic mice. This has been recently confirmed in another study, in which many miRNAs were found dysregulated in type 2 diabetes<sup>156</sup>. We also observed that miR-709 was one of the most abundant miRNAs in murine liver, and recent studies have also showed high abundance of miR-709 in this tissue<sup>97,145,157</sup>. However, the increase of miR-709 in *db/db* mice livers could not be validated by Taqman PCR assay. This suggests that the increased miR-709 levels detected in *db/db* mice could potentially be pre-miR-709, given that the chip assay detects both, precursor and mature form, while the Taqman assay detects only mature miR-709. We have shown that the levels of miR-709 precursor are highly abundant in liver. It has been shown that miR-709 has a function in the nucleus of fibroblasts, regulating levels of another miRNA (see next page). Thus, it is possible that in hepatocytes, the precursor also has a role in this cellular compartment, and the upregulation of miR-709 in *db/db* liver has implications for this unknown function.

Given that miRNA are largely regulated by RNA polymerase II, we anticipated that their levels would change to repress/derepress genes that are not required during the physiological responses that take place between the fasted and refed conditions. Remarkably, of all 61 miRNAs differentially expressed, all but one were downregulated during the refed state, indicating that miRNA silence genes during fasting conditions, and their role as inhibitors of gene expression is more important in this state than during refeeding. Likewise, in the process of aging, it has been reported that hepatic miRNAs increase, but none decreases<sup>97</sup>. This phenomenon is also seen in aging-related Alzheimer disease in human brains<sup>97</sup>. Nevertheless, miR-709 was not influenced by the change in hepatic nutritional/hormonal changes, suggesting it is not a critical miRNA for the response that controls glucose, fatty acid and ketone body metabolism.

Post-transcriptionally, miRNAs are processed through multiple steps and eventually form a linear miRNA:miRNA\* duplex. Only one of these strands is selected to be incorporated into RISC, based on the thermodynamic instability and weaker base-pairing at the 5' end of the strands<sup>158,159</sup>. For some miRNAs, both strands can be loaded into RISC. For miR-709, the 3p has been reported as the active strand (data from the miRBase database). Our data confirms that this is also the case in liver, where the miR-709-3p is the only strand used as guide.

Mammalian miRNAs can target multiple genes from various pathways<sup>160</sup>. In murine liver, miR-709 has been reported to increase with aging<sup>97</sup>. Correlation of the predicted targets with a proteome and transcriptome profile of aging liver suggested that

this miRNA impacts genes in cytoskeletal function<sup>97</sup>. Thus, given the lack of knowledge on validated targets of miR-709, and its high abundance in liver, we sought to find its target genes. Our data indicates that miR-709 downregulates genes important in cytoskeleton structure, endocytosis and cellular adhesion pathways, as well as lipid metabolism. We confirmed that at least three of the identified genes, Rab11b, Ces1g and Pctp, are direct targets of miR-709 and that the absence of miR-709 binding site/s in the 3' UTR of these target genes leads to lack of inhibition. Downregulation of several targets, including Rab11b, was confirmed at the protein level in murine liver cells and the hepatoma cell line Hepa1c1c.

There has been a lot of disparity between the predicted targets of a miRNA across various databases and the bona fide miRNA targets<sup>161</sup>. Hence, we compared the results from the microarray with the predicted targets of miR-709 across multiple databases to evaluate the extent of overlap with observed gene targets. Of the 6 databases used, we found that miRanda, miRWalk, DIANAmT and PICTAR5 had algorithms that best predicted miR-709 targets, with 60-70% of gene predictions being identified by microarray analysis. miRDB, TargetScan and RNA22 predicted less than 22% of the genes that were found downregulated in the microarray analysis. Hence, using multiple databases with good prediction score is a key to identifying miRNA targets.

In the three dimensional structure of the liver, hepatocytes must be polarized with apical and basolateral membranes to be functional<sup>12</sup>. The two domains are separated by tight junctions<sup>8</sup>. Bile canaliculi are formed on the apical membrane of two adjacent

hepatocytes and bile acid transporters are confined to this area<sup>8,143</sup>. Based on the pathways targeted by miR-709, we hypothesized that this miRNA might regulate the capacity of hepatocytes to polarize and form functional bile canaliculi. Our data suggests that miR-709 does not affect the capacity of hepatocytes to maintain the apical-basolateral polarity. Cells transfected with miR-709 and cultured in a sandwich culture model were able to form bile canaliculi and transport sodium fluorescein in a similar manner as Cel-239b-treated cells, implying that increased levels of mature miR-709 does not compromise liver organization. In addition, miR-709 sandwich cultures had similar survival times as Cel-239b-transfected cultures. Furthermore, primary hepatocytes cultured in a monolayer and transfected with miR-709 did not have faster rates of cell death over the course of 5 days relative to Cel-239b transfected hepatocytes (data not shown). Thus, miR-709 regulates genes that in a quiescent tissue do not affect cell survival or the capacity to maintain normal cellular architecture. Instead, our data suggests that miR-709 may be needed to facilitate cellular detachment from the extracellular matrix and cytoskeletal reorganization, processes that are needed after liver injury and repopulation, or during tumorigenesis.

In fibroblasts, it was shown that miR-709 controls the maturation of miR-15a/16-1<sup>145</sup>. In humans, this miRNA cluster is most commonly found deleted in chronic lymphocytic leukemia (CLL)<sup>162</sup>. The miR-15a/16-1 cluster of miRNAs has been shown to target the anti-apoptotic gene, Bcl-2<sup>145</sup> as well as genes involved in cell cycle<sup>163</sup>. Under apoptotic stimuli, miR-709 changed its nuclear localization and was transported into the cytoplasm in fibroblasts<sup>145</sup>. This resulted in loss of inhibition of miR-15a/16-1 processing



and led to downregulation of Bcl-2<sup>145</sup>. However, Bcl-2 is not expressed in murine liver<sup>164,165</sup> and therefore, it is unlikely that in this tissue miR-709 regulates apoptosis through the same mechanism. Furthermore, miR-709 has been shown to control expression of Brother Of the Regulator of Imprinted Sites (BORIS) in mouse testis<sup>166</sup>. BORIS is a testes-specific gene and an important regulator of DNA methylation and imprinting, and regulates epigenetic reprogramming during differentiation of germ cells<sup>167</sup>. However, this gene is not expressed in liver<sup>167</sup>. Thus, miR-709 may target distinct genes in different tissues.

It has recently been reported that mature miR-709 is predominantly a nuclear miRNA in various cell lines and tissues<sup>145</sup>. The data were generated by analysis of RNA from nuclear and cytoplasmic fractions, as well as by transfection of L929 fibroblasts with a synthetic 5'-FAM-labeled miR-709 duplex probe<sup>145</sup>. Tamminga and colleagues have shown by *in situ* hybridization that miR-709 is predominantly located in the nucleus in testis<sup>166</sup>. Thus, we used a 3'-FAM-labeled synthetic miR-709 mimic to study the cellular localization of the mature miR-709 in liver. Our data indicates that mature miR-709 is localized only in the cytoplasm of primary hepatocytes and Hepa1c1c cells under normal and metabolic stress culture conditions. It is possible that the location of mature miR-709 is different depending on the tissue, and in fibroblasts it is more nuclear than cytoplasmic. We have shown that in the liver, the precursor of miR-709 is significantly more abundant than the mature form, opposite to what is typically observed for the majority of miRNA. This has been reported to be the case across other mouse tissues, including brain, spinal cord, and heart<sup>147</sup>. The *in situ* hybridization study by Tamminga *et*

*al.*<sup>166</sup>, is consistent with higher levels of precursor in the nucleus, as the probe is likely to have detected the precursor and mature forms. The study showed the majority of the signal was present in the nucleus. Interestingly, miR-709 is not the only miRNA displaying this pattern: miR-690 and miR-720 also abundantly accumulate their precursors, while the mature form is scarce. The biological significance of the large accumulation of precursor, is currently unknown.

We have also shown that in mouse models of cancer and liver regeneration, the levels of mature miR-709 increase significantly, suggesting a role in cell division. Supporting these observations, inhibition of miR-709 in hepatoma cells, leads to diminished cell survival. To determine the role of miR-709 in quiescent and actively dividing cells, antagomiRs were used to deplete endogenous levels of miR-709. Transfection of primary hepatocytes with antagomirs did not lead to a concomitant upregulation of miR-709 targets Rab11b and Ces1g. Instead, we observed a dose response increase in the expression of miR-709 as more antagomiR was used. This suggests that miR-709 may have vital functions in the liver and cannot be inhibited in hepatocytes, even though these cells seem to be able to tolerate a multiple-fold increase of mature miR-709. In Hepa1c1c cells, depletion of miR-709 resulted in a decrease in cell viability, which was not seen in primary hepatocytes at similar antagomiR concentration, suggesting that appropriate levels of this miRNA may be more critical for proliferating than quiescent cells.

The increase in miR-709 in liver tumors was accompanied by an increase in transcription of its host gene, Rfx1. Rfx1 is a transcription factor with transcription activation as well as repression activity. It is ubiquitously expressed, and is abundant in liver, with expression levels similar to genes implicated in metabolic functions such as insulin receptor substrate (Irs2), forkhead box protein O1 (Foxo1) or sirtuin 1 (Sirt1) (data not shown). Lack of Rfx1 results in early embryonic lethality<sup>168</sup>. Rfx1 inhibits its own expression, as well as genes implicated in cell proliferation such as PCNA and c-Myc<sup>151-153</sup>. Although information on its function in liver is scarce, it has been recently shown that Rfx1 binds to the promoters of silent genes, such as Cdx2, and inhibit their activation by FoxA2. Cdx2 is a homeodomain transcription factor that determines intestinal epithelium differentiation and its ectopic expression has been associated with neoplastic processes. Indeed, Rfx1 downregulation is associated with esophageal carcinoma<sup>169</sup>. The same study showed that using siRNA to knockdown Rfx1, a maximum of 50% silencing could be obtained in a mouse epithelial cell line. As the mRNA levels were downregulated by the siRNA, Rfx1 gene transcription would increase<sup>169</sup>. We have observed that miR-709 downregulation with antagomiRs leads to an increase in miR-709 levels. Thus, miR-709 and Rfx1 seem to work in a coordinated manner, and depletion of either one leads to feedback activation to compensate for the decrease in their levels. Perhaps miR-709 accumulates in the nucleus to regulate expression of its own host gene. Finally, it is possible that Rfx1 increases in our models of cell proliferation to inhibit expression of epithelial non-hepatic genes and retain liver function.

MiR-709 is not a conserved miRNA; the human ortholog is hsa-miR-1827, and shares the same seed sequence. Thus, an exciting study will be to determine whether the pathways regulated by hsa-miR-1827 are the same as those regulated by miR-709. Many of the predicted genes are the same or are within the same family. Thus, we predict that the hsa-miR-1827 will have a similar role to mmu-miR-709. It will be interesting to conduct studies in human samples and/or cell lines to establish its function in normal liver, as well as pathological conditions.

In summary, miR-709 is most abundant in the pre-miR-709 form in the normal liver and is processed further to mature miR-709 only under conditions requiring cell division, such as cancer and liver regeneration. It is then that the mature miR-709 can bind to targets such as Rab11b, Ces1g, Pctp and Timp3 and aid in cellular regeneration perhaps by shutting down pathways that are not vital to the cell at that stage.

## FUTURE DIRECTIONS

Our study identified miR-709 as one of the most abundant miRNAs in murine liver and for the first time identified Rab11b, Ces1g and Pctp as direct targets. Recently, miR-709 has been found upregulated by 3.6-fold in *db/db* mice, an animal model of type 2 diabetes mellitus<sup>156</sup>, by ~7-fold in livers of aging mice<sup>97</sup>, in X-ray irradiated mouse testis<sup>166</sup>, and during liver regeneration and hepatocellular carcinoma (this work). This suggests a role for this miRNA in the response of liver to stress conditions. Future *in vivo* studies are needed to address the physiological consequence of knocking down miR-709 in type 2 diabetes liver, aging liver and hepatocellular carcinoma to study its role in these conditions. It is also intriguing that such high levels of precursor accumulate in the nucleus, which suggests an additional role in this compartment. miR-709 is not a conserved miRNA, and the ortholog miRNA in humans is hsa-mir-1827, which has the same seed sequence. Given the role of miR-709 in hepatocellular carcinoma and its potential role in liver regeneration, future studies should include characterizing its function in normal human liver, as well as analyzing human carcinoma samples to determine whether hsa-mir-1827 is dysregulated, and establishing its potential as a therapeutic target.

## LIST OF REFERENCES

1. Reinhart BJ, Slack FJ, Basson M, et al. The 21-nucleotide let-7 RNA regulates developmental timing in *Caenorhabditis elegans*. *Nature* 2000;403:901-6.
2. Brennecke J, Hipfner DR, Stark A, Russell RB, Cohen SM. bantam encodes a developmentally regulated microRNA that controls cell proliferation and regulates the proapoptotic gene hid in *Drosophila*. *Cell* 2003;113:25-36.
3. Xu P, Vernooy SY, Guo M, Hay BA. The *Drosophila* microRNA Mir-14 suppresses cell death and is required for normal fat metabolism. *Curr Biol* 2003;13:790-5.
4. Chen CZ, Li L, Lodish HF, Bartel DP. MicroRNAs modulate hematopoietic lineage differentiation. *Science* 2004;303:83-6.
5. Krutzfeldt J, Rajewsky N, Braich R, et al. Silencing of microRNAs in vivo with 'antagomirs'. *Nature* 2005;438:685-9.
6. Ambros V. Control of developmental timing in *Caenorhabditis elegans*. *Curr Opin Genet Dev* 2000;10:428-33.
7. Lagos-Quintana M, Rauhut R, Yalcin A, Meyer J, Lendeckel W, Tuschl T. Identification of tissue-specific microRNAs from mouse. *Curr Biol* 2002;12:735-9.
8. Treyer A, Musch A. Hepatocyte polarity. *Compr Physiol* 2013;3:243-87.
9. Boyer JL. Bile formation and secretion. *Compr Physiol* 2013;3:1035-78.
10. Jungermann K. Role of intralobular compartmentation in hepatic metabolism. *Diabete & metabolisme* 1992;18:81-6.
11. Malarkey DE, Johnson K, Ryan L, Boorman G, Maronpot RR. New insights into functional aspects of liver morphology. *Toxicologic pathology* 2005;33:27-34.

12. Dunn JC, Tompkins RG, Yarmush ML. Long-term in vitro function of adult hepatocytes in a collagen sandwich configuration. *Biotechnology progress* 1991;7:237-45.
13. Decaens C, Durand M, Grosse B, Cassio D. Which in vitro models could be best used to study hepatocyte polarity? *Biology of the cell / under the auspices of the European Cell Biology Organization* 2008;100:387-98.
14. Abu-Absi SF, Friend JR, Hansen LK, Hu WS. Structural polarity and functional bile canaliculi in rat hepatocyte spheroids. *Exp Cell Res* 2002;274:56-67.
15. Watanabe N, Tsukada N, Smith CR, Phillips MJ. Motility of bile canaliculi in the living animal: implications for bile flow. *J Cell Biol* 1991;113:1069-80.
16. Takahashi S, Kubo K, Waguri S, et al. Rab11 regulates exocytosis of recycling vesicles at the plasma membrane. *J Cell Sci* 2012;125:4049-57.
17. Rahner C, Stieger B, Landmann L. Apical endocytosis in rat hepatocytes In situ involves clathrin, traverses a subapical compartment, and leads to lysosomes. *Gastroenterology* 2000;119:1692-707.
18. Enrich C, Pol A, Calvo M, Pons M, Jackle S. Dissection of the multifunctional "Receptor-Recycling" endocytic compartment of hepatocytes. *Hepatology* 1999;30:1115-20.
19. Saetrom P, Snove O, Nedland M, et al. Conserved microRNA characteristics in mammals. *Oligonucleotides* 2006;16:115-44.
20. Jung HJ, Suh Y. MicroRNA in Aging: From Discovery to Biology. *Current genomics* 2012;13:548-57.
21. Bentwich I, Avniel A, Karov Y, et al. Identification of hundreds of conserved and nonconserved human microRNAs. *Nat Genet* 2005;37:766-70.
22. Friedman RC, Farh KK, Burge CB, Bartel DP. Most mammalian mRNAs are conserved targets of microRNAs. *Genome Res* 2009;19:92-105.

23. Chekulaeva M, Filipowicz W. Mechanisms of miRNA-mediated post-transcriptional regulation in animal cells. *Curr Opin Cell Biol* 2009;21:452-60.
24. Guo H, Ingolia NT, Weissman JS, Bartel DP. Mammalian microRNAs predominantly act to decrease target mRNA levels. *Nature* 2010;466:835-40.
25. Behm-Ansmant I, Rehwinkel J, Doerks T, Stark A, Bork P, Izaurralde E. mRNA degradation by miRNAs and GW182 requires both CCR4:NOT deadenylase and DCP1:DCP2 decapping complexes. *Genes Dev* 2006;20:1885-98.
26. Borchert GM, Lanier W, Davidson BL. RNA polymerase III transcribes human microRNAs. *Nature structural & molecular biology* 2006;13:1097-101.
27. Faller M, Guo F. MicroRNA biogenesis: there's more than one way to skin a cat. *Biochimica et biophysica acta* 2008;1779:663-7.
28. Ceccarelli S, Panera N, Gnani D, Nobili V. Dual Role of MicroRNAs in NAFLD. *International journal of molecular sciences* 2013;14:8437-55.
29. Cai X, Hagedorn CH, Cullen BR. Human microRNAs are processed from capped, polyadenylated transcripts that can also function as mRNAs. *Rna* 2004;10:1957-66.
30. Filipowicz W, Bhattacharyya SN, Sonenberg N. Mechanisms of post-transcriptional regulation by microRNAs: are the answers in sight? *Nature reviews Genetics* 2008;9:102-14.
31. Bartel DP. MicroRNAs: genomics, biogenesis, mechanism, and function. *Cell* 2004;116:281-97.
32. Creighton CJ, Reid JG, Gunaratne PH. Expression profiling of microRNAs by deep sequencing. *Briefings in bioinformatics* 2009;10:490-7.
33. Okamura K, Phillips MD, Tyler DM, Duan H, Chou YT, Lai EC. The regulatory activity of microRNA\* species has substantial influence on microRNA and 3' UTR evolution. *Nature structural & molecular biology* 2008;15:354-63.
34. Ro S, Park C, Young D, Sanders KM, Yan W. Tissue-dependent paired expression of miRNAs. *Nucleic acids research* 2007;35:5944-53.



35. Du T, Zamore PD. microPrimer: the biogenesis and function of microRNA. *Development* 2005;132:4645-52.
36. Winter J, Jung S, Keller S, Gregory RI, Diederichs S. Many roads to maturity: microRNA biogenesis pathways and their regulation. *Nature cell biology* 2009;11:228-34.
37. Lynn FC. Meta-regulation: microRNA regulation of glucose and lipid metabolism. *Trends in endocrinology and metabolism: TEM* 2009;20:452-9.
38. Mencia A, Modamio-Hoybjor S, Redshaw N, et al. Mutations in the seed region of human miR-96 are responsible for nonsyndromic progressive hearing loss. *Nat Genet* 2009;41:609-13.
39. Hughes AE, Bradley DT, Campbell M, et al. Mutation altering the miR-184 seed region causes familial keratoconus with cataract. *American journal of human genetics* 2011;89:628-33.
40. de Pontual L, Yao E, Callier P, et al. Germline deletion of the miR-17 approximately 92 cluster causes skeletal and growth defects in humans. *Nat Genet* 2011;43:1026-30.
41. Llave C, Xie Z, Kasschau KD, Carrington JC. Cleavage of Scarecrow-like mRNA targets directed by a class of Arabidopsis miRNA. *Science* 2002;297:2053-6.
42. Yekta S, Shih IH, Bartel DP. MicroRNA-directed cleavage of HOXB8 mRNA. *Science* 2004;304:594-6.
43. Huntzinger E, Izaurralde E. Gene silencing by microRNAs: contributions of translational repression and mRNA decay. *Nature reviews Genetics* 2011;12:99-110.
44. Bhattacharyya SN, Habermacher R, Martine U, Closs EI, Filipowicz W. Relief of microRNA-mediated translational repression in human cells subjected to stress. *Cell* 2006;125:1111-24.
45. Orom UA, Nielsen FC, Lund AH. MicroRNA-10a binds the 5'UTR of ribosomal protein mRNAs and enhances their translation. *Molecular cell* 2008;30:460-71.

46. He A, Zhu L, Gupta N, Chang Y, Fang F. Overexpression of micro ribonucleic acid 29, highly up-regulated in diabetic rats, leads to insulin resistance in 3T3-L1 adipocytes. *Molecular endocrinology* 2007;21:2785-94.
47. Kerr TA, Korenblat KM, Davidson NO. MicroRNAs and liver disease. *Translational research : the journal of laboratory and clinical medicine* 2011;157:241-52.
48. Filipowicz W, Jaskiewicz L, Kolb FA, Pillai RS. Post-transcriptional gene silencing by siRNAs and miRNAs. *Current opinion in structural biology* 2005;15:331-41.
49. Walker MD. Role of MicroRNA in pancreatic beta-cells: where more is less. *Diabetes* 2008;57:2567-8.
50. Trajkovski M, Hausser J, Soutschek J, et al. MicroRNAs 103 and 107 regulate insulin sensitivity. *Nature* 2011;474:649-53.
51. Zheng L, Lv GC, Sheng J, Yang YD. Effect of miRNA-10b in regulating cellular steatosis level by targeting PPAR-alpha expression, a novel mechanism for the pathogenesis of NAFLD. *Journal of gastroenterology and hepatology* 2010;25:156-63.
52. Hu J, Xu Y, Hao J, Wang S, Li C, Meng S. MiR-122 in hepatic function and liver diseases. *Protein & cell* 2012;3:364-71.
53. Filipowicz W, Grosshans H. The liver-specific microRNA miR-122: biology and therapeutic potential. *Progress in drug research Fortschritte der Arzneimittelforschung Progres des recherches pharmaceutiques* 2011;67:221-38.
54. Girard M, Jacquemin E, Munnich A, Lyonnet S, Henrion-Caude A. miR-122, a paradigm for the role of microRNAs in the liver. *Journal of hepatology* 2008;48:648-56.
55. Chang J, Nicolas E, Marks D, et al. miR-122, a mammalian liver-specific microRNA, is processed from hcr mRNA and may downregulate the high affinity cationic amino acid transporter CAT-1. *RNA biology* 2004;1:106-13.
56. Esau C, Davis S, Murray SF, et al. miR-122 regulation of lipid metabolism revealed by in vivo antisense targeting. *Cell metabolism* 2006;3:87-98.

57. Callegari E, Elamin BK, Sabbioni S, Gramantieri L, Negrini M. Role of microRNAs in hepatocellular carcinoma: a clinical perspective. *OncoTargets and therapy* 2013;6:1167-78.
58. Fan CG, Wang CM, Tian C, et al. miR-122 inhibits viral replication and cell proliferation in hepatitis B virus-related hepatocellular carcinoma and targets NDRG3. *Oncology reports* 2011;26:1281-6.
59. Hsu SH, Wang B, Kota J, et al. Essential metabolic, anti-inflammatory, and anti-tumorigenic functions of miR-122 in liver. *The Journal of clinical investigation* 2012;122:2871-83.
60. Hoekstra M, van der Sluis RJ, Kuiper J, Van Berkel TJ. Nonalcoholic fatty liver disease is associated with an altered hepatocyte microRNA profile in LDL receptor knockout mice. *The Journal of nutritional biochemistry* 2012;23:622-8.
61. Najafi-Shoushtari SH, Kristo F, Li Y, et al. MicroRNA-33 and the SREBP host genes cooperate to control cholesterol homeostasis. *Science* 2010;328:1566-9.
62. Hua X, Yokoyama C, Wu J, et al. SREBP-2, a second basic-helix-loop-helix-leucine zipper protein that stimulates transcription by binding to a sterol regulatory element. *Proceedings of the National Academy of Sciences of the United States of America* 1993;90:11603-7.
63. Yokoyama C, Wang X, Briggs MR, et al. SREBP-1, a basic-helix-loop-helix-leucine zipper protein that controls transcription of the low density lipoprotein receptor gene. *Cell* 1993;75:187-97.
64. Horton JD, Goldstein JL, Brown MS. SREBPs: activators of the complete program of cholesterol and fatty acid synthesis in the liver. *The Journal of clinical investigation* 2002;109:1125-31.
65. Rayner KJ, Sheedy FJ, Esau CC, et al. Antagonism of miR-33 in mice promotes reverse cholesterol transport and regression of atherosclerosis. *The Journal of clinical investigation* 2011;121:2921-31.
66. Rayner KJ, Suarez Y, Davalos A, et al. MiR-33 contributes to the regulation of cholesterol homeostasis. *Science* 2010;328:1570-3.

67. Davalos A, Goedeke L, Smibert P, et al. miR-33a/b contribute to the regulation of fatty acid metabolism and insulin signaling. *Proceedings of the National Academy of Sciences of the United States of America* 2011;108:9232-7.
68. Cheung O, Puri P, Eicken C, et al. Nonalcoholic steatohepatitis is associated with altered hepatic MicroRNA expression. *Hepatology* 2008;48:1810-20.
69. Min HK, Kapoor A, Fuchs M, et al. Increased hepatic synthesis and dysregulation of cholesterol metabolism is associated with the severity of nonalcoholic fatty liver disease. *Cell metabolism* 2012;15:665-74.
70. Nakanishi N, Nakagawa Y, Tokushige N, et al. The up-regulation of microRNA-335 is associated with lipid metabolism in liver and white adipose tissue of genetically obese mice. *Biochem Biophys Res Commun* 2009;385:492-6.
71. Iliopoulos D, Drosatos K, Hiyama Y, Goldberg IJ, Zannis VI. MicroRNA-370 controls the expression of microRNA-122 and Cpt1alpha and affects lipid metabolism. *Journal of lipid research* 2010;51:1513-23.
72. Ahn J, Lee H, Chung CH, Ha T. High fat diet induced downregulation of microRNA-467b increased lipoprotein lipase in hepatic steatosis. *Biochem Biophys Res Commun* 2011;414:664-9.
73. Kumar S, Zou Y, Bao Q, Wang M, Dai G. Proteomic analysis of immediate-early response plasma proteins after 70% and 90% partial hepatectomy. *Hepatology research : the official journal of the Japan Society of Hepatology* 2013;43:876-89.
74. Betel D, Wilson M, Gabow A, Marks DS, Sander C. The microRNA.org resource: targets and expression. *Nucleic acids research* 2008;36:D149-53.
75. Park JS, Surendran S, Kamendulis LM, Morral N. Comparative nucleic acid transfection efficacy in primary hepatocytes for gene silencing and functional studies. *BMC Res Notes* 2011;4:8.
76. Kreamer BL, Staecker JL, Sawada N, Sattler GL, Hsia MT, Pitot HC. Use of a low-speed, iso-density percoll centrifugation method to increase the viability of isolated rat hepatocyte preparations. *In vitro cellular & developmental biology : journal of the Tissue Culture Association* 1986;22:201-11.

77. Swift B, Pfeifer ND, Brouwer KL. Sandwich-cultured hepatocytes: an in vitro model to evaluate hepatobiliary transporter-based drug interactions and hepatotoxicity. *Drug metabolism reviews* 2010;42:446-71.
78. Schindelin J, Arganda-Carreras I, Frise E, et al. Fiji: an open-source platform for biological-image analysis. *Nat Methods* 2012;9:676-82.
79. Wang X. miRDB: a microRNA target prediction and functional annotation database with a wiki interface. *Rna* 2008;14:1012-7.
80. Wang X, El Naqa IM. Prediction of both conserved and nonconserved microRNA targets in animals. *Bioinformatics* 2008;24:325-32.
81. Dweep H, Sticht C, Pandey P, Gretz N. miRWalk--database: prediction of possible miRNA binding sites by "walking" the genes of three genomes. *Journal of biomedical informatics* 2011;44:839-47.
82. Lewis BP, Burge CB, Bartel DP. Conserved seed pairing, often flanked by adenosines, indicates that thousands of human genes are microRNA targets. *Cell* 2005;120:15-20.
83. Vlachos IS, Kostoulas N, Vergoulis T, et al. DIANA miRPath v.2.0: investigating the combinatorial effect of microRNAs in pathways. *Nucleic acids research* 2012;40:W498-504.
84. Alexiou P, Vergoulis T, Gleditsch M, et al. miRGen 2.0: a database of microRNA genomic information and regulation. *Nucleic acids research* 2010;38:D137-41.
85. Griffiths-Jones S. The microRNA Registry. *Nucleic acids research* 2004;32:D109-11.
86. Griffiths-Jones S, Grocock RJ, van Dongen S, Bateman A, Enright AJ. miRBase: microRNA sequences, targets and gene nomenclature. *Nucleic acids research* 2006;34:D140-4.
87. Griffiths-Jones S, Saini HK, van Dongen S, Enright AJ. miRBase: tools for microRNA genomics. *Nucleic acids research* 2008;36:D154-8.

88. Kozomara A, Griffiths-Jones S. miRBase: integrating microRNA annotation and deep-sequencing data. *Nucleic acids research* 2011;39:D152-7.
89. Kozomara A, Griffiths-Jones S. miRBase: annotating high confidence microRNAs using deep sequencing data. *Nucleic acids research* 2014;42:D68-73.
90. Meyers BC, Axtell MJ, Bartel B, et al. Criteria for annotation of plant MicroRNAs. *The Plant cell* 2008;20:3186-90.
91. Ambros V, Bartel B, Bartel DP, et al. A uniform system for microRNA annotation. *Rna* 2003;9:277-9.
92. Krek A, Grun D, Poy MN, et al. Combinatorial microRNA target predictions. *Nat Genet* 2005;37:495-500.
93. Miranda KC, Huynh T, Tay Y, et al. A pattern-based method for the identification of MicroRNA binding sites and their corresponding heteroduplexes. *Cell* 2006;126:1203-17.
94. Kim SW, Li Z, Moore PS, et al. A sensitive non-radioactive northern blot method to detect small RNAs. *Nucleic acids research* 2010;38:e98.
95. Takata A, Otsuka M, Yoshikawa T, Kishikawa T, Ohno M, Koike K. MicroRNAs and liver function. *Minerva gastroenterologica e dietologica* 2013;59:187-203.
96. Sekine S, Ogawa R, Ito R, et al. Disruption of Dicer1 induces dysregulated fetal gene expression and promotes hepatocarcinogenesis. *Gastroenterology* 2009;136:2304-15 e1-4.
97. Maes OC, An J, Sarojini H, Wang E. Murine microRNAs implicated in liver functions and aging process. *Mechanisms of ageing and development* 2008;129:534-41.
98. Mullokandov G, Baccarini A, Ruzo A, et al. High-throughput assessment of microRNA activity and function using microRNA sensor and decoy libraries. *Nat Methods* 2012;9:840-6.

99. Zhang F, Xu X, Zhou B, He Z, Zhai Q. Gene expression profile change and associated physiological and pathological effects in mouse liver induced by fasting and refeeding. *PloS one* 2011;6:e27553.
100. Desert C, Duclos MJ, Blavy P, et al. Transcriptome profiling of the feeding-to-fasting transition in chicken liver. *BMC genomics* 2008;9:611.
101. Zhou L, He J, Zhang Y. MicroRNA-22 expression in hepatocellular carcinoma and its correlation with ezrin protein. *The Journal of international medical research* 2013;41:1009-16.
102. Shi C, Xu X. MicroRNA-22 is down-regulated in hepatitis B virus-related hepatocellular carcinoma. *Biomedicine & pharmacotherapy = Biomedecine & pharmacotherapie* 2013;67:375-80.
103. Zhang J, Yang Y, Yang T, et al. microRNA-22, downregulated in hepatocellular carcinoma and correlated with prognosis, suppresses cell proliferation and tumorigenicity. *British journal of cancer* 2010;103:1215-20.
104. Li LH, Gao Q, Wang XY, Guo ZJ. [miR-378 suppresses HBV-related hepatocellular carcinoma tumor growth by directly targeting the insulin-like growth factor 1 receptor]. *Zhonghua gan zang bing za zhi = Zhonghua ganzangbing zazhi = Chinese journal of hepatology* 2013;21:609-13.
105. Chen DL, Wang ZQ, Zeng ZL, et al. Identification of MicroRNA-214 as a negative regulator of colorectal cancer liver metastasis by way of regulation of fibroblast growth factor receptor 1 expression. *Hepatology* 2014.
106. Zhang J, Jin H, Liu H, et al. MiRNA-99a directly regulates AGO2 through translational repression in hepatocellular carcinoma. *Oncogenesis* 2014;3:e97.
107. Ding J, Huang S, Wang Y, et al. Genome-wide screening reveals that miR-195 targets the TNF-alpha/NF-kappaB pathway by down-regulating IkappaB kinase alpha and TAB3 in hepatocellular carcinoma. *Hepatology* 2013;58:654-66.
108. Chen Z, Ma T, Huang C, et al. MiR-27a modulates the MDR1/P-glycoprotein expression by inhibiting FZD7/beta-catenin pathway in hepatocellular carcinoma cells. *Cellular signalling* 2013;25:2693-701.

109. Henry JC, Park JK, Jiang J, et al. miR-199a-3p targets CD44 and reduces proliferation of CD44 positive hepatocellular carcinoma cell lines. *Biochem Biophys Res Commun* 2010;403:120-5.
110. Ji J, Zhao L, Budhu A, et al. Let-7g targets collagen type I alpha2 and inhibits cell migration in hepatocellular carcinoma. *Journal of hepatology* 2010;52:690-7.
111. Gong FX, Xia JL, Yang BW, Xu XJ, Wu WZ. [Effect of let-7c on the proliferation of human hepatocellular carcinoma cell HCCLM3]. *Zhonghua gan zang bing za zhi = Zhonghua ganzangbing zazhi = Chinese journal of hepatology* 2011;19:853-6.
112. Gramantieri L, Ferracin M, Fornari F, et al. Cyclin G1 is a target of miR-122a, a microRNA frequently down-regulated in human hepatocellular carcinoma. *Cancer research* 2007;67:6092-9.
113. Brockhausen J, Tay SS, Grzelak CA, et al. miR-181a mediates TGF-beta-induced hepatocyte EMT and is dysregulated in cirrhosis and hepatocellular cancer. *Liver international : official journal of the International Association for the Study of the Liver* 2014.
114. Duan X, Hu J, Wang Y, Gao J, Peng D, Xia L. MicroRNA-145: a promising biomarker for hepatocellular carcinoma (HCC). *Gene* 2014;541:67-8.
115. Heo MJ, Kim YM, Koo JH, et al. microRNA-148a dysregulation discriminates poor prognosis of hepatocellular carcinoma in association with USP4 overexpression. *Oncotarget* 2014;5:2792-806.
116. Dang YW, Chen G, Liao Y, Wang L. [Expression of miR-191 and miR-221 in hepatocellular carcinoma and its clinical significance]. *Zhonghua bing li xue za zhi Chinese journal of pathology* 2013;42:397-8.
117. Giray BG, Emekdas G, Tezcan S, et al. Profiles of serum microRNAs; miR-125b-5p and miR223-3p serve as novel biomarkers for HBV-positive hepatocellular carcinoma. *Molecular biology reports* 2014.
118. Yang H, Zheng W, Zhao W, Guan C, An J. [Roles of miR-590-5p and miR-590-3p in the development of hepatocellular carcinoma]. *Nan fang yi ke da xue xue bao = Journal of Southern Medical University* 2013;33:804-11.



119. Li L, Guo Z, Wang J, Mao Y, Gao Q. Serum miR-18a: a potential marker for hepatitis B virus-related hepatocellular carcinoma screening. *Digestive diseases and sciences* 2012;57:2910-6.
120. Xu D, He XX, Chang Y, Sun SZ, Xu CR, Lin JS. Downregulation of MiR-93 expression reduces cell proliferation and clonogenicity of HepG2 cells. *Hepato-gastroenterology* 2012;59:2367-73.
121. Li Y, Tan W, Neo TW, et al. Role of the miR-106b-25 microRNA cluster in hepatocellular carcinoma. *Cancer science* 2009;100:1234-42.
122. Yuan B, Dong R, Shi D, et al. Down-regulation of miR-23b may contribute to activation of the TGF-beta1/Smad3 signalling pathway during the termination stage of liver regeneration. *FEBS letters* 2011;585:927-34.
123. Salvi A, Sabelli C, Moncini S, et al. MicroRNA-23b mediates urokinase and c-met downmodulation and a decreased migration of human hepatocellular carcinoma cells. *The FEBS journal* 2009;276:2966-82.
124. Roderburg C, Mollnow T, Bongaerts B, et al. Micro-RNA profiling in human serum reveals compartment-specific roles of miR-571 and miR-652 in liver cirrhosis. *PloS one* 2012;7:e32999.
125. Lee CG, Kim YW, Kim EH, et al. Farnesoid X receptor protects hepatocytes from injury by repressing miR-199a-3p, which increases levels of LKB1. *Gastroenterology* 2012;142:1206-17 e7.
126. Li W, Wang J, Chen QD, et al. Insulin promotes glucose consumption via regulation of miR-99a/mTOR/PKM2 pathway. *PloS one* 2013;8:e64924.
127. Wen F, Yang Y, Jin D, Sun J, Yu X, Yang Z. MiRNA-145 is involved in the development of resistin-induced insulin resistance in HepG2 cells. *Biochem Biophys Res Commun* 2014;445:517-23.
128. Jordan SD, Kruger M, Willmes DM, et al. Obesity-induced overexpression of miRNA-143 inhibits insulin-stimulated AKT activation and impairs glucose metabolism. *Nature cell biology* 2011;13:434-46.

129. Huang da W, Sherman BT, Lempicki RA. Bioinformatics enrichment tools: paths toward the comprehensive functional analysis of large gene lists. *Nucleic acids research* 2009;37:1-13.
130. Huang da W, Sherman BT, Lempicki RA. Systematic and integrative analysis of large gene lists using DAVID bioinformatics resources. *Nature protocols* 2009;4:44-57.
131. Horgan CP, Hanscom SR, Jolly RS, Futter CE, McCaffrey MW. Rab11-FIP3 links the Rab11 GTPase and cytoplasmic dynein to mediate transport to the endosomal-recycling compartment. *J Cell Sci* 2010;123:181-91.
132. Lapierre LA, Dorn MC, Zimmerman CF, Navarre J, Burnette JO, Goldenring JR. Rab11b resides in a vesicular compartment distinct from Rab11a in parietal cells and other epithelial cells. *Exp Cell Res* 2003;290:322-31.
133. Butterworth MB, Edinger RS, Silvis MR, et al. Rab11b regulates the trafficking and recycling of the epithelial sodium channel (ENaC). *American journal of physiology Renal physiology* 2012;302:F581-90.
134. Casanova JE, Wang X, Kumar R, et al. Association of Rab25 and Rab11a with the apical recycling system of polarized Madin-Darby canine kidney cells. *Mol Biol Cell* 1999;10:47-61.
135. Chen W, Feng Y, Chen D, Wandinger-Ness A. Rab11 is required for trans-golgi network-to-plasma membrane transport and a preferential target for GDP dissociation inhibitor. *Mol Biol Cell* 1998;9:3241-57.
136. Sugawara K, Shibasaki T, Mizoguchi A, Saito T, Seino S. Rab11 and its effector Rip11 participate in regulation of insulin granule exocytosis. *Genes to cells : devoted to molecular & cellular mechanisms* 2009;14:445-56.
137. Horgan CP, Hanscom SR, Jolly RS, Futter CE, McCaffrey MW. Rab11-FIP3 binds dynein light intermediate chain 2 and its overexpression fragments the Golgi complex. *Biochem Biophys Res Commun* 2010;394:387-92.
138. Burkhardt JK. The role of microtubule-based motor proteins in maintaining the structure and function of the Golgi complex. *Biochimica et biophysica acta* 1998;1404:113-26.

139. Burkhardt JK, Echeverri CJ, Nilsson T, Vallee RB. Overexpression of the dynamin (p50) subunit of the dynactin complex disrupts dynein-dependent maintenance of membrane organelle distribution. *J Cell Biol* 1997;139:469-84.
140. Harada A, Takei Y, Kanai Y, Tanaka Y, Nonaka S, Hirokawa N. Golgi vesiculation and lysosome dispersion in cells lacking cytoplasmic dynein. *J Cell Biol* 1998;141:51-9.
141. Palmer KJ, Hughes H, Stephens DJ. Specificity of cytoplasmic dynein subunits in discrete membrane-trafficking steps. *Mol Biol Cell* 2009;20:2885-99.
142. Traer CJ, Rutherford AC, Palmer KJ, et al. SNX4 coordinates endosomal sorting of TfnR with dynein-mediated transport into the endocytic recycling compartment. *Nature cell biology* 2007;9:1370-80.
143. Marion TL, Perry CH, St Claire RL, 3rd, Brouwer KL. Endogenous bile acid disposition in rat and human sandwich-cultured hepatocytes. *Toxicology and applied pharmacology* 2012;261:1-9.
144. Shibukawa A, Sawada T, Nakao C, Izumi T, Nakagawa T. High-performance frontal analysis for the study of protein binding of troglitazone (CS-045) in albumin solution and in human plasma. *Journal of chromatography A* 1995;697:337-43.
145. Tang R, Li L, Zhu D, et al. Mouse miRNA-709 directly regulates miRNA-15a/16-1 biogenesis at the posttranscriptional level in the nucleus: evidence for a microRNA hierarchy system. *Cell research* 2012;22:504-15.
146. Earnshaw WC, Martins LM, Kaufmann SH. Mammalian caspases: structure, activation, substrates, and functions during apoptosis. *Annual review of biochemistry* 1999;68:383-424.
147. Tang X, Gal J, Zhuang X, Wang W, Zhu H, Tang G. A simple array platform for microRNA analysis and its application in mouse tissues. *Rna* 2007;13:1803-22.
148. Zou Y, Bao Q, Kumar S, Hu M, Wang GY, Dai G. Four waves of hepatocyte proliferation linked with three waves of hepatic fat accumulation during partial hepatectomy-induced liver regeneration. *PloS one* 2012;7:e30675.

149. Bail S, Swerdel M, Liu H, et al. Differential regulation of microRNA stability. *Rna* 2010;16:1032-9.
150. Ruegger S, Grosshans H. MicroRNA turnover: when, how, and why. *Trends in biochemical sciences* 2012;37:436-46.
151. Chen L, Smith L, Johnson MR, Wang K, Diasio RB, Smith JB. Activation of protein kinase C induces nuclear translocation of RFX1 and down-regulates c-myc via an intron 1 X box in undifferentiated leukemia HL-60 cells. *The Journal of biological chemistry* 2000;275:32227-33.
152. Liu M, Lee BH, Mathews MB. Involvement of RFX1 protein in the regulation of the human proliferating cell nuclear antigen promoter. *The Journal of biological chemistry* 1999;274:15433-9.
153. Lubelsky Y, Reuven N, Shaul Y. Autorepression of rfx1 gene expression: functional conservation from yeast to humans in response to DNA replication arrest. *Molecular and cellular biology* 2005;25:10665-73.
154. Ha TY. MicroRNAs in Human Diseases: From Lung, Liver and Kidney Diseases to Infectious Disease, Sickle Cell Disease and Endometrium Disease. *Immune Netw* 2011;11:309-23.
155. Miyoshi K, Miyoshi T, Siomi H. Many ways to generate microRNA-like small RNAs: non-canonical pathways for microRNA production. *Mol Genet Genomics* 2010;284:95-103.
156. Kornfeld JW, Baitzel C, Konner AC, et al. Obesity-induced overexpression of miR-802 impairs glucose metabolism through silencing of Hnf1b. *Nature* 2013;494:111-5.
157. Zhang J, Zhang F, Didelot X, et al. Maternal high fat diet during pregnancy and lactation alters hepatic expression of insulin like growth factor-2 and key microRNAs in the adult offspring. *BMC genomics* 2009;10:478.
158. Schwarz DS, Hutvagner G, Du T, Xu Z, Aronin N, Zamore PD. Asymmetry in the assembly of the RNAi enzyme complex. *Cell* 2003;115:199-208.

159. Khvorova A, Reynolds A, Jayasena SD. Functional siRNAs and miRNAs exhibit strand bias. *Cell* 2003;115:209-16.
160. Lewis BP, Shih IH, Jones-Rhoades MW, Bartel DP, Burge CB. Prediction of mammalian microRNA targets. *Cell* 2003;115:787-98.
161. Gennarino VA, Sardiello M, Avellino R, et al. MicroRNA target prediction by expression analysis of host genes. *Genome Res* 2009;19:481-90.
162. Calin GA, Dumitru CD, Shimizu M, et al. Frequent deletions and down-regulation of micro- RNA genes miR15 and miR16 at 13q14 in chronic lymphocytic leukemia. *Proceedings of the National Academy of Sciences of the United States of America* 2002;99:15524-9.
163. Klein U, Lia M, Crespo M, et al. The DLEU2/miR-15a/16-1 cluster controls B cell proliferation and its deletion leads to chronic lymphocytic leukemia. *Cancer cell* 2010;17:28-40.
164. de la Coste A, Fabre M, McDonnell N, et al. Differential protective effects of Bcl-xL and Bcl-2 on apoptotic liver injury in transgenic mice. *The American journal of physiology* 1999;277:G702-8.
165. Hockenbery DM, Zutter M, Hickey W, Nahm M, Korsmeyer SJ. BCL2 protein is topographically restricted in tissues characterized by apoptotic cell death. *Proceedings of the National Academy of Sciences of the United States of America* 1991;88:6961-5.
166. Tamminga J, Kathiria P, Koturbash I, Kovalchuk O. DNA damage-induced upregulation of miR-709 in the germline downregulates BORIS to counteract aberrant DNA hypomethylation. *Cell cycle* 2008;7:3731-6.
167. Loukinov DI, Pugacheva E, Vatolin S, et al. BORIS, a novel male germ-line-specific protein associated with epigenetic reprogramming events, shares the same 11-zinc-finger domain with CTCF, the insulator protein involved in reading imprinting marks in the soma. *Proceedings of the National Academy of Sciences of the United States of America* 2002;99:6806-11.
168. Feng C, Xu W, Zuo Z. Knockout of the regulatory factor X1 gene leads to early embryonic lethality. *Biochem Biophys Res Commun* 2009;386:715-7.

169. Watts JA, Zhang C, Klein-Szanto AJ, et al. Study of FoxA pioneer factor at silent genes reveals Rfx-repressed enhancer at Cdx2 and a potential indicator of esophageal adenocarcinoma development. *PLoS genetics* 2011;7:e1002277.

## **CURRICULUM VITAE**

**Sneha Surendran**

### **EDUCATION**

- 2008-2014    Indiana University, Indianapolis, IN, USA  
Ph.D. Medical and Molecular Genetics w/ Minor in Diabetes  
Dissertation: Role of microRNA-709 in murine liver  
Advisor: Núria Morral, PhD
- 2005-2007    University of Mumbai, Mumbai, India  
M.Sc. Bioanalytical Sciences
- 2002-2005    University of Mumbai, Mumbai, India  
B.Sc. Biochemistry and Zoology

### **HONORS AND AWARDS**

- 2005    S.I.E.S College of Arts, Science & Commerce, affiliated to the University of  
Mumbai 3<sup>rd</sup> place in B.Sc. Biochemistry and Zoology examinations
- 2007    University of Mumbai 5<sup>th</sup> place in M.Sc. Bioanalytical Sciences examinations
- 2008    Indiana University, School of Medicine Fellowship (Travel grant)
- 2011    Sigma Xi Graduate Research Competition (Third place)

### **GRANTS AND FELLOWSHIPS**

- 2010-2012    Diabetes & Obesity DeVault Pre-doctoral Fellowship
- 2012-2014    American Heart Association Pre-doctoral Fellowship

## **PROFESSIONAL ACTIVITIES**

06/12 Member of Sigma Xi through the Indiana University Medical Center Sigma Xi chapter

01/11 Member of AAAS (American Association for the Advancement of Science) through the Science Program for Excellence in Science

## **ABSTRACTS AND PRESENTATIONS**

1. "Study of role of microRNAs in metabolism and type-2 diabetes". Department of Medical and Molecular Genetics poster session, 2010.
2. "Study of role of microRNAs in liver metabolism and type-2 diabetes". Department of Medical and Molecular Genetics Research Club, 2011.
3. "Role of microRNA-709 in hepatic insulin resistance". Department of Medical and Molecular Genetics poster session, 2011.
4. "Study of role of miR-709 in hepatic insulin resistance". Sigma Xi research competition, 2011.
5. "Role of microRNA-709 on hepatic metabolism". Department of Medical and Molecular Genetics poster session, 2012.
6. "Differential expression of microRNAs under different hepatic nutritional status". Department of Medical and Molecular Genetics poster session, 2013.
7. "Differential expression of microRNAs under different hepatic nutritional status" at Metabolism Signaling & Disease: From cell to organism, Cold Spring Harbor Laboratory, New York, 2013.



## **PUBLICATIONS**

1. Park, JS., **Surendran, S.**, Kamendulis, LM., Morral, N. Comparative nucleic acid transfection efficacy in primary hepatocytes for gene silencing and functional studies. *BMC Research Notes* 4:8 (2011).
2. Ahn, M., Gamble, A., Witting, SR., Magrisso, J., **Surendran, S.**, Obici, S., Morral, N. Vector and helper genome rearrangements occur during production of helper-dependent adenoviral vectors. *Human Gene Therapy Methods* 24:1-10 (2013).
3. Ruiz, R., Jideonwo, V., Ahn, M., **Surendran, S.**, Hou, Y., Tagliabracci, VS., Kerner, J., Gamble, A., Irimia-Dominguez, JM., Puchowicz, MA., DePaoli-Roach, A., Hoppel, C., Roach, P., Morral, N. Silencing Sterol Regulatory Element Binding Protein-1 In Mouse Liver Dissociates Hepatic Steatosis From Insulin Resistance. *Journal of Biological Chemistry* 289(9):5510-7 (2014).
4. **Surendran, S.**, Jideonwo, V., Merchun, C., Ahn, M., Murray, J., Ryan, J., Dunn, K., Dai, G., Kota J., and Morral, N. miR-709 targets cystoskeleton organization genes in mouse liver and is up-regulated in proliferative states. Submitted.
5. **Surendran, S.**, Goswami, C., Truitt, B., Lui, Y. and Morral, N. Differential expression of microRNAs under different hepatic nutritional statuses. In preparation.
6. **Surendran, S.** and Morral, N. Role of microRNAs in Diabetes. In preparation.

## **RESEARCH AND TRAINING EXPERIENCE**

2009                    Molecular Biology workshop; Indiana University, School of Medicine.

- 2008-2009 Indiana University School of Medicine, Department of Medical and Molecular Genetics. Research rotations (Mentors: Nuria Morral, Ph.D., Elliot Rosen, Ph.D. and David Gilley, Ph.D.).
- 2008 Observer in the Genetics laboratory of the Dept. of Assisted Reproduction and Genetics, Jaslok Hospital & Research Centre, Mumbai, India.
- 2006 Trained in 'Chromatography and Spectroscopy'; Perkin Elmer Technical Center.
- 2006 Training in Microbiology, Chemical and Analytical Section, Quality Assurance Department, Johnson & Johnson Limited.
- 2006-2007 Trained in Animal Testing Centre (CPCSEA Approved), Ramnarain Ruia College, Mumbai.
- Pharmacokinetic study of different formulations on rabbits.
  - Anti-diabetic study on rats using Streptozotocin model.
  - Anti-diabetic study on rats using Alloxan model.
  - Efficacy study of oils for hair growth on rats.
  - Anti-estrogenic activity of spice extracts on Albino Wistar rats.
  - Acute toxicity studies on lice (LD50).
  - Draize Skin irritancy study of formulation on Rabbits.
  - Toxicity studies on rats and mice.
  - Learned techniques like Retro-Orbital of rat; cervical dislocation; intra-venous and intra-peritoneal mode of injection on rats; oral

dosing of rats, mice and rabbits; withdrawal of blood from rats and rabbits; Cardiac puncture of rats and mice; etc.